UNIVERSITÉ DE LORRAINE | BIBLIOTHÈQUES UNIVERSITAIRES

AVERTISSEMENT

Ce document est le fruit d'un long travail approuvé par le jury de soutenance et mis à disposition de l'ensemble de la communauté universitaire élargie.

Il est soumis à la propriété intellectuelle de l'auteur. Ceci implique une obligation de citation et de référencement lors de l'utilisation de ce document.

D'autre part, toute contrefaçon, plagiat, reproduction illicite encourt une poursuite pénale.

Contact bibliothèque : ddoc-theses-contact@univ-lorraine.fr
(Cette adresse ne permet pas de contacter les auteurs)

LIENS

Code de la Propriété Intellectuelle. articles L 122. 4
Code de la Propriété Intellectuelle. articles L 335.2- L 335.10
http://www.cfcopies.com/V2/leg/leg_droi.php
http://www.culture.gouv.fr/culture/infos-pratiques/droits/protection.htm

Université de Lorraine, Collegium Sciences et Technologies
Ecole Doctorale SIReNa

Thèse

Présentée pour l'obtention du titre de
Docteur de l'Université de Lorraine
Spécialité "Géosciences"

Par **Jessica STRYDOM**

Etude de la production d'eau douce à partir de formations argileuses dans les zones de foothills

Soutenance le 21/ 06/ 2022

Membres du jury :

Président de jury :

Mme. Jocelyne BRENDLE — Professeure, Université de Haute Alsace, France

Rapporteurs :

Mme. Patricia PATRIER — Professeure, Université de Poitiers, France

Directeur de thèse :

M. Dragan GRGIC — Maître de conférences - HDR, Université de Lorraine, France

Co-Directeur de thèse :

M. Jérôme STERPENICH — Professeur, Université de Lorraine, France

Invités :

M. Eric C. GAUCHER. — Ingénieur Géochimie, TOTAL SA, Pau, France


UNIVERSITÉ
DE LORRAINE

SIReNa

cnrs

cregu

geo
Ressources

TOTAL


UNIVERSITÉ
DE LORRAINE

SIReNa

cnrs

cregu

geo
Ressources

TOTAL


UNIVERSITÉ
DE LORRAINE

SIReNa

cnrs

cregu

geo
Ressources

TOTAL

Université de Lorraine, Collegium Sciences et Technologies
Ecole Doctorale SIReNa

Thèse

Présentée pour l'obtention du titre de
Docteur de l'Université de Lorraine
Spécialité "Géosciences"

Par **Jessica STRYDOM**

Etude de la production d'eau douce à partir de formations argileuses dans les zones de foothills

Soutenance le 21/ 06/ 2022

Membres du jury :

Président de jury :

Mme. Jocelyne BRENDLE — Professeure, Université de Haute Alsace, France

Rapporteurs :

Mme. Patricia PATRIER — Professeure, Université de Poitiers, France

Directeurs de thèse :

M. Dragan GRGIC — Maître de conférences - HDR, Université de Lorraine, France

Co-Directeurs de thèse :

M. Jérôme STERPENICH — Professeur, Université de Lorraine, France

Invités :

M. Eric C. GAUCHER M. — Ingénieur Géochimie, TOTAL SA, Pau, France

Table of contents

Acknowledgments 9
RESUME ETENDU 11
ABSTRACT 19
GENERAL OVERVIEW 23
SCIENTIFIC CONTEXT 23
OBJECTIVES OF THE STUDY 25
THESIS ORGANIZATION 26
1- STATE OF THE ART 29
1.1- FORMATION WATERS: PHENOMENA RESPONSIBLE FOR THE PRODUCTION OF FRESH WATER 29
1.1.1- Water-rock interactions 31
1.1.2- Mixing or dilution 34
1.1.3- Hydrocarbon maturation 35
1.1.4- Ultrafiltration 36
1.2- CL & BR IN FORMATION WATERS 39
1.2.1- The fractionation of clorine and bromine stable isotopes 39
1.3- THE EFFECT OF ORGANIC MATTER 41
1.4- THEORETICAL CONSIDERATIONS 43
1.4.1- The diffuse double layer (DDL) 43
1.4.2- Overlapping of DDL during clay compaction 44
1.4.3- Diffusion 45
2- MATERIALS AND EXPERIMENTAL METHODS FOR HYDRO-MECHANICAL EXPERIMENTS 51
2.1- STARTING MATERIALS 52
2.1.1- The clays 52
2.1.2- The stock ocean water 53
2.2- THE EXPERIMENTAL SETUP 54
2.3- EXPERIMENTAL PROTOCOL 55
2.3.1- Hydro mechanical loading path 56
2.3.1- Fluid and solid sample collection 57
3- METHODS OF ANALYSIS FOR FLUIDS AND SOLIDS 59
3.1- THE FLUIDS 59
3.1.1- Chemical Analyses of Fluids 59
3.1.2- Mass Balance Calculation 62

3.1.3- Water Chemistry Modelling / Calculated Water Content 64
3.2- THE SOLIDS 67
3.2.1- Physical characterization 67
3.2.2- Water content 70
3.2.3- Chemical characterization 71
3.2.4- Mineralogical characterization 71
4- RESULTS 75
4.1- MECHANICAL DATA 75
4.2- THE FLUID EVOLUTION 78
4.2.1- Cl and Br concentrations 79
4.2.1- Major elements 86
4.2.2- Cl and Br Isotopes 89
4.3- WATER CHEMISTRY MODELLING 98
4.3.1- PHREEQC 98
4.3.2- SURP 98
4.4- THE SOLID MATERIAL CHARACTERIZATION OF THE COMPACTED CLAYS 103
4.4.1- Physical characterization 103
4.4.2- Volumetric water content (Thermogravimetry) 104
4.4.3- Porosity 104
4.4.4- Solid material chemical composition 113
4.4.5- Solid material mineralogical composition 113
5- DISCUSSION 123
5.1- REACTIVITY OF THE SYSTEM 123
5.2- FLUID FLOW AND SOLUTE TRANSPORT IN COMPACTED CLAYS 125
5.3- ISOTOPE FRACTIONATION 128
5.4- THE CASE OF Br 132
5.5- POROSITY 134
5.6- POTENTIAL MECHANISMS DRIVING PORE WATER EVOLUTION 136
6- CONCLUSION 141
7- LIST OF FIGURES 143
8- LIST OF TABLES 147
9- REFERENCES 149

ACKNOWLEDGMENTS

This work was funded by the Centre de Recherches sur la Géologie des Matières Premières Minérales et Energétiques (CREGU), Project Reference number: FR00008990 / T30, and TOTAL EP-R&D.

An African proverb says;

"***It takes a village to raise a child***."

On that note, there is a long list of incredible humans that I am so greatful to, for the privilidge of this journey they took with me.

From TOTAL Energies, Eric Gaucher, thank you for giving me your confidence to excecute the project and the freedom to put my own spin on it. Also, for providing a supportive ear, gentle encouragement and never failing to believe that I can do it.

From the IPGP, exceptional gratitude is extended to Hans Eggenkamp, Pascale Louvat, Pierre Agrinier and Pierre Burkel. Thank you for receiving me, for invesiting so many hours in training me, and the endless perseverance to ensure high quality results. A special acknowledgment goes to Hans for the personal interest you took in my progress and development.

From the Laboratoire GeoRessources, great appreciation goes to Patrick Gaire for his patient assistance with all technical aspects for the entire duration of the experiments. Without you, none of this work would have been possible. Thank you Patrick, for always being friendly and endlessly patient. Abdelrahman Eid and especially Régine Mosser-Ruck, are thanked for going above and beyond with XRD analysis. Laurent Schoumacker and Andreï Lecompte are also thanked for their analytical contributions, and Antonin Richard for his generous contribution to revising and significantly improving various texts, with regards to conference contributions and publications.

Then, I thank Manuelle Peletier and Olivier Cuisinier for serving as my Thesis Committee members. I walked out of each meeting feeling encouraged. Thank you for the reassurance and support.

To my Thesis Supervisors, Dragan Grigc and Jerome Sterpenich, where to begin… Thank you for the opportunity you gave me, for welcoming me as part of the team, and putting your confidence in me (even when I didn't have any in myself at moments). Thank you for the hours and hours spent on reviewing and improving my work. In particular Jerome, I'm exceptionally greatful for the support and the extra work you put in towards getting our article published.

A special word of appreciation is extended to Nathalie Foucal, from CREGU. Nathalie, you made everything appear effortless. I say ‘appear’ because I know you work very hard to keep all the weels turning and making sure all of us are well taken care off, professionally and personally. Thank you for being an endless source of incredibly kind assistance, but also for being a friend. Thank you for being the anker that held it all together.

Lastly, from the bottom of my heart, I thank my supportive friends, who kept me going; my partner, Alexandre Petit, for continuously, encouragingly, pushing me to do my best, and for putting up with all my ups and downs; and lastly, to my loving family for who they are. *Ubuntu*…

RESUME ETENDU

La production d'eau douce par compaction des formations argileuses (effet mécanique), diagenèse des argiles gonflantes ou maturation de la matière organique (effet thermique) peut jouer un rôle majeur dans le régime de pression, la fracturation des roches et l'expulsion des hydrocarbures. L'objectif de ce travail est de rechercher des traceurs chimiques et isotopiques (notamment les isotopes du Cl et du Br) permettant de discriminer les différents processus de production d'eau douce et de quantifier les volumes produits. La relation existant entre les isotopes stables du Cl (exprimés en $\delta^{37}Cl$) et les concentrations en chlorures a déjà été utilisée pour déterminer la source de salinité des eaux de formation, qui peut être liée à l'évaporation de l'eau de mer ou à la dissolution de halite.

La première partie du travail de thèse consiste en une étude bibliographique des phénomènes responsables de la production d'eau douce dans les dépôts de piémont, zone de transition entre les plaines de faible relief et les chaînes de montagnes adjacentes. Dans les piémonts, les sédiments s'accumulent dans des cônes alluviaux étendus qui sont souvent recouverts par des argiles et/ou des marnes (Cazanacli et al., 2002). Ceci peut constituer un potentiel pour le piégeage des hydrocarbures dans les sables sous-jacents (Ab'Saber, 1961). Avec la compaction progressive des sédiments, la transformation des matières minérales et organiques est connue pour produire une eau moins salée (plus douce) que l'eau interstitielle d'origine qui est de composition similaire à l'eau de l'océan. Ce phénomène est appelé ultrafiltration. Cette étude se concentre spécifiquement sur la contribution à la production d'eau douce de la transformation des minéraux d'argile hydratée, qu'elle soit due à des mécanismes mécaniques, thermiques ou chimiques, ou de la transformation de la matière organique (uniquement considérée d'un point de vue bibliographique). Une attention particulière est portée aux éventuels fractionnements chimiques et isotopiques qui résultent de cette production d'eau douce, en se basant également sur une étude d'eaux de réservoirs connus et non salées (Eggenkamp, 2014). Alors que les principaux cations et anions dissous dans l'eau interstitielle des argiles de compactage sont étudiés en raison du fractionnement chimique qui se produit, l'accent est mis sur les variations isotopiques du Cl et du Br qui sont considérés comme des traceurs chimiques et isotopiques des mécanismes responsables de l'évolution de la salinité. En effet, Cl et Br sont fortement concentrés dans les eaux de formation (Hanor, 1987) et les grandes variations de salinité observées restent encore mal comprises (Neuzil et Person, 2017).

La deuxième et principale partie du travail de thèse est expérimentale. Les trois expériences menées visent à déterminer la composition et les quantités (volumes) d'eau libérées par une argile saturée soumise à une compression mécanique. Le principal mécanisme considéré à travers ces expériences de compaction est la transformation minéralogique de type smectite-illite traduisant une déshydratation des argiles (Tremosa et al., 2020) comme source de dilution/rafraîchissement.

Ces expériences ont fait appel à un dispositif expérimental spécialement conçu pour mesurer de très petits volumes de fluides aqueux échangés sous de très fortes contraintes de compaction (conditions oedométriques), de température et de pression de fluide sur une très longue période (plusieurs mois) compte tenu de la très faible perméabilité des matériaux et d'une cinétique de réaction très lente. Une quantification des mécanismes mis en jeu, en particulier l'étude des traceurs chimiques mais aussi isotopiques (Cl et Br), sera réalisée.

La troisième et dernière partie du travail de thèse consiste à réaliser des calculs d'équilibres géochimiques afin de quantifier la teneur en eau retenue par les minéraux argileux. Les paramètres cinétiques de la genèse de l'eau qui ont été déterminés par l'expérience ont été confrontés à une modélisation de pointe afin de quantifier spécifiquement la proportion d'eau douce produite par la transformation des minéraux par rapport au volume expulsé suite à la compaction mécanique.

Notre objectif est de simuler expérimentalement les processus diagénétiques (flux de fluide et de chaleur, compaction mécanique et compaction chimique) impliqués dans la production d'eau de formation à partir d'un échantillon d'argile saturée dans des conditions d'enfouissement profond (~6-7 km de profondeur). Les tests oedométriques simulent les conditions unidimensionnelles (verticales) de déformation et de drainage: aucun déplacement latéral de l'échantillon cylindrique n'est possible mais l'échantillon peut gonfler/se comprimer verticalement en réponse aux changements de la contrainte verticale (axiale) $\sigma 1$.

Pour ces expériences, une cellule oedométrique, avec des dimensions internes de 10 cm de diamètre et 10 cm de hauteur, est connectée à un ensemble de pompes pour générer à la fois une pression de fluide poreux (Pi) des deux côtés de l'échantillon (condition drainée) et une contrainte verticale atteignant 45 MPa et 150 MPa respectivement. Les pompes peuvent être contrôlées individuellement pour induire la contrainte verticale effective souhaitée sur l'échantillon ($\sigma 1' = \sigma 1 - Pi$). La cellule de compression oedométrique qui a été développée pour les besoins de cette étude est nouvelle et rare en raison des hautes pressions de fluide, contraintes mécaniques et températures qu'elle permet d'appliquer aux échantillons d'argile durant les expériences. L'originalité réside également dans la collaboration multidisciplinaire entre des laboratoires réputés afin de contribuer à une compréhension fonctionnelle du comportement du Cl et du Br dans les processus géologiques. Il n'existe pas d'expérience multidisciplinaire similaire à grande échelle (décimétrique) dans la littérature.

Nous avons réalisé trois expériences de compactage, qui ont duré environ 200 jours chacune, au cours desquelles nous avons enregistré en continu la contrainte axiale ($\sigma 1$), la pression du fluide interstitiel (Pi), la déformation axiale et les volumes de fluide dans les pompes d'injection et de collecte. Les expériences consistaient d'abord à saturer l'argile avec de l'eau de mer dans la cellule oedométrique, puis à la compacter en 5 ou 10 étapes d'augmentation de la contrainte verticale jusqu'à 150 MPa et

d'augmentation de la température jusqu'à 150°C, tout en maintenant la pression du fluide interstitiel aussi proche que possible de 45 MPa.

Les deux matériaux sélectionnés pour les expériences sont l'argile à smectite MX80 (contenant 71% de smectite) et la marne de Sainte-Suzanne (SSM contenant 61% d'illite) du bassin aquitain (forage LA 101 ; latitude 43,420648° et longitude -0,619980°). Pour simuler un environnement de bassin d'avant-pays sédimentaire, de l'eau naturelle filtrée de l'océan Atlantique (0,1 μm) prélevée sur la côte de Bidart (France) a été utilisée comme eau océanique de réserve pour saturer l'argile pour les trois expériences.

Les variations du protocole pour les trois expériences sont les suivantes :

Expérience 1 : compactage de la MX-80 saturée avec 5 étapes d'augmentation de la contrainte verticale et de la température.

Expérience 2 : compactage de la SSM saturée avec 5 étapes d'augmentation de la contrainte verticale et de la température.

Expérience 3 : compactage de MX-80 saturée avec 10 étapes d'augmentation de la contrainte verticale et à température ambiante.

Le suivi continu de la déformation axiale et la surveillance de la composition de l'eau d'entrée et expulsée ont permis d'établir un bilan massique hydrique et chimique du système. Nous avons donc pu évaluer la composition de l'eau interstitielle restante à chaque étape du compactage.

De plus, en collaboration avec le BRGM (Orléans, France), le volume d'eau produit par la transformation potentielle de la smectite en illite a également été calculé à partir des paramètres expérimentaux et des résultats de la première expérience de compaction du MX80 en utilisant un logiciel spécialisé développé en interne (appelé SURP). Le code SURP est un logiciel de modélisation qui traite simultanément les calculs thermo-hydro-mécaniques et les interactions chimico-minéralogiques pendant la compaction géologique, en couplant un code Python (v 2.7) avec IPHREEQC (Tremosa et al., 2020). Cette modélisation nous a permis de comprendre quelle proportion de cette eau expulsée est le résultat de la déshydratation des minéraux argileux.

Aucune transformation minérale importante n'a pas été mise en évidence, que ce soit suite à l'exercice de modélisation (Figure 1) ou suite à la caractérisation minérale par diffraction des RX.

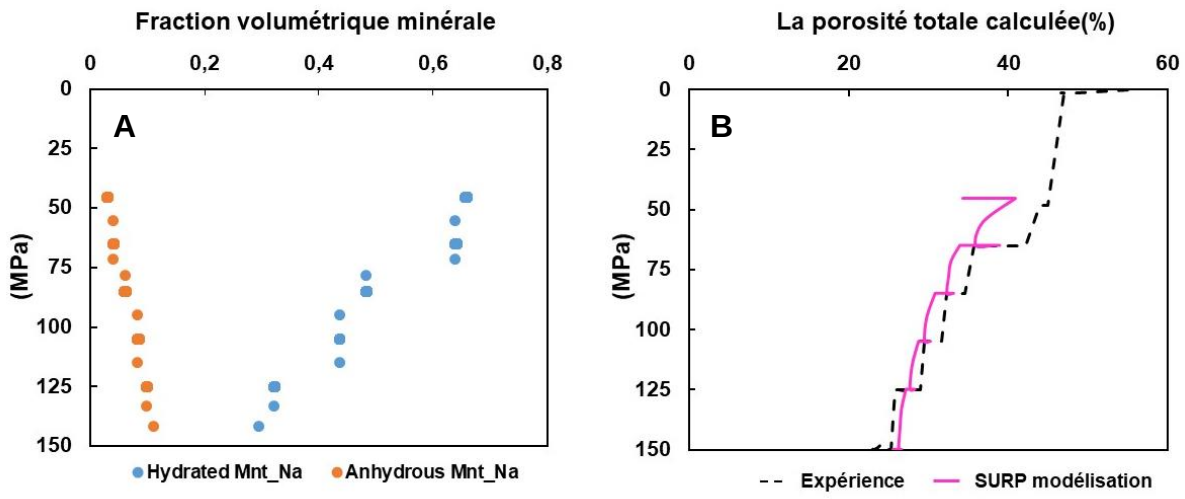


Figure 1: Profil minéralogique simulé montrant la Na-Montmorillonite hydratée (3, 2 ou 1 couches d'eau adsorbées) en orange et la Na-Montmorillonite anhydre en bleu en A. En B, la diminution de la porosité correspondante est représentée.

Nous avons constaté que la chimie de la solution et les variations des rapports isotopiques des halogènes sont considérablement différentes dans les expériences réalisées avec une argile gonflante (MX80 riche en smectite) et une argile non gonflante (SSM rich en illite). Concernant l'argile gonflante, nous avons observé une diminution générale des concentrations en cations et anions dans l'eau expulsée (Figure 2), tandis que sa concentration augmentait légèrement dans le fluide interstitiel restant. Ce n'était pas le cas pour l'argile non gonflante SSM. Ensuite, un rafraîchissement plus important de l'eau expulsée s'est produit pendant l'expérience de compactage à une température plus élevée.

Nous avons également observé que le Br est beaucoup plus efficacement filtré et fractionné par les argiles que le Cl. Ceci peut être expliqué par son abondance naturelle beaucoup plus faible, son potentiel ionique hydraté plus élevé (fonction de la charge et du rayon) et sa masse atomique deux fois supérieure à celle du Cl. Cela se traduit également par une plus grande gamme de fractionnement isotopique pour le Br (valeur δ^{81}Br de l'eau expulsée de 0,9 ‰ jusqu'à 1,5‰) que pour le Cl (valeur δ^{37}Cl de l'eau expulsée de -0,1‰ jusqu'à -0,5‰), et ceci dans les trois expériences de compactage.

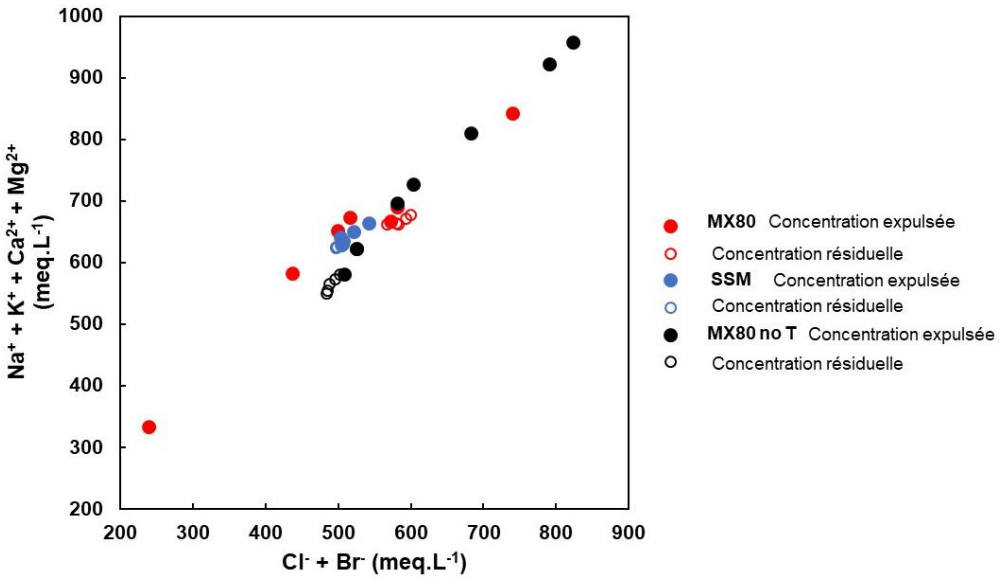


Figure 2: Concentrations en cations et en anions de l'eau expulsée au cours des trois expériences de compactage et composition calculée de l'eau interstitielle restant dans l'argile.

La gamme des valeurs isotopiques obtenues dans les trois expériences de compactage se situe dans la gamme de valeurs attendues (Eggenkamp, 2014), à savoir des rapports de $\delta^{37}Cl$ entre -8‰ et 1,5‰ et des rapports de $\delta^{81}Br$ entre -1,5‰ et 4‰. On remarque que plus la concentration en Cl est faible dans l'eau expulsée, plus la valeur de $\delta^{37}Cl$ est faible également. Les valeurs de $\delta^{37}Cl$ sont aussi négativement corrélées avec celles de $\delta^{81}Br$.

La Figure 3 permet de faire deux observations importantes. La gamme de fractionnement de Br observée est plus grande que la gamme de fractionnement de Cl et, deuxièmement, il est intéressant de noter que l'expérience de compaction de SSM a provoqué un fractionnement des isotopes du Br du même ordre que lors des compactions de MX80, alors qu'aucun fractionnement isotopique ne s'est produit pour le Cl pendant la compaction de SSM. Les isotopes du Br ont également subi un fractionnement significatif dans les marnes riches en illite (SSM). Ce résultat soutient l'idée que le fractionnement est le résultat combiné des phénomènes de diffusion et de la diminution de la porosité. La charge négative plus faible de l'illite aura un effet plus faible sur l'exclusion anionique. La réduction de la taille des pores liée à la compaction peut être invoquée pour expliquer le fractionnement des isotopes du Br qui possèdent une masse atomique double de celle des deux isotopes stables du Cl. Le Br a également une mobilité plus faible que les deux isotopes du Cl.

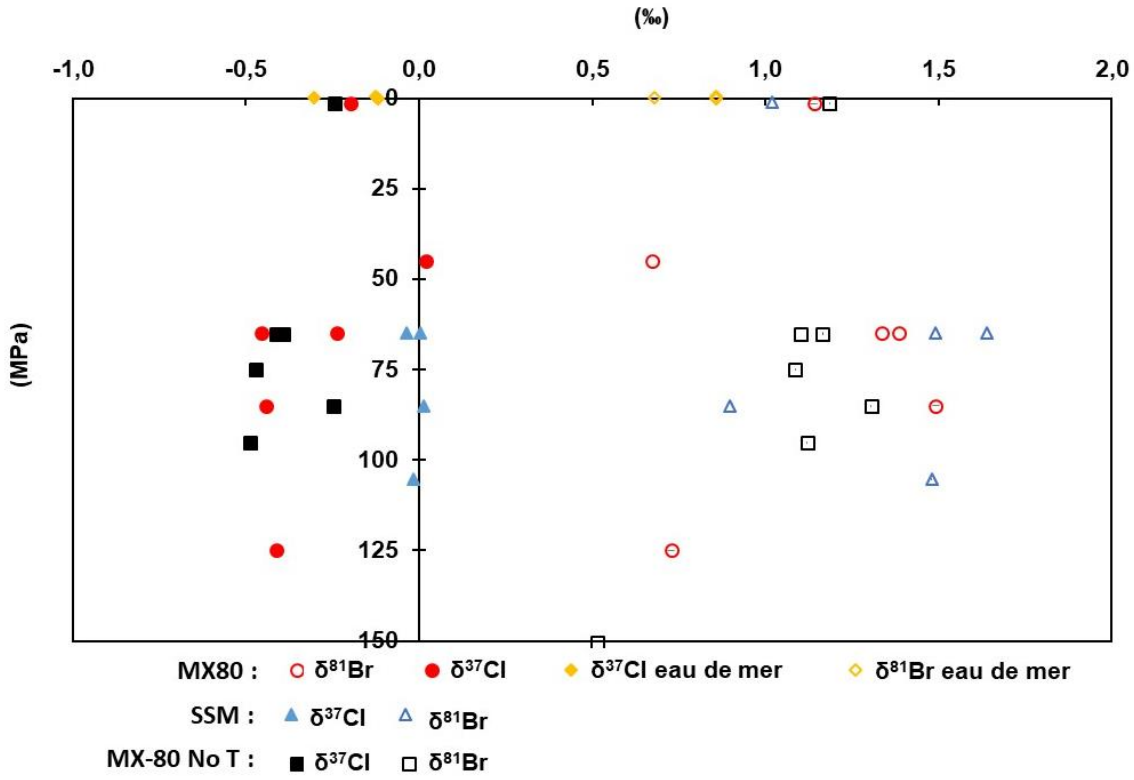


Figure 3: Gammes de fractionnement isotopique du Cl et du Br observées dans l'eau expulsée lors des trois expériences de compaction. Les formes pleines représentent les valeurs de δ37Cl et les formes vides représentent les valeurs de δ81Br. Les losanges jaunes colorés et vides représentent les valeurs initiales de l'eau océanique de δ^{37}Cl et δ^{81}Br respectivement.

La compaction de l'échantillon SSM a conduit à une porosité finale connectée au mercure plus faible (8%) que celle de MX80 (17% dans l'expérience 1, et 15% dans l'expérience 3). Cependant, la porosité piégée est plus grande pour MX80 (9% et 8%) que pour SSM (3,6%). Dans l'expérience 1 de compaction (MX80), la diminution la plus importante de la porosité calculée (42% à 35,6%) pendant l'étape à 65MPa et 30°C conduit à un fractionnement significatif à la fois pour Cl (-0,24‰ à -0,45‰ pour δ37Cl) et Br (1,38‰ à 1,33‰ pour δ81Br). La deuxième diminution la plus importante de la porosité pendant la compaction de MX80 s'est produite à 125 MPa et 120°C. La porosité a été réduite de 4% (de 29 à 25 %). Un fractionnement significatif est observé uniquement pour Br au cours de cette étape (1,5‰ à 0,7‰ pour δ81Br). Dans la compaction de SSM, la plus grande perte de porosité (35% à 25%) se produit également à 65MPa et 30°C, ce qui correspond à un faible fractionnement du Br (de 1,65‰ à 1,5‰ pour δ81Br). En revanche, la deuxième diminution la plus importante de la porosité (de 25% à 21%) s'est produite à 85 MPa et 60°C et correspond à un fractionnement important du Br (de 1,5 à 0,9‰ pour δ81Br). Le fractionnement des isotopes du Br se poursuit pour des étapes de compaction plus poussées par compassion au Cl. Ceci est potentiellement dû à la plus grande taille des anions Br. Pour les deux argiles, la réduction de la porosité et ses conséquences sur les fractionnements isotopiques ne peuvent être corrélées avec certitude.

Nos données confirment le modèle proposé selon lequel les argiles ont le potentiel, en théorie, de fractionner les isotopes stables du chlore parce que les couches d'argile chargées négativement repoussent l'ion ^{35}Cl chargé négativement légèrement plus que l'ion ^{37}Cl pendant la diffusion de l'eau interstitielle. La force de répulsion créée par les barrières de charges négatives dans l'argile sous compactage devrait généralement être plus forte sur le Br que sur le Cl (et donc le retardement/expulsion préférentielle plus important). Le Br a également une mobilité plus faible par rapport aux deux isotopes du Cl. Le Br est potentiellement plus susceptible d'être piégé en raison des effets d'exclusion des anions et de l'augmentation de la tortuosité.

Nos données confirment également que pour les isotopes du Cl, l'effet de fractionnement est plus fort pour les argiles plus chargées négativement, comme cela est observé pour les sédiments naturels. Les valeurs de $\delta^{37}Cl$ des eaux interstitielles des argiles riches en smectite sont systématiquement plus faibles (-8,5‰ & -6,8‰ dans Agrinier et al. 2019 ; Underwood et al. (2013) Saito et al. (2010) ; Henry et al. (2012)), que les valeurs de $\delta^{37}Cl$ pour les eaux interstitielles de sédiments riches en argile à dominante non gonflante, comme la kaolinite, la chlorite et l'illite (-1,9‰ & -2,1‰ dans Bonifacie et al. (2007) ; Bonifacie et al. (2005) ; Elderfield et al. (1999) ; Underwood et Hoke (2000)). Pour les isotopes du Br, ce n’est pas le cas.

Cependant, nos calculs de bilan de masse montrent que le ^{35}Cl s'enrichit légèrement dans la couche d'argile elle-même. Par conséquent, nous pouvons comprendre que le rafraîchissement observé n'est pas seulement le résultat du retardement des solutés dissous (filtration) mais aussi le résultat du piégeage des solutés par la couche d'argile elle-même. Ce piégeage des anions dans la couche d'argile est une combinaison d'interactions physiques et chimiques entre les surfaces minérales de l'argile et le fluide interstitiel.

En conclusion, nous suggérons que :

1. L'évolution des teneurs en anions et des rapports isotopiques du Cl et du Br pendant la compaction des argiles est fonction des interactions chimiques et physiques entre l'eau et le matériau. La chimie de surface de l'argile, combinée à la diminution de la porosité, entraîne un rééquilibrage des doubles couches diffuses comprimées et superposées qui, dans l'ensemble, conduisent à une évolution des concentrations en anions et des rapports isotopiques en accord avec les mécanismes de transport par diffusion.

2. L'argile avec une charge de surface plus négative est plus efficace dans l'ultrafiltration/le rafraîchissement de l'eau expulsée pendant la compaction, indépendamment de son degré de compaction.

3. Un rafraîchissement plus efficace est également obtenu lorsque la température est augmentée de manière incrémentale en même temps que la pression.

4. La réduction de la porosité et la barrière de charge résultant du chevauchement des DDL entraîne le piégeage des anions dans la couche d'argile. L'effet de rétention est légèrement plus prononcé pour le Br que pour le Cl.

5. Des chemins de transport plus longs au sein de la porosité des argiles n'ont pas eu d'effet significatif sur la concentration des anions dans l'eau expulsée mais ont eu un effet significatif sur la composition isotopique.

6. La gamme de fractionnement isotopique observée pour le Br est plus large que celle observée pour le Cl.

7. La barrière de charge résultant de la compaction des argiles chargées négativement a provoqué l'expulsion préférentielle de l'isotope le plus lourd pour le Cl et de l'isotope le plus léger pour le Br. Ce phénomène est encore mal expliqué.

8. Le fractionnement des isotopes du Cl est plus important lors des premières étapes de la compaction (pressions et températures plus basses). Le fractionnement des isotopes du Br devient plus prononcé lors des étapes ultérieures de la compaction (pressions et températures plus élevées).

ABSTRACT

With progressive compaction of the sediments, mineral and organic matter transformation are known to produce water that is less saline than the original pore water, which would have been similar in composition to ocean water. This freshening has been linked to over pressure generation as a consequence of the material transformation. The aim of our experimental investigation/work was to simulate the diagenetic processes of fluid and heat flow, and mechanical compaction that are involved in the freshening of formation water from a saturated clay sample. Our objective was to use the general water chemistry, as well as Cloride and Bromide isotopic tracers, to track the evolution of freshwater production with time.

The large-scale oedometric compression cell that was developed for the purpose of this study is novel and rare due to the high fluid pressures, mechanical stresses and temperatures that could be applied on the clay samples during the experiments, and the multi-disciplinary collaboration between well-reputed laboratories in order to contribute to a functional understanding of Cl and Br behaviour in geological processes. There are no similar multi-disciplinary large-scale experiments in the literature.

We did three compaction experiments that lasted up to around 200 days each during which we continuously recorded axial stress, pore fluid pressure, axial deformation, and the volumes of fluids in injection and collector pumps. The experiments constituted first saturating the clay with ocean water in the large oedomertic cell, and then compacting it in either 5 or 10 steps of increasing vertical stress and temperature up to 150 MPa and 150°C, while maintaining the pore fluid pressure as close as possible to 45 MPa. Continuously following the axial deformation, and monitoring the composition of the input and expelled water allowed for a water and chemical mass balance of the system. We could therefore calculate what the remaining pore water composition should be, with each consecutive compaction step. Furthermore, the state of the art modelling software, SURP, developed by the BRGM, helped us to understand what proportion of that expelled water, was the result of clay mineral dehydration. True mineral transformation was not observed. Neither through the modelling exercise, nor through XRD mineral characterization.

We found that the chemistry and isotope behavior is considerably different between swelling clay (MX80 containing 75 wt% smectite) and non-swelling clay (Sainte Suzanne marl containing 61 wt% illite & 7 wt% kaolinite). In our study we observed a general decrease of the cation and anion concentrations in the expelled water for swelling clay while its concentration slightly increased in the remaining pore fluid. This was not the case for non-swelling clay. Then, more freshening of the expelled water occurred during the compaction MX80 experiment at higher temperature.

We also observed that as Br is much more effectively filtered by the clays than chlorine due to its much lower natural occurrence, this translates to a larger range of isotopic fractionation for Br (δ^{81}Br value of the expelled water from 0.9 ‰ up to 1.5‰) than for Cl (δ^{37}Cl value of the expelled water from -0.1‰ down to -0.5‰), in all three compaction experiments.

It is supposed that significant retention of Cl and Br in the pore water of the compacted MX80 is indicative of ultrafiltration and that the surface chemistry of the clay in combination with decreasing porosity result in re-equilibration of compressed and overlapping diffuse double layers which in part, drive the anion and isotope evolution. δ^{37}Cl and δ^{81}Br are promising tracers to better interpret the origin and evolution of formation waters in sedimentary basins.

Disclaimer – a number of analysis following the completion of the last experimental work, have not been completed due to the onset of the global Covid 19 pandemic and the consequent confinement regulations that was imposed in France.

Introduction

GENERAL OVERVIEW

SCIENTIFIC CONTEXT

In foothills, the production of fresh water by compaction of clay formations (mechanical effect), diagenesis of swelling clays, or maturation of organic matter (thermal effect) can play a major role in the pressure regime, rock hydro fracking, and hydrocarbon expulsion. The objective of this work is to investigate tracers (chemical and isotopic) that help to discriminate the different processes of freshwater production and to quantify the volumes produced.

The first part of the thesis work consists of a bibliographic study of the phenomena responsible for the production of fresh water foothill deposits, the transition zone between low relief plains, and the adjacent mountain ranges. In foothills, sediments accumulate in extended alluvial fans which are often overlain or capped by clays and/or marls (Cazanacli et al., 2002). This can be a potential for hydrocarbons trap in the sands underneath (Ab'Saber, 1961). With progressive compaction of the sediments, mineral and organic matter transformation are known to produce water that is less saline (fresher) than the original pore water which would have been similar in composition to ocean water, often referred to as ultrafiltration. This study focuses specifically on the contribution to freshwater production from hydrated clay mineral transformation, whether driven by mechanical, thermal or chemical mechanisms, or the transformation of organic matter (only considered in the bibliography). Particular attention is paid to the possible chemical and isotopic fractionations that result from this production of fresh water, based also on a case study of known and unsalted reservoir waters (Eggenkamp, 2014). While the major cations and anions dissolved in the pore water of compacting clays are studied for chemical fractionation, the focus for isotopic fractionation is on the Cl and Br anions specifically, as chemical isotopic tracers. Cl and Br are highly concentrated in formation waters (Hanor, 1987) and the large variations observed remain not well-understood (Neuzil and Person, 2017).

The second and major part of the thesis work is experimental. The three experiments conducted aim to determine the composition and quantities (volumes) of water released by a saturated clay subjected to a mechanical compression. The main mechanism considered through these compaction experiments is the mineralogical transformation of smectite-illite type reflecting a dehydration of the clays (Tremosa et al., 2020) as a source of dilution/freshening. These experiments involved a specially designed experimental device capable of measuring very small volumes of aqueous fluids exchanged under very high compaction, temperature, and fluid pressure constraints over a very long period (several months) in view of very low material permeability and very slow reaction kinetics.

The quantification of the mechanisms involved, in particular, the study of chemical but also isotopic tracers (Cl and Br).

The third and final part of the thesis work consists of carrying out geochemical equilibrium calculations in order to quantify the water content retained with clay minerals. The kinetic parameters of water genesis that have been determined by the experiment were applied to state-of-the-art modeling software in order to specifically quantify the proportion of fresh water produced from mineral transformation compared to the volume expelled as a result from mechanical compaction.

OBJECTIVES OF THE STUDY

The overhead focus of this study is to develop a functional understanding of freshwater production as a function of compaction of clay-rich formations, specifically considering the evolution of Cl and Br anions and their respective stable isotopes.

The research project is underwritten by three main aims, each with a number of related objectives. The aims and objectives are as follows:

1. *Develop a functional understanding of the various chemo-mineralogical mechanisms that contribute to the production of fresh formation waters.*

1.1 Smectite mineral dehydration from a fully hydrated state (four water interlayers) to two water interlayers when clay mineral transformation becomes a possible consequent contributor. The final question arising here is then how much of the total available interlayer and structural water can be retrieved.

1.2 The role of smectites clay in process of ultrafiltration with special regard to chloride and bromide stable isotopes, will be investigated as a consequence of vertical compaction.

1.3 The contribution of organic matter to the production of fresh water will just be considered from literature and not experimentally.

2. *Employ water chemistry and specific isotopic tracers to track the evolution with time of freshwater production.*

2.1 Change in major dissolved cation composition – Na, Ca, K, Mg & Si

2.2 Change in major dissolved anion composition – Br, Cl

2.3 Change in stable isotopes ^{37}Cl, ^{81}Br

3. *Be able to ascribe a volume and quality of water produced to a specific load/and or temperature increments/gradient.*

Careful monitoring of fluid volumes produced to balance input, expected production, and actual production accounting for periodic extractions for analysis (weight produced).

THESIS ORGANIZATION

This thesis manuscript is organized into 6 chapters. Chapter 1- presents the state of the art in the current understanding of 1) the mechanisms responsible for freshening of water during sediment compaction; 2) Cl and Br fractionation in a formation water setting, and 3) explores the application of well-established theoretical bases relevant to our study. Chapter 2- focuses on the experimental design and protocol, highlighting the novelty of the study and motivating the selection of materials and experimental conditions for three compaction experiments conducted during this study. Chapter 3- describes the methods and techniques used to reach the research objectives. The methods involve mainly; geochemistry of the fluids, characterization of the solid materials, and the specific modeling techniques employed. In Chapter 4- the results of three experimental studies are compared. and the modeling of a part the experimental data is presented. Chapter 5- is a combined discussion synthesizing a general understanding of possible application of the theoretical mechanisms that fit the results for the three experiments. The key conclusions extracted from our complete work is presented in the final chapter.

State of the Art

STATE OF THE ART

The purpose of this chapter is to present a bibliographic overview of research on the filtration effects responsible for the freshening of water in foothill zones. This bibliographic section focusses specifically on the contribution to freshwater production from hydrated clay mineral transformation, whether driven by mechanical, thermal or chemical mechanisms, or the transformation of organic matter; how clays behave during compaction and how pore waters behave during compaction. Special focus is given to the Cl and Br in the compaction environment. Particular attention is paid to the possible chemical and isotopic fractionations that result from this production of fresh water, based on a key case study of known and unsalted reservoir waters (Eggekamp, 2014).

1.1- FORMATION WATERS: PHENOMENA RESPONSIBLE FOR THE PRODUCTION OF FRESH WATER

Formation waters are of importance in many geological processes, including metal mineralization, and hydrocarbon migration. Understanding the geochemical evolution in formation water can help to recognize important rock-fluid interactions and so, interpret the fluid flow of a basin. Migration of free-flowing formation water is an important factor in mass movement/transport and diagenesis due to the inevitable chemical reactions with rocks along its migration path (Bethke and Marshak, 1990; Bjorlykke, 1999). Despite the significance of subsurface fluid chemistry, the evolution process of formation water, however, is not always clear, especially in abnormally pressured environments. In particular, several hydrocarbon-bearing basins have been found to be abnormally over pressured systems. This includes the North Sea basin (Rudkiewicz et al., 1999; Yardley and Nwozor, 2017) and the Gulf of Mexico basin (Zhao and Li, 2017).

Among the processes explaining fluid overpressure in sedimentary basins, clay compaction is one of the most significant. The microstructure of the clay rocks creates a very tortuous and electrically charged pore network where long pathways and ionic repulsions obstruct the movement of water and dissolved ions in the clay rocks (Melkior et al., 2009). Recently, two types of water produced during burial of clay formations were clearly described by Tremosa et al. (2020). The first is produced by mechanical compaction. The second is produced by the mineralogical transformation of the clays due to the increasing temperature (chemical compaction). These two types of water are diluting the former formation waters. Before we elaborate, let us first clearly define the term formation water. It simply describes water that saturates sedimentary rocks (among them deep oil or gas reservoir rocks).

It refers to water that is free to move under appropriate hydrodynamic conditions, as opposed to water that is electrostatically bound on clay surfaces, or water associated with the hydration of interlayer cations (Bagheri et al., 2014).

Studying formation waters is beneficial to understand the source of the waters, which could potentially link to the origin of the hydrocarbon resource (Garven, 1995; Ziegler et al., 2001; Kharaka and Hanor, 2003). Formation waters can range from very saline (Solley et al., 1983; Coleman, 1992; Kharaka and Hanor, 2003; Bagheri et al., 2014) to remarkably fresh (low salinity or dilute). Mechanisms responsible for the origin of saline groundwater that have been proposed include, 1) membrane- /ultrafiltration (the relative retardation of solutes with respect to flowing solution when passing through fine-grained material), 2) halite and potash salt dissolution, 3) concentration due to evaporation of seawater, and evaporation of non-marine fluids or 4) water-rock interactions in sediments. Dilution or freshening of formation waters, contrariwise, are attributed to; 1) ultrafiltration; 2) condensate water (water produced from the condensation of water vapor present in hydrocarbon gas reservoirs when the pressure is reduced during production); 3) mixing with external fluids (meteoric water or diluted continental waters (rivers, lakes)) or 4) water-rock interactions (including clay mineral transformation). Salinity in groundwater will likely result from a combination of the abovementioned processes and will depend on the evolution of the local hydro-chemical environments and the degree to which water derived from different mechanisms has been mixed.

Another interest for studying formation water evolution relates to understanding the build-up of overpressures. Clay dehydration has been discussed as a possible source for abnormal pressures in sedimentary basins (Bruce, 1984; Shaw and Primmer, 1989) due to the observation "that the onset of the overpressure coincided with the smectite-to-illite transformation". However, it is necessary to distinctly clarify between two relevant mechanisms to 'smectite-to-illite transformation': *illitisation of smectite* VS *dehydration of smectite*. The former refers to mineralogical transformation due to the loss of structural water (discussed in section 1.1.1- . The latter refers to the loss of water layers adsorbed to the surface of the negatively charged smectite clay. However, clay dehydration and transformation have often been ruled out as a mechanism contributing to overpressure because of the small volume increase from the water produced. It was estimated that below a depth of 1 km, which is the depth at which overpressures are observed to develop, only a 1.4% volume increase occurs from the water produced from smectite illitisation (Swarbrick and Osborne, 1998). Recently Tremosa et al., (2020) further distinguished between the two mechanisms. They confirmed that water release by smectite illitisation has much less influence on the pressure profile than smectite dehydration.

Similarly, it's been calculated that smectite dehydration can contribute 20 – 30 % to overpressuring (Audet, 1995; Wangen, 2001; Tanikawa et al., 2008). In the case of Tanikawa et al. (2008), it was suggested that clay dehydration was more significant than hydrocarbon generation in generating overpressures. The water production during hydrocarbon maturation is discussed in section 1.1.3- .

1.1.1- Water-rock interactions

A short summary of the main chemical and physical characteristics of clay minerals is necessary to follow the mechanisms of water and solute interaction with the clays. Clays are fine-grained (<2µm) aluminosilicate minerals that exhibit particular plasticity and consist of alternating sheets of tetrahedra and octahedra (Guggenheim and Martin, 1995). Clay minerals are classified according to their structure, i.e. silicate sheet composition and stacking, as well as their interlayer spaces and interlayer constituents (Wenk and Bulakh, 2004). There are two basic clay mineral sheets structures. In the tetrahedral sheet, Si^{4+} (or Al^{3+}) coordinates with four O^{2-} ions. Three of these occur in a basal position and the other in an apical position. Each of the basal O^{2-} ions bind to another to form a lattice with hexagonal cavities with all apical O^{2-} toward the same side. In the octahedral sheet, the central cation, ideally Mg^{2+} or Al^{3+}, coordinates with six O^{2-} (or OH^{-}) ions, four on the same plane and the remaining two as opposite apexes. Each of the six sides can be shared with another octahedron to laterally extend the sheet so that two planes of closest-packed oxygen (or hydroxyls) make up the top and bottom of the octahedral sheet. Such a structural composition allows for each anion to be bonded to three cations. When Al^{3+} fills two-thirds of the available cation positions, the unit cell is said to be dioctahedral (or gibbsite-like) or trioctahedral (or brucite-like) if Mg^{2+} fills three cation positions. These individual sheets combine into layers with a ratio of a tetrahedral sheet(s) to an octahedral sheet of 1:1 (two-layer structure) or 2:1 (three-layer structure). This occurs when the apical oxygen of the tetrahedral sheet is shared with the surface oxygen of the octahedral sheet. Necessary deformations occur due to differences in the size of the basic tetrahedral and octahedral sheets as well as differences induced by cation substitution resulting in ditrigonal symmetry. Cation substitution is a process wherein Si^{4+} in tetrahedrons are often exchanged by Al^{3+} while in octahedrons Mg^{2+} will often be substituted by Al^{3+} in dioctahedral sheets or vacant sites creating a net negative charge for the layer. The layer charge can be neutralized either by ions, as in micas (K^{+}, Na^{+} or Ca^{2+}), or sheets, as for chlorite and vermiculite (Fe^{2+}, Mg^{2+}, Al^{3+} or Fe^{3+}; hydroxides (OH^{-})), in the interlayer space. Larger cations such as Na^{+}, K^{+} and Ca^{2+} are often also adsorbed on the external surface to satisfy the charges.

The most important clay naturally occurring clay mineral groups are:

- Kaolinites - simple alternation of tetrahedral- and octahedral sheets (1:1 stacks). Cation substitution in the basic sheets are not very common.
- Illites and micas - a 2:1 structure of two tetrahedral sheets on either side of an octahedral sheet (TOT). A negative unbalanced charge due to possible substitution of Al in the in the tetrahedral layer is generally balanced by the adsorption of interlayer cations, especially K^+.
- Smectites and vermiculites – a permanent structural negative charge results from cation substitution in both the tetrahedral and octahedral layers (2:1 structure). These clays therefore have a large capacity to adsorb cations in various states of hydration.
- Chlorites – have a 2:1:1 structure as the negative structural charge is balanced by an interlayer hydroxide sheet. Many possible cation substitutions results in highly variable chemical composition within this group.

1.1.1.1- Smectite Illitisation

Clay minerals are equilibrated to their surrounding environment and the interaction between rock/mineral and water. Their formation is governed by the thermodynamics of the system of concern. The minerals that form will possess the lowest possible amount of free energy at that time in those particular conditions, will be more highly ordered, and be of larger particle size .

During the burial and compaction of clay-rich sediments, illitisation is a pronounced diagenetic process, resulting in alteration of smectite and kaolinite to illite and silica cement (micro quartz) plus water (Boles and Franks, 1979; Thyberg and Jahren, 2011). Illite content progressively increases with increasing temperature and increasing concentration of K^+ in the pore water. Increasing the water/rock ratio and geological time also promotes illitisation (Altander and Ylagan, 1997; Whitney, 1990). In sedimentary prograde alteration systems, the illite → smectite series and their intermediary mixed layers, are the most abundant clays (around 45%), followed by kaolinite (15%), and chlorite (6%) (Srodon et al., 2001; Srodon, 2010). Basic illitisation of smectite, evolves to muscovite (K) or paragonite (Na), depending on the Na to K ratio. For the Ca^{2+} - Mg^{2+} - smectite clay minerals, the fundamental transformation is chloritization of smectite, usually through corrensite. The reactions steps that occur are consistent with the Ostwald step rule (Merriman, 2005), which states that each progressive step (polymorph) that forms will be the one closest in energy to the previous.

(1)

$$smectite + K^+ = illite + silica + H_2O$$

(2)

$$kaolinite + K^+ = illite + silica + H_2O$$

As seen in the equations, the illitisation process involves the release of structural water, whereas the cementation potentially reduces the permeability and prevents excess pore-water expulsion.

There are two possible mechanisms for smectite-to-illite transformation:

(i) dissolution–recrystallization without mixed layering (Inoue and Kitagawa, 1994; Clauer et al., 1997; Srodon, 1999; Srodon et al., 2000) and,

(ii) intermediate I–Sm mixed-layering (Eberl and Srodon, 1988; Inoue et al., 1988; Christidis, 1995; Nieto et al., 1996).

The transformation process (mechanism (ii)) entails the formation of intermediate I-Sm phases which involves solid-state layer-by-layer transformation, including random interstratification, transition to ordered mixed-layer minerals, and development of long-range order (Bethke and Altaner, 1986). The sequence for transformation through I–Sm mixed-layer phases can be described as:

$$\text{Smectite} \rightarrow \text{I-Sm (R=0)} \rightarrow \text{I-Sm (R=1)} \rightarrow \text{I-Sm (R=3)} \rightarrow 1M_d \text{ illite} \rightarrow 2M_1 \text{ muscovite}$$

Where R is the Reichweite index which describes the layer stacking sequence. R¼0 is a random, I–Sm with 0–60% illite layers; R¼1 is an ordered I–Sm with 65–85% illite layers; and R¼3 is an ordered I–Sm with 85–100% illite layers. In the early stage of burial diagenesis, discrete smectite and randomly interstratified I-Sm coexist. Illite content will progressively increase. When the illite content exceeds ~60%, short-range ordered (R1) interstratified I-Sm can be observed (Inoue et al., 1987). Intermediate I-Sm phases and I-Sm-Chlorite phases may coexist (Lanson et al., 2009). For the most illite-rich I-Sm (> 85% illite), long-range ordered interstratified I-Sm (R≥3) occurs (Inoue et al., 1987). The transformed minerals replace pre-existing minerals or fill pore space.

Clay mineral diagenesis research leads to the observation that oil and gas reservoirs lie within the temperature (depth) window of 60–120°C depth where illitization of smectite occurred (Nadeau, 2011). This became known as the ‘Golden Zone’. As a result, the interest in effect of permeability, porosity, overpressure, and fluid migration evolution during diagenetic transformation of clay minerals on the entrapment and recovery of petroleum, increased.

1.1.2- Mixing or dilution

1.1.2.1- Smectite dehydration

All clays attract water to adsorb it onto its surface or absorb it into its structure. In the first 3–5 km of burial compaction, free or weakly bound water is eliminated and the porosity decreases from 80% to about 20% (Galan and Ferrell, 2013). This mechanical compaction from overburden loading increases the bulk density of sediment as the pore volume decreases. The rate of decline in pore volume (porosity reduction) is relatively fast at the beginning of mechanical compaction before slowing down when a more rigid frame is formed during deeper burial (e.g., Mondol et al., 2007). This behavior is particularly pronounced in fine-grained clay-rich sediments which initially have very high porosity (80 – 90%) at the surface and lose most of the porosity at relatively shallow depths (Poelchau et al., 1997; Mondol et al., 2007). Decreasing the pore volume is directly related to the expulsion of pore fluid. Expelling water from clays requires a certain force to break the mineral surface-water bond. Closer to the surface, the properties of water molecules may vary significantly from that of free water (Sacchi et al., 2001). Van Olphen (1965) showed that the 11th water layer from a montmorillionite clay surface requires ~5 MPa to be removed, whereas the 2nd water layer requires ~250 MPa and the closest water layer requires ~500 MPa to break the bond between clay mineral surface and a water molecule. Retention of water may be related to the salinity of the pore- and interlayer water due to difficulty stripping water molecules from cations. Water molecules in saline solutions exhibit reduced mobility. From a thermodynamic point of view, brines display a water activity (a) that is smaller than 1. Thermodynamic activity refers to the "effective concentration" of a species in a mixed solution. The activity of a species *i* characterizes its chemical potential or chemical reactivity in relationship with the ionic activity coefficient of the solution (γ) in:

(3)

$$a_i = c_i \gamma$$

Where c_i is the molarity or molality of the species *i*. Increasing salinity increases the ionic strength of the solution leading to a decrease of the activity coefficient thus to the activity of ions in solution. So, to reach equilibrium, you will need a more concentrated solution to precipitate for example. Or the solubility will be greater for a mineral in a saline solution. In addition, salinity may also cause some fractionation affecting the different cations during solute expulsion (Sofer and Gat, 1972, 1975; Yechieli et al., 1993). The mobility of solutes is more related to their hydration radii than to the dimension of the ion itself. For example, hydraulic drag, the shear stress caused by a fluid moving against a rigid surface boundary, is larger on divalent cations than on monovalent cations (Kharaka and Berry, 1973).

Fine-grained, clay-rich sediments can maintain high amounts of bound water due to their large specific surface area and high cation exchange capacity (Henry, 1997; Conin et al., 2011). On the other hand, these sediments have relatively low permeabilities which make it even more difficult to expel the pore water out of the pore space during compaction (Mondol et al., 2008). Thus, mudstones and shales are prone to develop overpressure during mechanical compaction. This occurs when the rate of pore fluid expulsion is less than what would result from drained stress-induced compaction, thus the pore pressure will exceed the hydrostatic pressure. Overpressure caused by disequilibrium compaction begins at the depth where sediment permeability becomes so low that mechanical compaction and, therefore, porosity reduction is retarded. This is known as the fluid retention depth.

1.1.3- Hydrocarbon maturation

Hydrocarbons form from organic matter buried in an anoxic marine environment. Organic matter (OM) in sediments underlying the oceans is derived from different sources including marine phytoplankton, phytobentos in shallow water with sufficient light, bacteria, and land-derived material (Emerson and Hedges, 1988).

Within organic-rich mudstones and shales, hydrocarbon generation and/or cracking to lighter hydrocarbons (i.e., oil to gas cracking) can increase pore pressure due to the low expulsion rate of hydrocarbons particularly in mud-dominated rocks (Mann, 1994), and due to the increase in volume and release of water during the maturation transformation.

The organic matter contained in clay rich sediments subject to burial and lithification, undergoes many changes. These changes can be grouped into three stages: diagenesis, catagenesis, and metagenesis (Tissot and Welte, 1984). The main drivers are, most importantly, increasing temperature, -time, and -pressure. An average geothermal gradient is about 3°C per 100 m of depth. Diagenesis occurs in the shallow subsurface at near-normal temperatures and pressures, up to 2 km and 60° C. Methane, carbon dioxide, and water are driven off from the organic matter to leave a complex hydrocarbon termed kerogen mainly through microbial degradation (Arndt et al., 2013). With increasing burial, the source bed is subjected to rising temperature due to the prevailing geothermal gradient and rising pressure due to overburden loading. Diagenesis merges into catagenesis. This is the principal phase of petroleum generation and is mainly driven by thermal degradation of organic matter. Initially, oil is given off once temperatures are above about 60 °C. The oil generation window is 60–120 °C and 2-4 km. Above this temperature, oil generation declines and is replaced by methane gas generation which ceases at about 200 °C. The gas window is at 4-6 km depth. This temperature differentiates the transition between catagenesis and metamorphism.

The maturation process during burial compaction is a very complex biophysiochemical process impacted by many different factors and passes through many intermediary steps to effectively lower hydrogen to carbon and oxygen to carbon ratios due to the generation and liberation of hydrocarbons, carbon dioxide, and water. During this maturation process, the molecules progressively become more ordered which results in a volume increase of ~15% during catagenesis and up to ~35% in metagenesis (Ungerer et al., 1983; Duppenbecker et al., 1991). Organic matter contains an average of 60 weight % water content which is driven off mainly during diagenesis and catagenesis (Tissot and Welte, 1984). For this reason, organic matter maturation is related to the generation of overpressure (Neuzil 1995; Swarbrick and Osborne, 1998; Zhao et al., 2019). Overpressure, in turn, can retard the continuation of organic matter maturation because the activation energies required increases, and progressive molecular ordering is hindered (Zou and Peng, 2001).
Organic matter transformation has also been observed to enhance smectite illitisation due to the potential substitution of K^+ with NH^{4+} in the illitisation process (Williams and Ferrell, 1991).

1.1.4- Ultrafiltration

(Alternatively referred to as: Ion filtration/ Hyperfiltration/ Solute-sieving)

Ultrafiltration is a naturally occurring geologic membrane process that occurs in the subsurface (Bredehoef, et al., 1963; Bredehoef et al., 1983; Fritz 1986). Membrane processes refer to the interaction of two solutions of different concentrations that are separated by a semipermeable membrane. The filtration effects of geological materials, and clays in particular, have been studied since the 1930's (Russell, 1933). Fine-grained clay-rich lithologies characterized by layered fabric have been shown to be particularly effective geological membranes (McKelvey and Milne, 1962; Benzel and Graf, 1984). The efficiency of geological material to function as a membrane almost doubles for oriented fabrics, such as clays, versus non-oriented fabrics (Benzel and Graf, 1984).

When the flux of water and solute across the membrane is a function of the concentration gradients, it is called osmotic pressure which is defined as the pressure necessary to stop the flow of solute from high to low concentration across the membrane (Martin 1964; Letey, et al., 1969; Neuzil and Provost 2009). During ultrafiltration, an external force in excess of the osmotic pressure is applied and the result is the restriction or retardation of solute migration through a membrane relative to the migration of the solvent (Hart 2013). Naturally, this should result in more saline solution on the inflow (high-pressure) side of the membrane lithology, and less saline solution on the outflow side of the membrane lithology (Fritz and Whitworth, 1994).

This pattern is observed in nature. For example, in water slowly flowing upward through confining clay layers that do restrict the flow of ions (which are in the recharge water or the formation water), the concentration of ions in the lower layers would increase (De Sitter; 1947; Bredehoeft et al., 1963; Agrinier, 2019 and resources therein). This phenomenon of ultrafiltration is therefore easily and often invoked to explain the freshening of subsurface water, as well as abnormally high salinities (Berry and Hanshaw, 1960; Graf et al., 1966; Coplen and Hanshaw, 1973; Kharaka and Berry, 1973; Haydon and Graf, 1986; Phillips and Bentley, 1987; Demir, 1988; Agrinier, 2019 and resources therein).

The 'puzzling large ^{37}Cl-depletion in pore fluids in sedimentary basins, vs. seawater and evaporates' have also been attributed to ultrafiltration processes (Agrinier et al., 2018; Kaufmann et al., 1984 ; Phillips and Bentley, 1987). Recently Neuzil and Person (2017), on the basis of numerical modeling of transport of ions through clay membranes, suggested that modest salinity gradients are created and therefore ion filtration could not generate high salinity brines. Ultrafiltration remains not well explained.

The extent of ultrafiltration is controlled by the efficiency of the clay baring membrane. Membrane efficiency (σ) can be defined as the ability of a membrane to selectively let one substance pass relative to another (Hart 2013). A membrane filtration efficiency value of 0, indicates no membrane effects. A membrane filtration efficiency value of 1 is the perfect membrane that completely prevents the passing of a solute relative to a solvent. McKelvey and Milne (1962), from their forced flow experimental study, first linked the efficiency of filtration to the ion exchange capacity of the clay. However, membrane efficiency decreases with increasing solution salinity (Neuzil and Person, 2017). Kemper (1961), and Kemper and Maasland (1964) first accounted for the influence of diffusive flow driven by the concentration gradient (according to Fick's law (see section 1.4-), on membrane efficiency. Furthermore, Van Everdingen (1968) found that membrane efficiency is also highly dependent on the size of the hydrated ionic radius. Berry in 1969 illustrated that an increase in temperature would decrease membrane filtration efficiency because the increased temperature might decrease dissociation, reduces the ion-exchange capacity of the membrane, and possibly reverses the ion selectivity sequence that was proposed by Eisenman (1962). Along with major elemental concentration variations, Colpen and Hanshaw (1973) and Campbell (1985) contributed, early on, that isotopes of hydrogen, oxygen, and chlorine also experienced fractionation when flowed through clays. Anion exclusion effect (or Donnan exclusion) due to the interaction of negatively charged anions and negatively charged clay particle surfaces was proposed by Colpen and Hanshaw (1973) as a prominent active mechanism of ultrafiltration.

However, isotope fractionation, as well as solute composition variation, was also observed to result from diffusion-dominated systems, therefore without the membrane effect (Phillips & Bentley, 1987; Campbell, 1985; Mazurek et al., 2011). The fractionation of Cl isotopes by clay membranes has been linked by Campbell (1985) in her pioneering work to 1) cation exchange capacity of the clay due to the possible anion exclusion when ionic double layers associated with the negative surface charge of the clay particles overlap, 2) decreasing pore size as a result of increasing pressure which is argued to restrict the flow of certain components based on their ionic radii and, 3) fluid concentrations with the membrane being more effective with decreasing salinity. She chooses to label the mechanism most likely to be responsible for the fractionation produced by both her fluid flow and diffusion experiments – "back diffusion" corresponding to the model described by Phillips and Bentley in 1984. This model basically states that both the Cl isotopes are repulsed by the negative charge of the clay but due to the greater inertia of the slightly heavier ^{37}Cl, the ^{35}Cl can more easily be repulsed (and removed). Therefore, the effluent becomes enriched in ^{37}Cl.

Some studies have found fractionation of various isotopes to correspond to ion filtration as shown by Kaufman et al. (1984), while others have shown enrichment and depletion in increasing depth (Campbell, 1985).

Diminishing/low porosity in itself retard dissolved ions according to their radius and charge, in effect acting as a filter (Sacchi et al., 2001). Horseman et al. (1996) states that if pores are less than 10nm in diameter, studies have shown that water and solutes will only flow if a threshold pressure gradient is exceeded.

1.2- CL & BR IN FORMATION WATERS

Formation waters contain some of the highest recorded naturally occurring concentrations of the highly soluble Br anion (Hanor, 1987). Along with Cl, the hydrophilic and unreactive nature of these monovalent halide anions causes them to dissolve easily and remain in solution with very little incorporation into minerals (Davis et al., 1998; Alcalá and Custodio, 2008). Therefore, by studying Cl and Br anions as tracer elements, one can follow the fluid transport without much interference from water-rock interactions (except for evaporites). Br/Cl ratios can be significantly affected by interaction with organic matter (Kendrick et al., 2011) but this is not within the scope of the current study.

Chlorine and bromine are the two most abundant halogens in sedimentary formation waters with concentrations ranging from less than 100 $mg.L^{-1}$ to more than 250 000 $mg.L^{-1}$ for Cl and a much lower concentration range for Br of less than 1 $mg.L^{-1}$ to over 6000 $mg.L^{-1}$ (Worden, 1996). Most formation water has vastly different compositions form the connate water or ocean water at the time of burial of the original sediments. As can be seen in the contrast to the average concentrations for these specific halogens in ocean water given by Drever (1997) as 19 350 $mg.L^{-1}$ and 67.3 $mg.L^{-1}$ for Cl and Br respectively, as well as the much larger Cl to Na ratio found in formation waters. With depth in the crust, decreasing water/rock ratio generally results in increased fluid salinity. Fluid convection, hydrodynamic dispersion, and diagenetic reactions are motivated by Hanor (1994) as the essential influences that drive subsurface water compositions. In deeper settings, the contribution of the dehydration mud-rich sediments is considered a major contributor to subsurface fluid composition as well. Water – salt interaction and the input from organic matter sources are major influencers on the Cl and Br content of subsurface waters (Kendric et al., 2011; Worden, 1996). To the contrary, the anion total charge is considered as a master variable, along with pressure and temperature, to drive diagenetic reactions. While the major solute composition is buffered by rock interaction, the unbuffered components (such as Cl and Br as well as isotopic compositions) are therefore considered very useful to derive information on the pathways of reaction.

1.2.1- The fractionation of clorine and bromine stable isotopes

Because dissolved Cl and Br are so un-reactive, it is also interesting to consider their stable isotopes to understand what physical processes are influencing the fluid evolution. The two stable isotopes that exist for both chlorine (^{35}Cl and ^{37}Cl) and bromine (^{79}Br and ^{81}Br) are fractionated by natural and anthropogenic processes during their cycling between reservoirs. Stable isotope ratios of Cl have been used to describe various physical processes that could have contributed to formation water composition, including salt precipitation (Eggenkamp et al., 1995), ion filtration (Phillips and

Bentley, 1987), ion-exchange (Musashi et al., 2004) and diffusion (Eggenkamp and Coleman, 2009), Beekman et al. 2011). Sedimentary basins that originated from ocean water display negative δ^{37}C1 (≤0.0‰; Eggenkamp et al., 1995; Eastoe et al., 2001). With fewer focused studies on the natural variation of isotope ratios of Br (Shouakar-Stash et al., 2007; Shouakar-Stash, 2008; Stotler et al., 2010), the behavior and application of Br stable isotope ratios are still not well understood. From previous literature, we know that the isotopic ratios of chlorine in formation waters are usually negative and can vary significantly, down to -8‰ (Agrinier et al., 2019). From the few studies that have measured the isotopic ratios of Br in formation waters, the δ^{81}Br values are mostly positive and vary up to +4‰ (Eggenkamp, 2014a). Both being halogens, isotopes of Cl and Br have originally been assumed to react similarly. As capabilities to measure Br isotopes have developed, it has become clear that the stable isotopes of these anions fractionate differently despite their similar chemical behavior. The fractionation of Cl isotopes by the well-known process of diffusion has been clearly illustrated in fine-grained low porosity clay rich materials (Kaufman et al., 1984; Phillips and Bentley, 1987; Lavastre, 2005). There seems to be a decreasing trend for δ^{37}Cl with increasing depth (Giunta et al., 2017; Agrinier et al., 2019). The fractionation of Br isotopes due to diffusion has only been studied experimentally where it's been shown to correlate with the diffusion of Cl (Eggenkamp and Coleman, 2009). In the past, it has been assumed that due to the larger ionic radius and higher atomic mass, Br should fractionate at a rate about half of that of Cl (Eggenkamp, 2014). δ^{81}Br trends with increasing depth have not been studied. Interestingly, comparing published δ^{37}Cl and δ^{81}Br values of natural formation waters, those samples with very negative Cl isotope ratios often show surprisingly positive Br isotope values. It is regularly suggested that these values might be the result of ion filtration through semi-permeable clay membranes (Coplen and Hanshaw, 1973; Kharaka and Berry, 1973; Campbell, 1985) as a consequence of clay surface charges (Tournassat and Appelo, 2011).

1.3- THE EFFECT OF ORGANIC MATTER

Natural organic matter shows a strong affinity for clays. (Theng, 1974; Maurice et al., 1998). Organic matter bound to clay particles present an increase reactive surface for interaction with dissolved solutes in the pore water solution. It may play a role in the buffering solution acidity and ion concentrations in solution. Decomposition of organic matter during burial and diagenesis has been linked to the high Br content of deep foreland basin water (Boschetti et al., 2011).

Organohalogen compounds (OHCs) are a large group of natural and synthetic chemicals, containing one or more halogens combined with carbon and other elements, widely distributed in the environment. OHCs differ widely in chemical reactivity depending on the halogen. Newer studies have shown that there are more than 3700 organohalogen compounds (Gribble, 2010), mainly containing chlorine and bromine, from simple gaseous methyl halides to much larger and sometimes very complex structures, which are naturally produced by living organisms or formed during natural abiotic processes such as volcanoic activity, forest fires and other geothermal processes (Gribble, 1999, 2010).

The particulate phase of sediments is thought to be associated entirely with organic matter, though neither the chemical nature nor origin of this association is understood. Many primary producers, especially macroalgae, are known to synthesize brominated organic compounds (Gribble, 1998). Heterotrophic organisms, especially invertebrates but including bacteria (Gribble, 1998), also produce brominated compounds. Last, bromination may occur via nonbiological reactions. Anthropogenic oxidation processes such as chlorination are well known to cause bromination of various organic moieties and natural versions of this type of reaction may occur. Inorganic compounds of bromide are highly soluble. Therefore, evaporation to partial dryness will leave a residual brine rich in bromide that will sorb on organic solids (Reeve, 2002).

Recently a study compared industrially and naturally produced 2,4-bromophenol. They found that the δ^{81}Br value for a naturally produced and industrially produced 2,4-dibromophenol sample has a statistically significant difference of about 1.4‰ higher in case of natural origin. They concluded that different pathways of formation of these compounds lead to the difference in δ^{81}Br isotope value (Carrizo et al., 2011). Horst et al. (2013), and Horst et al. (2014) attempted to determine isotope fractionation of bromomethane during its release from plant matter. They investigated bromomethane formed from pectin (fortified with KBr) and from *Salicornia fruticosa*, a halophytic plant with high salt content. They found that the bromomethane released from both pectin and *Salicornia fruticosa* showed δ^{81}Br values that were about 2‰ lower than the original KBr suggesting a fractionation of this order during the formation of bromomethane. These results may be attributed to the coexistence of both mass-dependent and mass-independent isotope fractionation of the carbon-bromine bond cleavage.

In water, this effect was only found for 4-bromophenol, while in the case of 2-bromophenol no fractionation was observed and in the case of 3-bromophenol only fractionation of bromine was observed. It was suggested that these different results might be explained in the case of 2-bromophenol with the fact that carbon bromine bond cleavage is not a rate-limiting step in the reaction, and in the case for 3-bromophenol that a mass-independent fractionation effect takes place (Eggenkamp, et al., 2014).

Organic matter decomposition can potentially impact mineral transformations. Apart from releasing water in the process of OM transformation, organic acids and carbon dioxide released during organic matter decomposition/decarboxylation can have effect on mineralogical transformations and material porosity. It can promote the dissolution of feldspars and calcite and authegenic precipitation (Davisson and Criss, 1996), thereby exentially also influencing the pore water composition.

1.4- **THEORETICAL CONSIDERATIONS**

1.4.1- The diffuse double layer (DDL)

The mostly negative surface charge inherent to clay minerals causes individual sheets to accumulate in stacks and stacks to arrange in edge-to-edge or edge-to-face structures (Figure 4). This arrangement creates interlayer - and interparticle spaces. The double layer refers to two parallel layers of charge surrounding clay particle surfaces as first described by Langmuir (1918). In the first layer (Stern layer) with a mostly negative surface charge, immobile hydrated cations are adsorbed directly onto the adjacent particle surface due to various chemical interactions (Stern, 1924). The second layer is composed of ions more loosely attracted to the surface via Coulomb forces. In the second layer, ions can move in the fluid under the influence of electric attraction, thermal motion or concentration gradients. It is therefore called the diffuse layer. Together it is called the diffuse double layer (DDL), or the electric double layer.

The concentration of counter-ions decreases with distance from the charged particle surface until there will be no distinction between the DDL and the bulk aqueous solution. Cations of higher valence are preferentially adsorbed, and for a given periodic group of elements (same valence), the smallest hydrated ionic radius would be preferentially adsorbed (Sparks 2003). For anions, the ones with the greatest polarization potential (ability of an anion to be distorted by a cation) is preferentially adsorbed. This is usually the largest anions. The adsorbed ions are also governed by the composition and the ionic strength of the solution surrounding the particle (Brady and Weil, 2008). Smaller cations are prominent in interlayer and bound water while the largest anions dominate the free water fraction in the interparticle space. Cl and Br form sufficiently strong associations with cations to occur as neutral or positively charged ion pairs or clusters in the DDL (Neuzil and Person, 2017). According to Celejewski et al. (2018), chlorine can be included in the diffuse layer (bound water) while bromine will remain in the free water fraction as Cl^- preferentially associates with cations compared to Br^- (Eggenkamp and Coleman, 2009). The thickness of the diffuse double layer is a response to both the surface charge distribution and the ionic strength of the solution and is defined by the Debye length (Sparks, 2003).

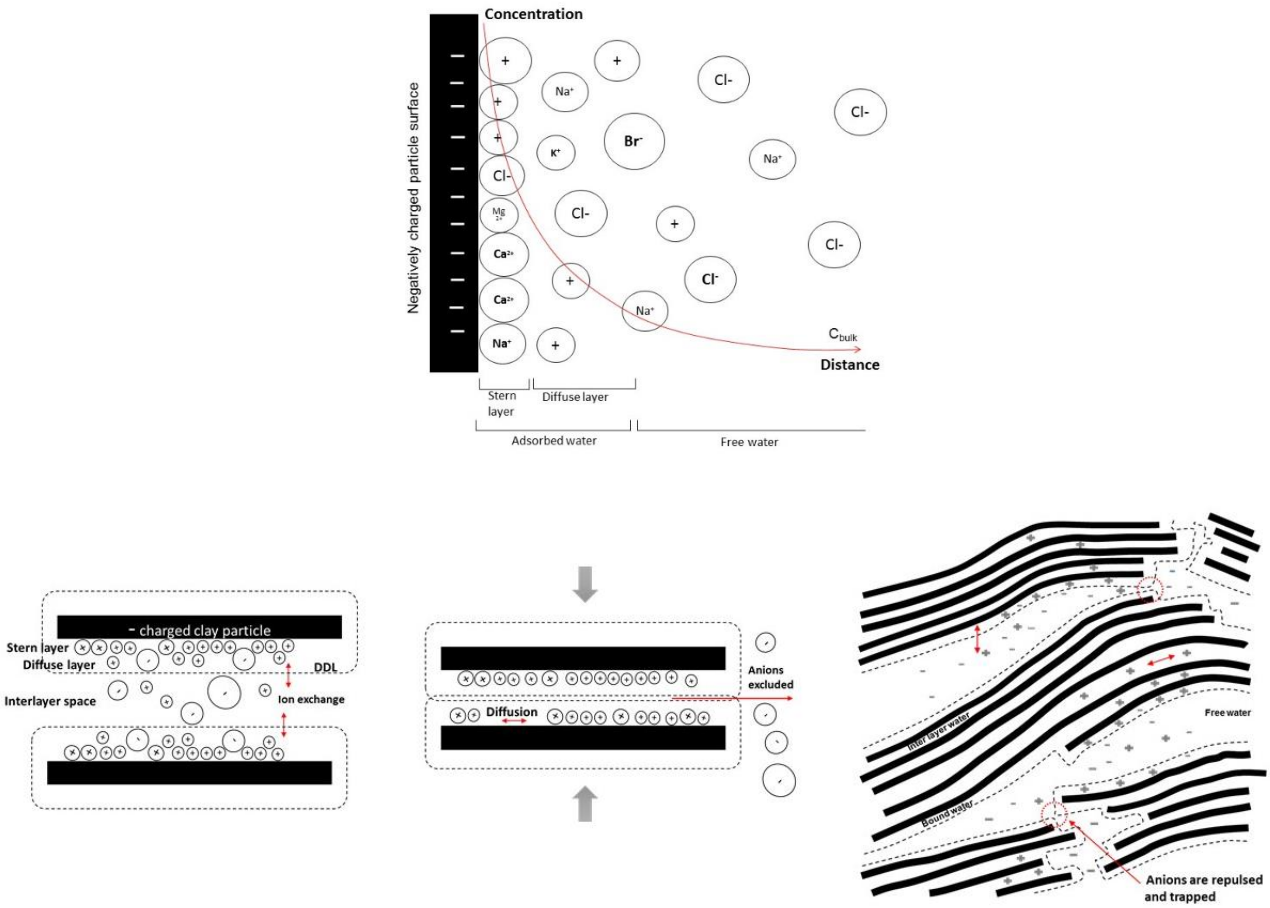


Figure 4: An illustration of the influence of the negative charge of clay particles on the physical and chemical morphology of clay rock pore spaces showing progressive expulsion and trapping and of the Cl and Br anions during compaction of negatively charged stacks. *Red arrows represent the possible motions of ions in interlayer water and between free water and bound water* (Partly modified from Apello et al. 2010).

1.4.2- Overlapping of DDL during clay compaction

During compaction of clays, the interparticle space will decrease first while the interlayer space will remain more or less constant (Muurinen et al., 2004). With increasing compaction, the interlayer space will also start to decrease (bulk dry density >1300 kg/m^3, (Van Loon et al., 2007). Due to the very narrow spaces created between clay particles within clay mineral stacks, the double layers in the interlayers approach one another until they finally overlap. As a result, the negative electric potential in the interlayer space increases, and all anions will be expelled from the interlayer (Bolt and de Haan, 1982; Pusch et al., 1990; Wersin et al., 2004). The interlayer water now contains only cations while anions dominate the larger interparticle pore space. This is referred to as 'the anion exclusion effect'.

In the case of high ionic strength of the free pore solution, the effect of anion exclusion will be smaller because the double layers are already compressed.

In addition to anion exclusion, overlapping DDL's also creates a charge barrier or blockage between converging clay particle stacks (Appelo et al., 2010). This prevents the passage of anions in free water. Therefore, anions can either get trapped inside the diminishing pore spaces or anions are forced to travel via longer transport routes through the clay layer, slowing down transport, as illustrated in Figure 4.

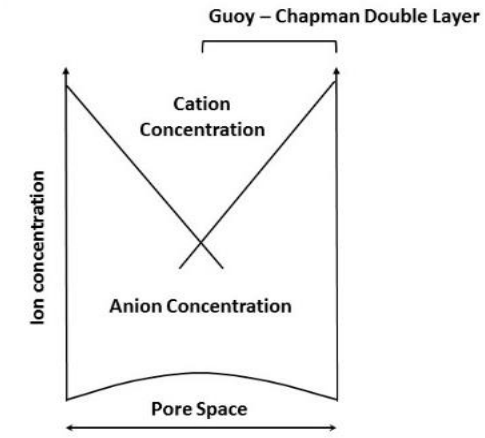


Figure 5: Cations in an electrolyte solution are attracted to the clay surface. As the pore is compacted, the double layers overlap, lowering the concentration of the anions in the pore solution, leading to anion exclusion (from Campbell 1985).

1.4.3- Diffusion

In fine grained low porosity clayey aquitards, where advective flow is low or absent, diffusion is the dominant transport mechanism. Diffusion is a process through which concentration differences within a stagnant solution will even out by random Brownian movement of molecules. Fick's laws (1855) define diffusion as a change in concentration (∂c) of a system as a function of space (∂x) as distance in one dimension/length (first law), and time (second law). Fick's first law is expressed as:

(4)

$$J = -D\frac{\partial c}{\partial x}$$

Where J is the flux of a chemical component in mol.m^{-2}.s^{-1}, D is the diffusion coefficient in m^2.s^{-1}. The concentration is usually a molality and the distance is in meters. In the second law, t is the time in seconds.

(5)

$$\frac{\partial c}{\partial t} = D\frac{\partial^2 c}{\partial x^2}$$

The diffusion coefficient (D) is an expression of ion mobility i.e. the friction experienced as a function of ion size (radius) and the viscosity of the solution. The diffusion coefficient decreases when solution concentration increases (Schauble et al., 2003; Rotenberg et al., 2007). Interaction between ions to maintain charge neutrality, will also influence the diffusion coefficient (for example more mobile Cl^- can drag along slower diffusing Na^+, while the Na^+ will simultaneously slow down the Cl^- diffusion.) Diffusion in sediment pore waters differs from diffusion in "free" water in that circumnavigating sediment grains, considerably increases the distance/length of the pathway (referred to as tortuosity) (Melkior et al, 2009). Results from other diffusion experiments with clay-rich materials have shown that cation diffusion is normally enhanced compared to anion diffusion due to interlayer and DLL diffusion (Shackelford and Daniel, 1991; Sato et al., 1992; Kozaki et al., 1998; Molera and Eriksen, 2002; Van Loon 2004; 2007; Descostes et al., 2008). The Nerst-Planck approach to the equation extends Fick's law for diffusion for the case where the diffusing particles are also moved with respect to the fluid by electrostatic forces. It is a time-dependent conservation of mass equation that describes the influence of an ionic concentration gradient and that of an electric field on the flux of chemical species, specifically ions.

Temperature changes influence the rate of diffusion. Heat causes atoms to vibrate and vibration increases with increasing temperature. The diffusion of species needs enough energy (thermal energy) to break their chemical bonds and move through its neighbors. The energy necessary for this motion is called the activation energy (Ea). The average thermal energy of an atom at room temperature (kBT = 0.026 eV) is usually much smaller than the activation energy Ea (~ 1 eV.atom-1) and a certain fluctuation in energy is needed for a movement. The probability of such fluctuation in energy is exponentially dependent on temperature (i.e. Arrhenius dependence). With regards to temperature, the diffusion coefficient (D) follows the Arrhenius dependence. Therefore, increasing temperature will result in an enhanced diffusion coefficient (Desaulniers et al., 1986; Eggenkamp et al., 1994; Hendry et al., 2000; Hesse et al., 2000; Luo et al., 2014; Bernachot et al., 2017):

(6)

$$\boldsymbol{D = D_0\, exp\left(-{Ea}/{RT}\right)}$$

where D_0 is the temperature-independent pre-exponential diffusion coefficient ($m^2.s^{-1}$), *Ea* is the activation energy for diffusion ($J.mol^{-1}$ or $eV.atom^{-1}$), *R* is gas constant (8.31 $J.mol^{-1}K^{-1}$ or $8.62\times10^{-5}eV.atom^{-1}.K^{-1}$) and *T* is the absolute temperature in Kelvin.

In 1921, Lindemann proposed, theoretically, that due to the differences in masses, the different stable isotopes of an element would fractionate during the process of diffusion. Isotopic fractionation is defined as the relative partitioning of the heavier and lighter isotopes between two coexisting phases in a natural system, i.e. fractionation is a function of the relative difference of masses of the different isotopes. Fractionation is driven either by the equilibrium or kinetics of a system. Therefore, the nature of the chemical bonds (Nygård et al., 2004) and the temperature (Urey, 1947) can influence isotopic fractionation. Fractionation decreases with increasing temperature (Richet et al., 1977; Schauble et al., 2003; Balan et al., 2019) and stronger chemical bonds generally preferentially involve the heavier isotope (Schauble, 2004). The fractionation in natural systems, such as in sediments, are dictated more by kinetics rather than equilibrium fractionations (solution and precipitation). The chlorine and bromine isotope compositions are reported using standard delta notation (respectively $\delta^{37}Cl$ and $\delta^{s}Br$), expressed in per mil (‰) units, as follows:

(7)

$$\delta(‰) = \left(\frac{R_x - R_{std}}{R_{std}}\right) \times 1000$$

where R is the ratio of the heavy isotopes relative to the light isotopes. R_x and R_{std} refer to the R value of the sample (x) and standard (std) respectively. The international standards are SMOC (Standard Mean Ocean Chloride, Kaufmann *et al*., 1984) for chlorine and SMOB (Standard Mean Ocean Bromide, Eggenkamp and Coleman, 2000) for bromine. This means when the δ value decreases, there is a depletion of the heavier isotope and when the value becomes more positive, there is an enrichment in the heavier isotope. In order to assess element and isotopic fractionation during diffusion, there are three things that should be considered separately: (1) the relative atomic mass difference between Cl and Br, (2) the relative mass difference between ^{81}Br and ^{79}Br and (3) the relative mass difference between ^{37}Cl and ^{35}Cl. The Cl anion has a smaller radius than Br at 167 picometer and 182 picometer respectively. However the atomic mass of Br isotopes (78.9 and 80.9 $g.mol^{-1}$ for ^{79}Br and ^{81}Br respectively), are more than twice that of Cl isotopes (34.9 and 36.9 $g.mol^{-1}$ for ^{37}Cl and ^{35}Cl respectively). Therefore, Br is clearly expected to move slower, so fractionate less, than Cl during diffusion processes (Eggenkamp and Coleman, 2009).

Scientific Approach

MATERIALS AND EXPERIMENTAL METHODS FOR HYDRO-MECHANICAL EXPERIMENTS

To supplement the numerous studies on pore water evolution, Le Gallo et al. (1998) provided valuable simulations of mineral evolution in reservoirs. Limitations of the water/rock interaction models require that the pore water composition and its evolution are known. For proper constraining of the interaction model, the mineralogical and petrographical data are necessary (Person et al., 1996). For example, the depths of the smectite dehydration reactions and the smectite-to-illite transformation may vary significantly depending on the chemical composition of the clay phases or the variation of the thermodynamic parameters. For this study, we are experimentally investigating ion-filtration effects on ocean water by means of a high-pressure squeezing experiment. It has been specifically designed to extract pore water volumes large enough to measure chlorine and bromine stable isotope composition, in parallel with the evolution of pore water chemistry during stepwise pressure and temperature increases, in order to follow the effect of clay compaction. We compare two distinctly different clay-rich materials. The first, MX-80, is a well-studied and well-characterized clay with high smectite clay content. The second material used is the Sainte Suzanne marl (SSM) from the Aquitaine basin (France) and is of interest as it acts as a flow and thermal barrier between the upper (less saline) and lower (more saline) Lacq reservoirs (Elias Bahnan et al., 2019). The SSM contains a smaller quantity of clay minerals which are mostly non-swelling in nature (predominantly illite rich). Expulsion of water from the compaction of the clay-rich SSM could have contributed to dilution of the aquifer water in the upper Lacq reservoir according to Elias Bahnan et al., (2019). Our data is combined with state of the art geochemical basin modeling software (SURP) to determine what proportion of the pore water results from smectite illitisation, and to assess the chemical reactivity of the systems, geochemical modeling was performed with PHREEQC code (Parkhurst and Apello, 1999) using Thermoddem database (Themoddem 1.10 version 6 June 2017). Equilibrium calculations were carried out to check the saturation state of the sampled solutions (phases expected to precipitate) and to follow the possible mineralogical transformations due to the change of physico-chemical conditions.

2.1- **STARTING MATERIALS**

2.1.1- The clays

The two materials selected for this experiment were MX80 smectite clay and Sainte-Suzanne marl (SSM) from the Aquitaine basin (borehole LA 101; latitude 43.420648° and longitude -0.619980°). MX-80 is well characterized and widely studied in numerous compaction studies (Sauzéat et al. (2001), Neaman et al. (2003), (Mondol et al., 2007), Karnland et al. 2007). It consists of 75 mass % Na-Ca montmorillonite ($(Si_{3.98}Al_{0.02})(A_{1.55}Mg_{0.28}Fe^{III}_{0..9}Fe^{II}_{0.08})Na_{0.18}Ca_{0.10}(OH)_2$), 15 wt% quartz, 5-8 wt% feldspars (plagioclase and microcline) with lesser amounts of kaolinite, phlogopite, calcite, siderite, pyrite and organic carbon (Bradbury and Baeyens, 2003). In contrast, the clay component of the SSM, as characterized with SEM and XRD, consists of 61 wt% illite, 16 wt% quartz, 10 wt% feldspars (anorthite and albite), 7 wt% kaolinite, 3.5 wt% calcite, while the remainder of the rock comprising cristobalite and pyrite. In terms of particle size of the materials, ~80% < 63 µm for the MX-80 and ~90% < 63 µm for the marl. Due to the high smectite content, the MX-80 has a brut cation exchange capacity (CEC) of 70 meq/100g while the CEC for marl is 10 meq/100g. Their respective chemical compositions are described inTable 1.

Table 1: The total chemical composition for MX-80 and Sainte Suzanne marl as weight % of major elements oxides. MX-80 composition is from (Rapport caractérisation MX80, n.d.) and marl composition is determined by ICP-OES at SARM (Nancy).

Major elements (wt %)	MX-80	Sainte Suzanne marl
SiO_2	59.00	53.29
Al_2O_3	18.70	11.88
Fe_2O_3	4.20	3.79
MnO	0.042	0.040
MgO	2.22	1.42
CaO	1.99	10.71
Na_2O	2.28	1.00
K_2O	0.84	2.44
TiO_2	0.17	0.57
P_2O_5	0.19	0.10
Loss on Ignition	9.90	14.67
Total	**99.51**	**99.89**

Regarding the source and complete characterization of MX-80 smectite clay, the reader is referred to Sauzéat et al. (2001). The marl was provided from storage at TOTAL Centre Scientifique et Technique Jean Féger (CSTJF) and characterized in terms of chemistry, mineralogy, petrophysical properties, grainsize, CEC.

2.1.2- The stock ocean water

To simulate a sedimentary foreland basin environment, filtered natural Atlantic Ocean water (0.1 μm) sampled of the coast of Bidart (France), was used as stock ocean water to saturate the clay for all three experiments. The ocean water was collected and filtered (0.1 μm) by TOTAL. The composition of the stock ocean water is presented as major elements in Table 2 (including Br), which accounts to a charge balance (of -3%). The $\delta^{37}Cl$ of the ocean water is -0.14‰ (very close to the Standard Mean Ocean Chlorine that has a $\delta^{37}Cl$ of 0.00‰) and the $\delta^{81}Br$ is 0.86‰. The ocean water has a pH of 8.1 and electrical conductivity of 48.59 $ms.cm^{-1}$ and contained 32.58 $g.L^{-1}$ total dissolved solids.

Table 2: The initial chemical composition of the stock ocean water from Bidart, France, used in the three compaction experiments.

Major cations			**Major anions**		
	(mmol.L^{-1})	**(meq.L^{-1})**		**(mmol.L^{-1})**	**(meq.L^{-1})**
Na^+	481.92	481.92	**Cl^-**	524.11	524.11
K^+	10.08	10.08	**SO_4^{2-}**	27.7	55.4
Mg^{2+}	54.63	109.26	**HCO_3^-**	1.9	1.9
Ca^{2+}	10.73	21.46	**Br^-**	0.88	0.88
Sr^{2+}	0.09	0.18			
Total	557.45	622.9	Total	554.59	582.29

2.2- **THE EXPERIMENTAL SETUP**

A high stress/fluid pressure/temperature oedometric type cell was designed to experimentally simulate the diagenetic processes (fluid and heat flow, mechanical compaction and, chemical compaction) involved in the production of formation water from a saturated clay sample under deep burial conditions (~6 – 7 km deep). Oedometer tests simulate the one-dimensional (vertical) deformation and drainage conditions: no lateral displacement of the cylindrical sample is possible but the sample can swell/compress vertically in response to changes in vertical (axial) stress σ_1.

For this experiment an oedometric cell, with internal dimensions of 10 cm diameter and 10 cm height, is connected to a set of pressure pumps for generating both pore fluid pressure (Pi) at both sample sides to allow drainage conditions, and a vertical stress up to 45 MPa and 150 MPa respectively, which can be individually controlled to induce the desired effective vertical stress to the sample (σ_1'=σ_1-P_i). Figure 6 shows the experimental setup for the study: the oedometric cell [A], the oil-pressure generator (for the axial stress) [B] the fluid circulation system [C], the control and data acquisition systems [D], the system for heating control [E].

The oedometric cell is encased by two thermal heating rings to regulate the temperature up to 150°C. An inlet/outlet for fluid from the pore pressure generator pumps are positioned at both the top and bottom of the cell. Two 3 mm thick porous plates (retaining 98% of particles > 16μm) sit on opposite sides of the sample. The fluid can therefore uniformly percolate into/out of the sample. Due to valves placed between the pressure generator pumps and the inlet/outlet of the cell, flow can occur in both directions. The pore pressure generator pumps [C1 & 2], each with a capacity of 100 mL, can apply a constant fluid flow (0.00001–30 ml/min) or a constant fluid pressure. Fluid temperature in the pore pressure generator pumps can also be temperature regulated. The data acquisition system allows for recording both the axial stress (σ_1) and pore fluid pressure (P_i). Axial deformation is recorded from an externally fitted linear variable differential transformer (LVDT) sensor. The volumes of fluids in both of the pore pressure pumps are also continuously recorded thus allowing for a water and chemical mass balance of the system.

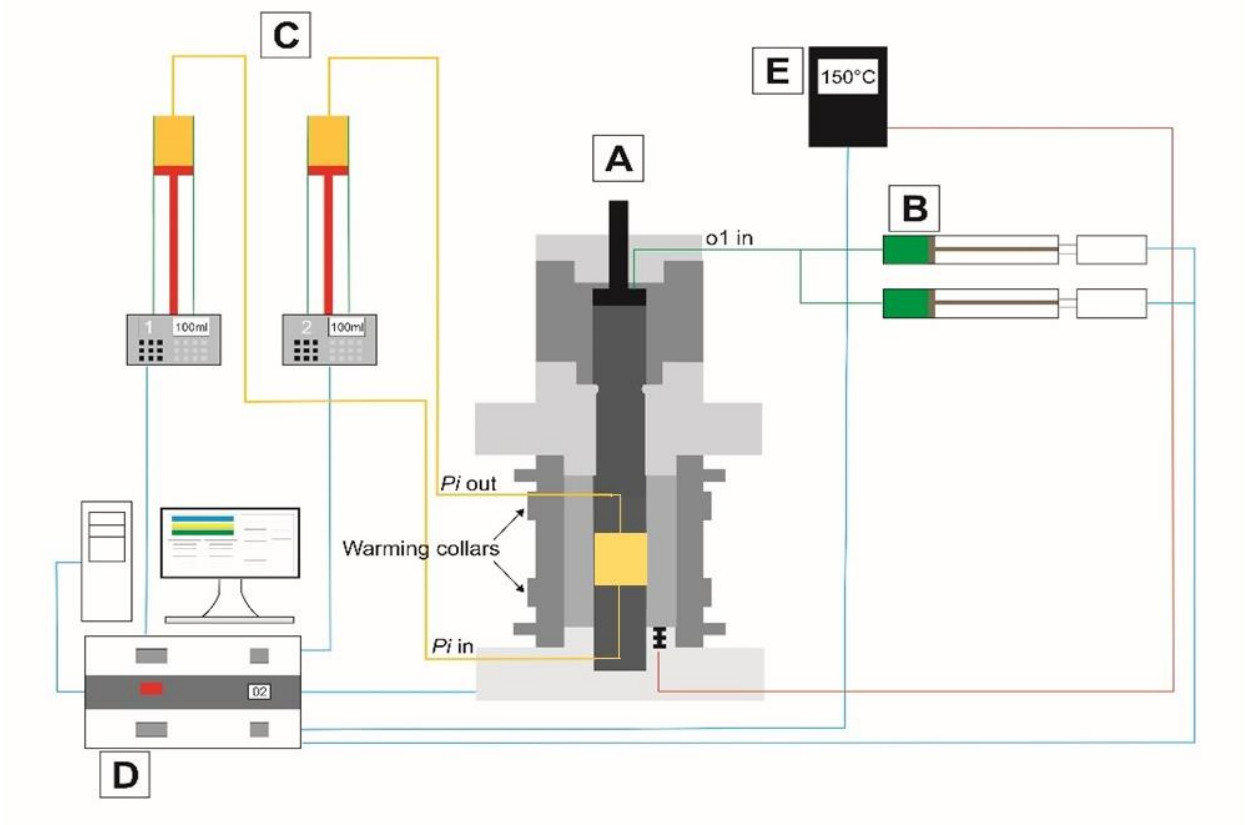


Figure 6 : Illustration of the experimental system showing the compaction (oedometric) cell [A] and various operation systems; the oil-pressure generator (for the axial stress) [B] and the fluid circulation system [C]; the control and data acquisition systems [D]; the system for heating control [E].

2.3- **EXPERIMENTAL PROTOCOL**

For this study, the results from three long-term clay compaction experiments are compared. The compaction protocol followed a series of axial vertical stress and temperature steps for up to 200 days (Figure 7). The variations of the protocol for the three experiments are:

Experiment 1: Compaction of saturated MX-80 with 5 steps of increasing vertical stress and temperature **(MX80)**.

Experiment 2: Compaction of saturated SSM with 5 steps of increasing vertical stress and temperature **(SSM)**.

Experiment 3: Compaction of saturated MX-80 with 10 steps of increasing vertical stress and constant low (ambient) temperature **(MX80 no T)**.

2.3.1- Hydro mechanical loading path

The compaction protocol followed a series of axial stress and temperature steps for up to 200 days.This study was not attempting to reproduce a specific basin or reservoir, therefore, common values for the axial load (23 $kPa.m^{-1}$) and thermal gradients (25°$C.km^{-1}$) and a constant pore pressure were selected. For the duration of the experiment it was attempted to maintain the pore pressure at 45 MPa while the vertical stress was increased from 45.5 MPa to 150 MPa (maximal effective stress: 105 MPa) by increments of ~ 25 MPa, and temperature increments of 30°C for the MX80 and SSM compaction experiments 1 and 2, and in increments of ~ 15 MPa for the MX80 no T compaction experiment 3.

The experimental conditions were progressively applied in the following order:

1. application of a low axial stress ($\sigma1$ = 1.5 MPa) for the sample saturation;
2. hydration of the dry powdered material in the cell from both the top and bottom inlet at low injection pressure of 1 MPa;
3. when the clay was fully hydrated (i.e. no more fluid was taken up by the clay material), a pressure gradient was applied (from the bottom to the top) until the bottom injection pump C1 was emptied, thus allowing water flow and complete chemical equilibration. At the end of this step, the injection pump at the bottom C1 was isolated from the oedometric cell with a valve, so that no new water will be injected during compaction. The injection pump at the top C2 was almost entirely emptied; only asmall amount ocean water was kept to maintain pore pressure in the sample and to collect the expelled water during the experiment.
4. Application of the vertical stress ($\sigma1$ = 45.5 MPa) using a loading rate of 0.001 MPa/s;
5. Application of the interstitial pressure (Pi = 45 MPa) using a loading rate of 0.002 MPa/s;
6. Beginning of the stepwise incremental increase of the vertical stress ($\sigma1$ max = 150MPa) using a loading rate of 0.001 MPa/s and simultaneous application of incremental temperature increase.

The duration of the steps varied between two and four weeks to allow for the stabilization of the axial compaction (deformation) curves. Expelled fluid was sampled as soon as a minimum required volume of 2 ml has accumulated in the collection pump C2, or before the next axial pressure step was applied. Fluid was not expelled at each step.

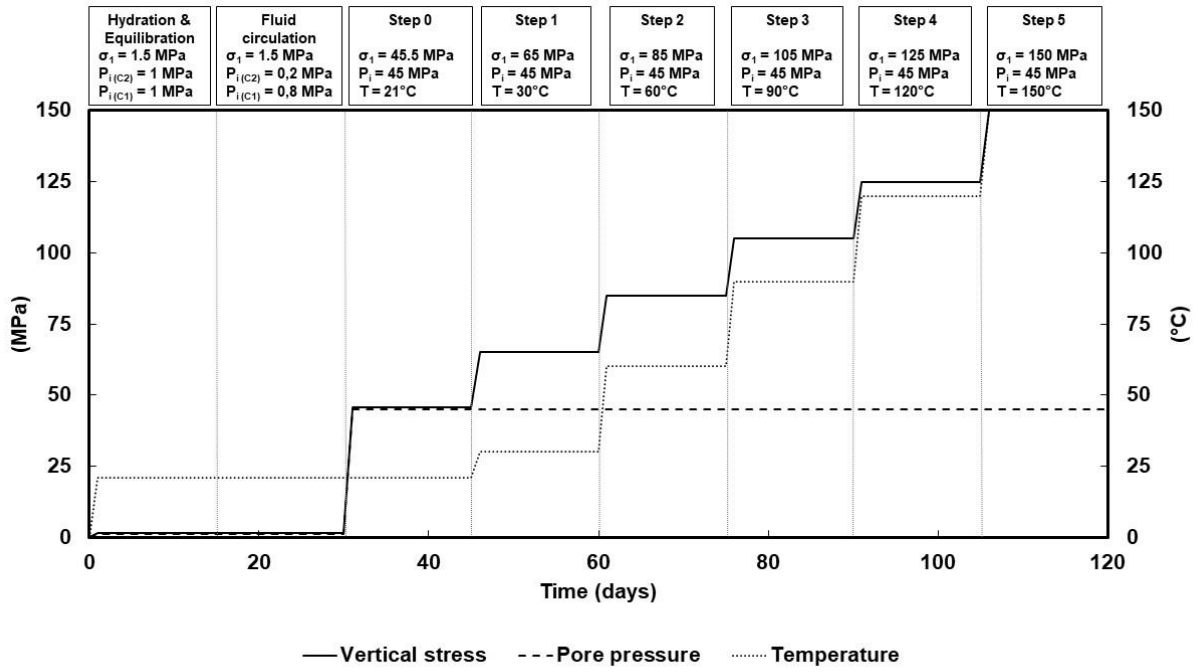


Figure 7 : Schematic presentation of the pressure and temperature increments followed in the experiments. The pore pressure was maintained at 45 MPa while the axial stress was increased from 45.5 MPa to 150 MPa (maximal effective stress: 105 MPa) by increments not exceeding 25 MPa, and temperature increments of ~ 30°C.

2.3.1- Fluid and solid sample collection

2.3.1.1- The fluid collection

Fluid expelled from the clay compaction was sampled as soon as the minimum required volume of 2 mL has accumulated in the collection pump. To collect the fluid, the valve between the cell and pump was closed. The pressure in the pump had to be decreased to < 10 MPa before it could be collected. The pressure in the pump was then increased back to 45MPa before the valve between the pump and the cell was opened again. The water samples were collected in airtight polyethylene dual-position snap cap flasks. Both the ICP-MS as well as isotope analysis were done at the Institute de Globe du Physique de Paris (IPGP).

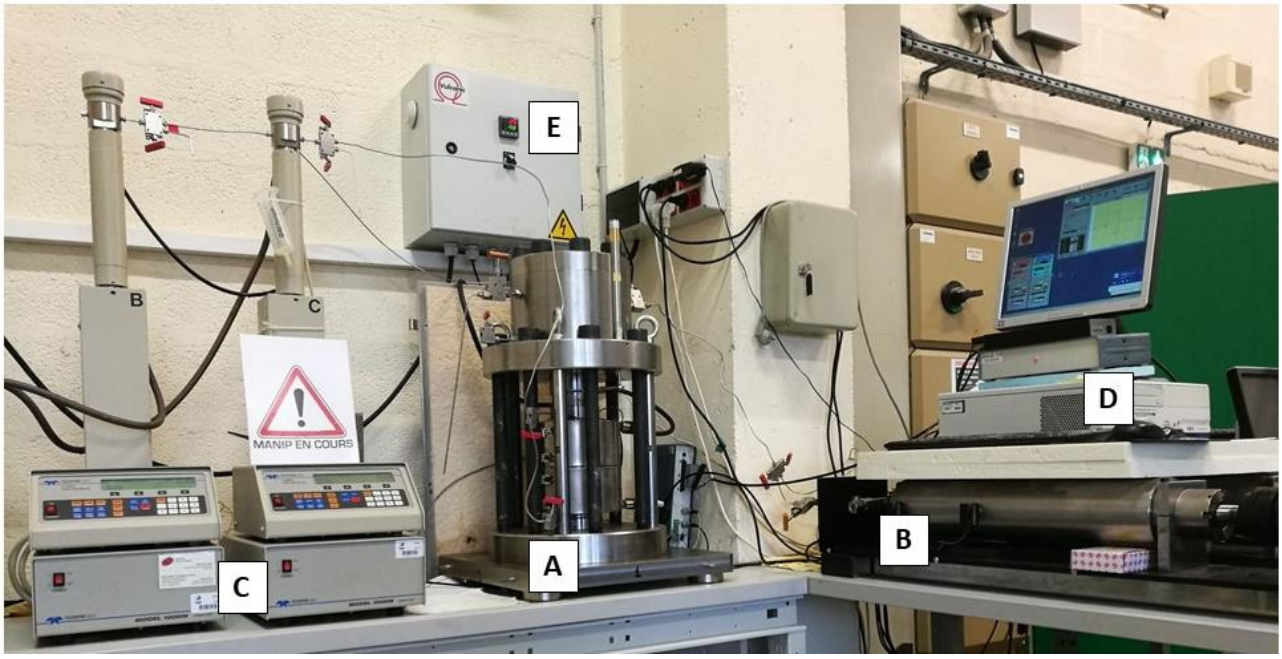


Figure 8 : A photo of the experimental system showing the compaction (oedometric) cell [A] and various operation systems; the oil-pressure generator (for the axial stress) [B] and the fluid circulation system [C]; the control and data acquisition systems [D]; the system for heating control [E].

2.3.1.2- Compacted core collection

The compacted solid had to be carefully drilled from the cell. No fluid was used during this drilling process. Unfortunately, a proportion of solid material was lost during this process as dust generated from this drilling. Each of the cores were weighed and their dimensions measured. They were then sealed in impermeable plastic film until needed.

METHODS OF ANALYSIS FOR FLUIDS AND SOLIDS

3.1- THE FLUIDS

Despite the small number of samples that could be collected in each experiment, the volumes collected were sufficient for ICP-MS analysis to quantify the major and trace elements in the fluid, as well as stable isotope measurements of Cl and then Br.

3.1.1- Chemical Analyses of Fluids

3.1.1.1- ICP-MS

Upon collection; (1) the pH was measured (InLab Semi-micro 6 mm combined probe); (2) the sample was filtered (0.024 µm PP membrane syringe filters) and (3) split into two aliquots. A proportion was prepared for ICP-MS and the remainder was refrigerated for later isotope analyses. Preparation of ICP-MS entailed diluting each sample to ~ 100 ppm and acidification with HNO_3 (2%). Elemental concentrations were assessed using an Agilent 7900 quadrupole ICP-MS at the Institut du Globe de Physique de Paris (IPGP). Liquid samples were sprayed through a micro-nebulizer in a Scott spray chamber prior to ionization. Elements with masses between that of sodium (23) and bromine (81) were measured using a collision-reaction cell with helium gas (5 $mL.min^{-1}$) to remove polyatomic interferences. All other elements were measured without collision gas. Scandium, indium, and rhenium internal standards were injected after inline mixing with the samples to correct for signal drift and matrix effects. Two sets of multi-element calibration standards (one for major and one for trace elements) were analyzed to compute the calibration curves that were used to convert elemental signals to concentrations. The reported uncertainties were calculated using algebraic propagation of blank subtraction and sample count standard deviations (n=3).

3.1.1.2- Cl isotopes

For the extraction and measurement of Cl isotopic content, the protocol thoroughly described by Eggenkamp et al., (2016) was closely followed. To separate the Cl^- isotopes for analysis, 50 -100 µl of the expelled ocean water is mixed with 4 ml of a 1 M KNO_3 solution to keep a high ionic strength that results in finer AgCl grains and better reaction with CH_3I. Next, a citric acid-phosphate buffer is added to keep pH low to avoid precipitation of Ag_2S. This mixture is heated until almost boiling and then reacted with 1 ml of 0.2 M silver nitrate to precipitate silver chloride. This reaction occurs fast and as AgCl is light sensitive, the precipitate should be vacuum filtered quickly and quantitatively. The precipitate and filter on which it had been collected is oven-dried in a dark container overnight.



Figure 9 : Gas column used for precipitation of silver chloride, preceding Cl isotope measurements.

The dried filter is then transferred to a glass ampule from which the air is evacuated and an excess amount of iodomethane gas is introduced, before the ampule is sealed (Figure 9). Allow at least 48 hours for the CH_3I to slowly react with the AgCl precipitate to form $CH_3Cl_{(g)}$ and $AgI_{(s)}$. The $CH_3Cl_{(g)}$ is separated from the remaining excess CH_3I by gas chromatography by means of difference in velocity of movement when traveling past a thermal conductivity detector filament and adsorption by a gas exchange resin (Porapak Q 80–100 mesh). The separated CH_3Cl is measured on a dual inlet mass spectrometer (a ThermoFisher DeltaPlus XL), configured to allow precise measurements on CH_3Cl (m/z 52 and 50), typically at 4 V on m/z 94 and≈4V on m/z 96. Two repeated measurements were used to calculate the $\delta^{37}Cl$ and standard deviation.

3.1.1.3- Br isotopes

For the extraction and measurement of Br isotopic content, the protocol thoroughly described by Eggenkamp & Louvat, (2018) was closely followed. Br is extracted by distillation in the presence of nitric acid and trapping it in an ammonia solution. The distillation method has been shown to be an effective alternative to the customary extraction by ion exchange chromatography on anion- exchange resin (Louvat et al., 2016) in cases where high Cl content can be problematic to Br extraction due to supersaturation of the resin by Cl.



Figure 10: Distillation of the ocean water to extract bromine.

A dilute nitric acid solution will oxidize Br^- to Br_2 but won't oxidize Cl^- therefore a solution containing little to no Cl^- can be produced from solutions with large Cl/Br ratios. Trapping the solution in a strongly reducing alkaline environment such as an ammonia solution disproportionates the Br_2 to Br^- and BrO_3^- in a ratio of 5:1. Due to the reducing nature of the ammonia solution the BrO_3^- is then reduced to Br^-. Enough sample should be used to provide a minimum of 20 μg Br. For ocean water, the distillation requires that 1 ml HNO_3 (69%) is added to ~ 0.5 ml sample plus 3.5 ml de-ionized water, immediately closed up, and vigorously boiled over a low heat source for 8 -10 minutes until the 1 ml of 0.5 M NH_3 on the trapping end of the distillation has doubled in volume - i.e. 1 ml has been distilled. This solution is then measured with a Thermo Neptune multi-collector inductively coupled plasma mass spectrometer. The measurement protocol proposed by Eggenkamp & Louvat (2018), was closely followed. An average of 5 repeated measurements was used to calculate the $\delta^{81}Br$ and standard deviation.

3.1.2- Mass Balance Calculation

3.1.2.1- Major element concentrations

The balance between what goes in, what is expelled and, what remains in the system, has to be recalculated each time water is expelled from the clay under compaction, as illustrated in the diagram of Figure 11. At the initial state of the saturation, volume of fluid absorbed by the clay is V_i. The concentration is C_i. Therefore the number of moles initially in the pore fluid is Q_i:

(8)

$$Q_i = V_i * C_i$$

Compaction expel from the clay, a volume Vex of concentration Cex, containing Qex number of moles.

(9)

$$Q_{ex} = V_{ex} * C_{ex}$$

Pore water of volume V_r remains in the clay.

(10)

$$V_r = V_i - V_{ex}$$

From the number of moles in the expelled water, the number of moles in the remaining pore water will be Qr.

(11)

$$Q_r = Q_i - Q_{ex}$$

Considering the volume of pore water remaining in the clay, the concentration of the remaining pore water C_r can then be calculated.

(12)

$$C_r = Q_r / V_r$$

For each following expelled volume of water, the balance between what is expelled and what remains in the pore water is calculated accordingly.

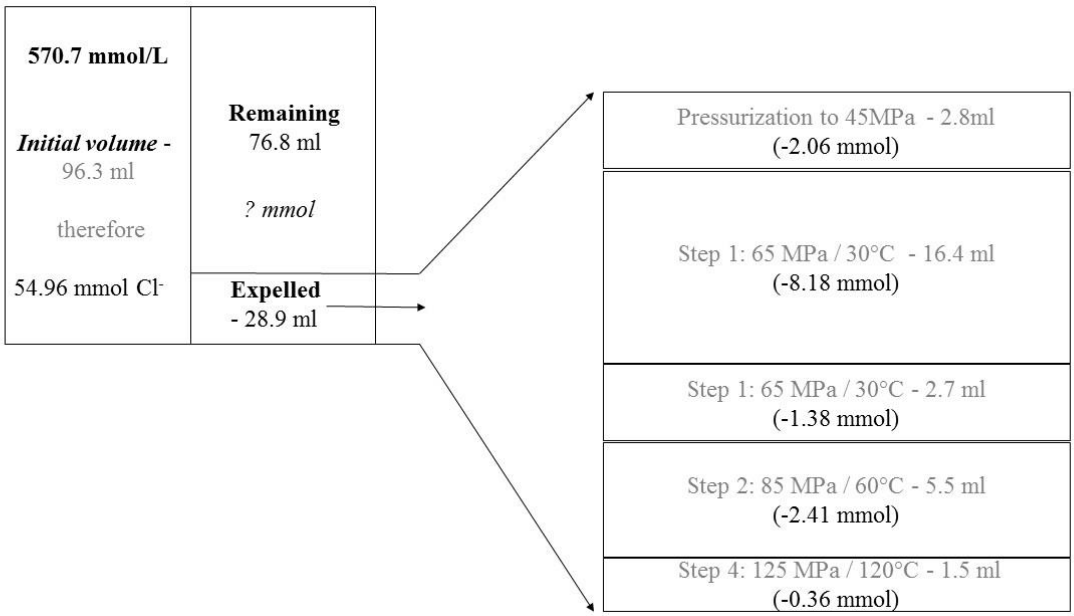


Figure 11 : Diagram to illustrate the mass balance calculation between expelled and remaining pore water composition for a given element.

3.1.2.2- Isotope ratios

An isotope mass balance to compute the isotopic composition of isotopes trapped in MX-80 was done according to the same assumptions as for the major element concentrations. The example given is for Cl isotopes in the MX80 compaction experiment 1. As for the major elements, we assume that the clay and ocean water has reached equilibrium after an extended period of fluid circulation through the clay. We, therefore, take the composition of the re-equilibrated ocean water to be the same as the composition as the pore water at this time, and that the isotopic ratio in this water will also be the same. We refer to this as the initial composition. Therefore the number of ^{35}Cl and ^{37}Cl is calculated from the measured δ^{37}Cl value:

(13)

$$^{35}Cl = Cl/(1 + \left(1 + \frac{d37Cl}{1000}\right) * {}^{35}Cl\ of\ SMOC$$

and

(14)

$$^{37}Cl = d^{37}Cl - {}^{35}Cl$$

The ^{35}Cl and ^{37}Cl for the next expelled sample is the subtracted from that of the initial composition. This gives the ^{35}Cl, ^{37}Cl and corresponding δ^{37}Cl value in the pore water.

The ^{35}Cl and ^{37}Cl of each expelled sample is then subtracted from ^{35}Cl and ^{37}Cl of the previous the remaining pore water composition. From the resulting ^{35}Cl and ^{37}Cl, the $\delta^{37}Cl$ is then recalculated from equation (14)(13) above.

3.1.3- Water Chemistry Modelling / Calculated Water Content

3.1.3.1- PHREEQC

To assess the chemical reactivity geochemical modelling was performed with PHREEQC code (Parkhurst and Apello, 1999) using Thermoddem database (Themoddem 1.10 version 6 june 2017) to compare Experiment 1 (MX80) and Experiment 2 (SSM). Equilibrium calculations were carried out to check the saturation state of the sampled solutions (phases expected to precipitate) and to follow the possible mineralogical transformations due to the change of physico-chemical conditions. The considered mineral phases were:

For Experiment 1 and 3 (MX80): C (element), calcite, gypsum, kaolinite, microcline, muscovite (ordered, dissolve only), pyrite, quartz, siderite, smectite (MX80) for the initial minerals, and montmorillonite (HcNa), albite (low), anorthite and anhydrite for the phases likely to precipitate.

For Experiment 2 (SSM), albite (low), anorthite, calcite, cristobalite, quartz, kaolinite, illite, pyrite for the initial minerals, clinochlore and anhydrite for the phases likely to precipitate.

The silicate minerals expected to precipitate are chosen in agreement with the results of XRD. The initial solution is that of the Bidart ocean water sample (Table 2).

3.1.3.2- SURP

In collaboration with the Bureau de Recherches Géologiques et Minières (BRGM, Orleans, France), the volume of water produced due to the potential transformation of smectite to illite was calculated for the MX80 compaction experiment 1 using their internally developed specialist software (named SURP). The SURP code is a modeling software that simultaneously processes thermo-hydro-mechanical calculations and chemical-mineralogical interactions during geological compaction, through coupling a Python code (v 2.7) with IPHREEQC (Tremosa et al., 2020). The architecture of the code is set out in Figure 12.

The purpose for developing the code was to be able to calculate the effect of water released by smectite mineralogical transformations on the pore pressure, and the generation of overpressure, of clay-rich sedimentary layers. Due to the SURP code's capacity to incorporate 1) the influence of temperature and pressure (effective stress) evolution of a sedimentary pile and 2) the influence of the water released by smectite clay dehydration during illitisation, for this study, in collaboration with the developer, the SURP code was modified to apply the compaction and chemical data from a long

term laboratory compaction experiment of smectite rich MX80 clay equilibrated with ocean water under high fluid pressure (45 MPa), mechanical stress up to 150 MPa and temperature up to 150 °C. In the laboratory compaction experiment, the pore pressure is known and controlled. We aimed to calculate the volume of water that could have been produced from smectite dehydration or mineral transformation.

A detailed account of the development of the code and the base calculations is given in Tremosa et al., (2020). In brief, a stepwise approach is followed. For each timestep, after updating the thermo-hydro-mechanical parameters, IPHREEQC is launched from Python, for the chemical and mineralogical reactions calculations. From the IPHREEQC output, the mineralogical evolution, the balance of water produced and consumed by the minerals, and the solution density are returned into the thermo-hydro-mechanical calculations in Python for calculation of the following timestep's thermo-hydro-mechanical parameters.

The smectite dehydration model in the SURP code was largely adapted from the model presented by Vidal and Dubacq (2009). For practicality, the smectite-to-illite transformation described in the SURP model is simplified to not involve the formation of interstratified I/S. The conversion requires a potassium and aluminum source and generates quartz and water. The following simplified equation roughly describes/illustrates the transformation.

(15)

$$Mnt_Na + K^+ + Al^{3+} = illite + quartz + H_2O$$

In the SURP code, three solid solutions between the hydrated montmorillonite end-member, and the dehydrated end-member are defined. The hydrated components, Mnt_Na.3w (3 water layers), Mnt_Na.2w (2 water layers), and Mnt_Na.1w (1 water layer), contain respectively 7, 4, and 2 $H_2O/O_{10}(OH)_2$. Within the development of the SURP code, the effect of pressure on the stability domains of the smectite solid solutions has been taken into account in expressing the functions of the dependency of the molar volume on the number of water layers, the nature of the interlayer cation (Na and Ca) and the substitution rate Al-Mg in the octahedral sites of the smectite.

The experimental data and results from the MX80 compaction experiment 1 were used as input for the SURP code. Certain adjustments were necessary. For the compaction experiment, the effective pore pressure was known, as well as the vertical stress applied, the amount of water produced during the various steps, and the composition of the water produced. The objective was therefore to rework the model to find, for these experimental conditions and results, what intermediary mineral transformation steps could have occurred, and if that was the case, what volume of the water expelled during the clay compaction, resulted from the mineralogical transformation of smectite to illite.

From mass balance calculations for each step, the remaining pore water composition for each step was calculated (what is inside minus what is expelled). From knowing the composition (and so ionic strength) of the remaining pore water, other relevant parameters could be determined.

This includes the thickness of the diffuse double layer (Debey length) and because the porosity/pore size is also known from the SURP model, consequently the proportion of the pore space that's subjected to anion exclusion could be calculated and so the proportion of the pore space that contains free water (the proportion that contains all the anions). With the pore size and ionic strength for the pore solutions known, the membrane efficiency of the MX-80 clay for Cl and Br respectively was derived.

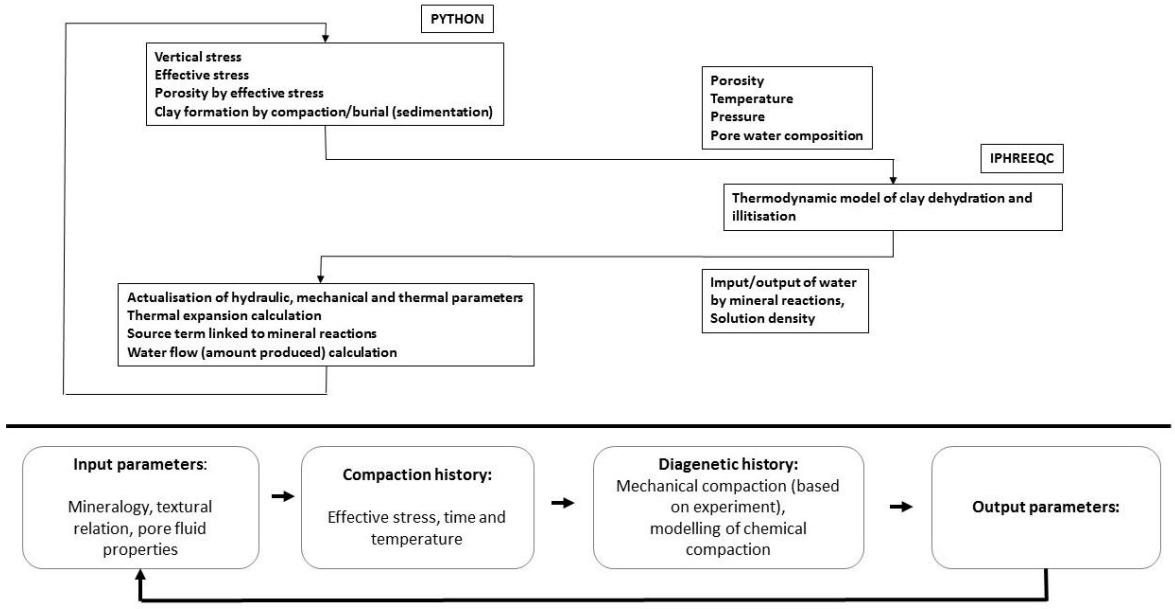


Figure 12 : Architecture of the calculations made by the SURP code, including the coupling of the thermo-hydro-mechanical calculations with Python language and the thermodynamic reactive calculations made using the IPHREEQC code (from Tremosa et al., 2020).

For the thermos-hydro-mechanical model, the steps of compaction is set out in Table 3 was used. Initial porosity of the dry clay loaded in the compaction cell was 55%. And the pore pressure was set and maintained at 45 MPa.

Table 3: Steps of compaction applied during the SURP during the geochemical modeling approach.

	Vertical Mechanical Stress	Temperature	Duration (days)	ml expelled (28.9mL)	Amount resulting from clay mineral dehydration. (7.4 mL)
Pore pressurization	45.5 MPa	21°C	26	2.8	1.88
Step 1:	65 MPa	30 °C	15	16.4 + 2.7	0.57
Step 2:	85 MPa	60 °C	12	5.5	0.57
Step 3:	105 MPa	90 °C	17	-	0.91
Step 4:	125 MPa	120 °C	22	1.5	1.87
Step 5:	150 MPa	150 °C	18	-	-0.003

3.2- THE SOLIDS

3.2.1- Physical characterization

3.2.1.1- Particle size distribution of the marl

The particle size distribution was determined to characterize the marl before the compaction experiment. The core was gently crushed and pulverized. The powder was riffled down to 50 g which was washed through a set of sieves with apertures of 350 µm and 63 µm respectively. The wet fractions were dried overnight at 55°C and weighed. This fraction (<63 µm) was decarbonated, as described by Komada et al., (2008), followed by sedimentation separation of the smallest fractions according to the principles of Stoke's law. To determine the carbonate fraction of the marl, the simple process of dissolving the carbonate content by acidification of the sample in suspension serves to indicate what proportion of the weight of the rock material constitutes carbonate species and in parallel liberate the fine particles for a better extraction of the fine fractions. The total of the sub 63 µm-fraction was dispersed in 200 ml of pure (de-ionized water). A 1 M solution of HCl was used to systematically lower the pH of the suspension to pH 4. Between each addition of HCl, the pH of the solution was allowed to stabilize before the next addition of HCl. The decarbonisation was considered complete when there was no more change in pH. The suspension was left to sediment and the supernatant decanted and discarded. The remaining solid fraction was re-dispersed in pure water to rinse whereafter it was oven-dried at 55°C and weighed once dry. The difference in mass is attributed to the carbonate content.

3.2.1.2- Material density (ρ_g) of the marl.

Particle density, also called material density (ρ_g) is a measure of the mass of the solid sample in a given volume (mass divided by volume). Material density focuses on just the solid particles of a material and excludes air and water that occupy the pore spaces in the material. The material density is a result of the chemical composition and structure of the minerals in the material. Material density data are used with bulk density data to calculate the porosity before the compaction experiment.

The material density was determined by Water Pycnometer (ASTM D 854-00) by adding 25 g of slightly crushed oven-dried marl (48h @ 55°C) to a pure water in a pycnometer flask. To remove entrapped air from the sample, the pycnometer flask is placed under vacuum for 10 minutes.
After the vacuum is removed, more water is added to the mixture to fill the flask up to the watermark. The mass of the pycnometer and content is measured. Subtract the mass of the pycnometer filled only with water from the mass of the pycnometer with solids and water. An average material density for the marl was obtained from three repetitions.

3.2.1.3- Porosity

3.2.1.3.1. Mercury intrusion porosimetry

Mercury intrusion porosimetry (MIP) is a technique used to determine the distribution of the entrance radii of pores, therefore, presenting pore size distribution under the assumption that pores are cylindrical flow channels. This method allows the measurement of pore size over a wide range, from a few nanometers up to several tens of micrometers. With MIP, the cumulative mercury volume intruded corresponding to steps of increasing mercury pressure is given as a function of the equivalent pore radius. The pore radius (r) associated with each mercury pressure increment, is described by the following equation:

(16)

$$r = \frac{2T_s \cos \alpha}{P}$$

T_s is the surface tension of the liquid mercury (0:485 N m^{-1}), α is the contact angle of the interface between fluid and solid (140° on average for the mercury–air interface as explained in Cuisinier and Laloui (2004). P corresponds to the pressure difference.

3.2.1.4- Total Porosity

Since the degree of compaction was continuously recorded in terms of vertical displacement (by means of the LVDT sensor), the continuous change in total volume (V_t) can be calculated. The V_t includes the volume of solids (V_s), the volume of air (V_a), and the volume of water (V_w). Knowing the initial mass of the solid material (M_s), the bulk dry density (ρb - $g.cm^{-3}$) can be calculated as follows:

(17)

$$\rho_b = (M_s/V_t)$$

As the material density (ρ_g) is also known, it is therefore possible to calculate a corresponding porosity (n) from the following equation:

(18)

$$n = 1 - (\rho_b/\rho_g)$$

This calculated porosity is used as an approximation to follow the change in porosity through the compaction process.

3.2.1.5- N_2 gas adsorption study

Gas adsorption isotherms are measured in order to investigate the porous nature and characteristics of a sample. For example the pore size, the pore volume, and the pore area as well as the surface area. This is actually a process of physical adsorption as we are describing the interaction between absorbing atoms, the absorbate, and the sample, the absorbante. Physical absorption occurs through interaction of weak forces of attraction such as Van der Waals forces. They are of low enthalpy, typically lower than 50 KJ/mole and typically they don't involve in the formation of chemical bonds. The most common absorbate is N_2. N_2 is adsorbed at 77 Kelvin, liquid nitrogen temperature. So, in this case we are actually referring to adsorption of the liquid phase rather than the adsorption of the gaseous phase.

Together the adsorption and desorption isotherms can give us a lot of information on the pore size and pore shape in a sample. The shape of the isotherms will change dramatically depending on the pore sizes and the pore shapes actually present. Micropores are classified as < 2 nm, mesopores between 2 -50 nm, and macropores >50 nm (IUPAC). These dimensions refer to the diameter of cylindrical-shaped pores or the width of a slit-shaped pore. Super- or ultra micropores are <1 nm. Not all samples have micro-, meso- and macropores present.

Before analysis, the sample is thoroughly degassed at 110 °C to clean it through the removal of moisture, or any other extraneous materials that are present. The sample is held under vacuum in the analysis tube and as we start to admitN_2 gas. To determine the surface area, the sample is put under vacuum, to cryogenic temperature (using liquid nitrogen). Nitrogen gas is dosed to the sample in controlled increments.

After each dose of adsorptive gas, the pressure is allowed to equilibrate, and the quantity of gas adsorbed is determined. The quantity of gas adsorbed is plotted as a function of pressure. From this plot the quantity of gas required to form a monolayer over the external surface of the solid is determined. The surface area can be calculated from the quantity of gas required to form a monolayer, using the BET (Brunauer, Emmett and Teller) equation. To determine the pore volume and pore size distribution, the gas pressure is increased further incrementally until all pores are filled. Next, the gas pressure is reduced incrementally, evaporating the condensed gas from the system. Evaluation of the adsorption and desorption isotherms reveals information about the pore volume and pores size distribution. The BJH (Barrett, Joyner and Halenda) calculation is used to determine pore volume and pore size distribution.

3.2.2- Water content

3.2.2.1- Thermogravimetry

Thermogravimetric analysis (TGA) is a method of thermal analysis in which changes in physical and chemical properties of materials are observed as a result of heating at a constant rate. increase in temperature. Thermogravimetric analysis is a complete, accurate, and responsive method of moisture determination by monitoring the weight change that occurs by the process of water vaporization. The process respectively distinguishes loss of adsorbed water, the deshydroxylation of the clay layers, and re-crystallisation. The TG analysis was done, at the Laboratoire Interdisciplinaire des Environnements Continentaux (LIEC), Nancy, with a crushed sample in a range from room temperature to 1000 °C. The maximum sample capacity is 20 g, for a measurement range of +/- 1 g with a resolution of 0.2 µg, or a measurement range of +/- 200 mg with a resolution of 0.02 µg.

3.2.3- Chemical characterization

3.2.3.1- Whole rock chemistry

Analyses of the major elements of solid materials are carried out on an Inductively Coupled Plasma-Optical Emission Spectrometry (ICP-OES) using a Thermo Fischer ICap 6500 spectrometer at the Service d'Analyses des Roches et des Minéraux (SARM) of the Centre de Recherches Pétrographiques et Géochimiques (CRPG), Nancy. The solid material is crushed and pulverized. The powder is then melted with $LiBO_2$ and dissolved with HNO_3 before it is introduced into the ICP-OES. The detection limit is 0.01 wt % as oxides.

3.2.3.2- Cation exchange capacity

The cation exchange capacity (CEC), expressed in milliequivalents, measures the quantity of cations that a sample can retain in exchangeable form on the surface of the clays. CEC is determined by UV measurement after exchange with cobaltihexamine according to the methodology of Aran et al., (2008). A solution of $Co(NH_3)_6^{3+}$) which is put in contact with the sample. In order to allow the exchange of cations, the solution is stirred for two hours at 35°C, then centrifuged.

The remaining cobaltihexamine ion concentration is then determined by colorimetric determination (λ=475nm) using a Shimadzu UV2501-PC spectrophotometer. The CEC is calculated by the difference between the concentration before and after exchange.

3.2.4- Mineralogical characterization

3.2.4.1- X-Ray Diffraction

After completion of the experiments, the compositions of the two compacted cores were characterized by semi–quantitative X-ray diffractometry. XRD patterns were collected on a D8 Advance Bruker AXS diffractometer at 35 kV and 45 mA with non-monochromatic CoKα radiation (λ = 0.17903 nm), equipped with a LynxEye fast linear detector. Intensities were recorded from 3 to 75°2θ with a 0.035°2θ step using a 3s counting time per step. For the fine clay fraction (< 2 microns), intensities were recorded from 2 to 40°2θ with a 0.02°2θ step using a 4s counting time per step. Data reduction and analysis were performed with the EVA software (DIFFRACplus from Bruker) and diffraction peaks were identified by comparison with powder diffraction files (PDF2 database from the International Center for Diffraction Data, ICDD).

3.2.4.2- Scanning Electron Microscopy

The scanning electron microscope (SEM) was used to identify mineral phases, complimentary to X-Ray diffraction. A high-energy electron beam is focused on polished surfaces. X-rays are common products of interactions between the electron beam and the atoms in the sample. These emitted X-rays and the spectra generated by the energy dispersive spectrometer (EDS) are specific for each chemical element thus allowing qualification and quantification of major elements (Girão et al., 2017). A section with maximum dimensions of 60 mm x 80 mm in length and width, and 40mm thickness, was polished to obtain a smooth surface. All air was evacuated from the samples under vacuum. The surfaces of the sample were then carbon-coated to avoid electron charging. Selected samples were studied with a JEOL JSM-7600F scanning electron microscope (SEM) equipped with an Oxford Instruments Silicon Drift Detector (SDD)-type EDS spectrometer at the GeoRessources Laboratory (Nancy, France). Analyses were performed at 15 kV with a beam current of around 1 nA.

Results

RESULTS

This section is divided into subsections presenting in section 4.1- the compaction results, in section 4.2- the fluid evolution and mass balances, and in section 4.3- geochemical modelling. The solid material characterization comparing before and after compaction, is presented in section 4.4-

4.1- MECHANICAL DATA

In this section, the compaction curves of the three experiments are discussed. Figure 13 to Figure 15 represents compaction curves for the three experiments. The convention of positive compressions for stress and displacement is used. The plotted curves show the stress (primary y-axis) and vertical deformation (secondary y-axis) as a function of time (number of days).

In the absence of swelling clay minerals, the marl hydrated and compacted faster (132 days) than the MX80 (200 days for the MX80 compaction experiment 1 and 189 days for experiment 3). The initial vertical stress of 45 MPa caused an immediate 15% vertical compaction in experiment 1 (MX80) on bentonite, a 25% vertical compaction in experiment 2 (SSM) on marl, and 20% vertical displacement in experiment 3 (MX80 no T) on bentonite. This significant difference between the two materials is due to an important swelling pressure maintained by the MX80 from strongly adsorbed interlayer water during the hydration step. The total vertical displacement was 42% for experiment 1 (MX80), 47 % for experiment 2 (SSM), and 44% for experiment 3 (MX80 no T). The marl was generally more compactable and compacted faster than the MX80. As can be seen from Figure 14, the vertical displacement curve stabilized/flattened immediately after compaction for each step. The MX80 vertical displacement compaction curves in Figure 13 and Figure 15 were much slower to stabilize/flatten. With the shorter (fewer days) and smaller (reduced pressure increments) compaction steps of experiment 3 (MX80 no T), the compaction curve did not fully stabilize during most of the steps.

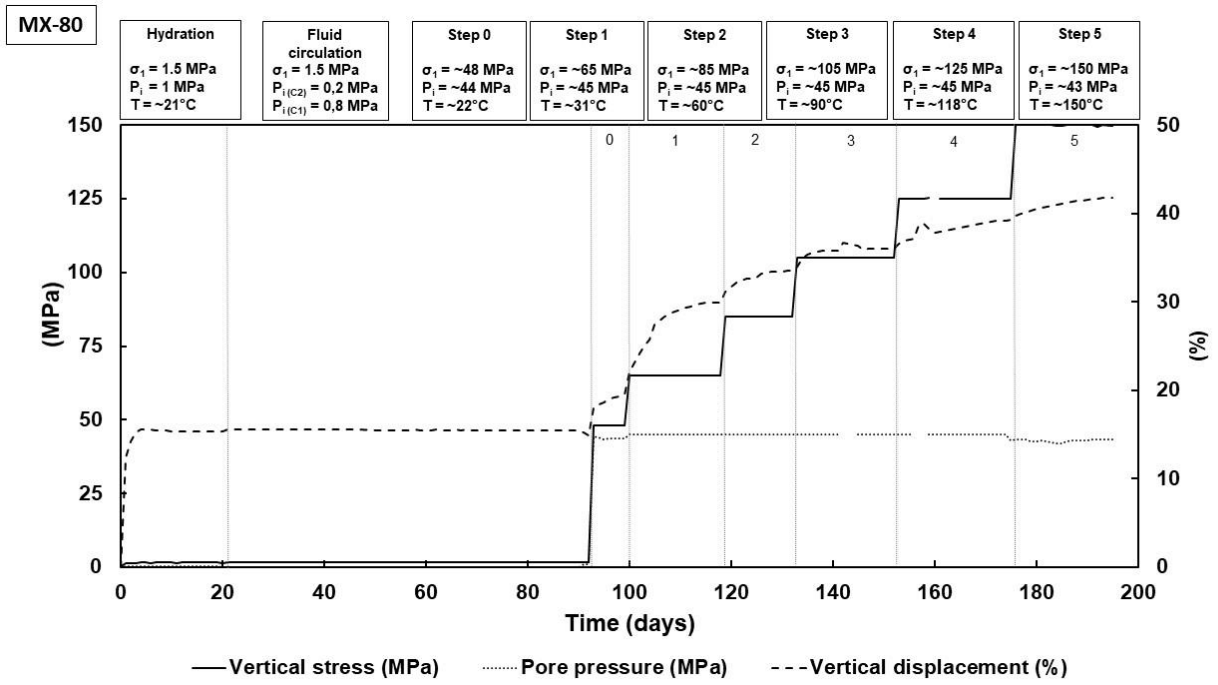


Figure 13: The compaction curve for the compaction of MX-80 in Experiment 1 that lasted from 22/11/2017 to 12/06/2018.

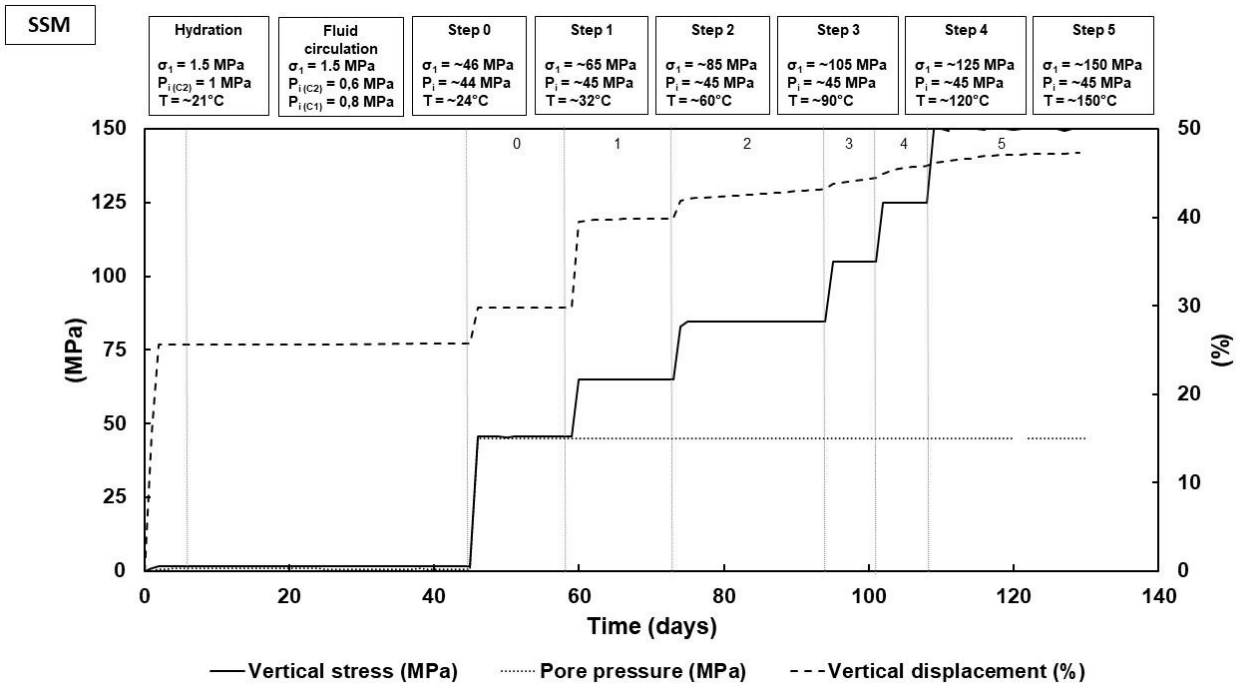


Figure 14: The compaction curve for the Sainte Suzanne marl in Experiment 2 that lasted from 16/07/2018 to 23/11/2018.

The compaction curves show the duration of the various experimental steps. For each of the steps the average axial stress (σ), pore pressure (P_i), and average temperature (T) for the duration of the step, are indicated on the compaction curves. For experiments 1 and 2, the five compaction steps were on average 2 weeks each while, for experiment 3, the number of steps was doubled to 10 and therefore the length of each step was reduced to around 1 week each.

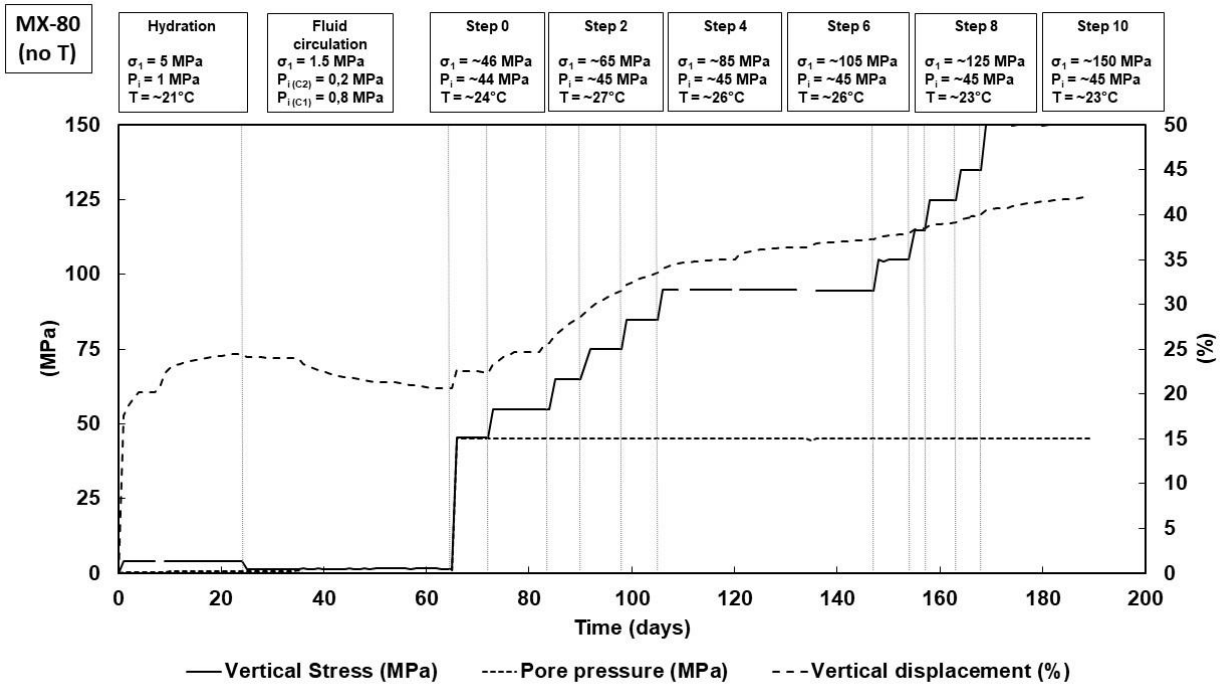


Figure 15 : The compaction curve for MX-80 in Experiment 3 that lasted from 02/04/2019 to 09/10/2019.

4.2- **THE FLUID EVOLUTION**

Table 4 shows the volumes of water that were collected during the various compaction steps for the experiments and the chemistry of the expelled solutions are given in Table 5, Table 7 and Table 8. Both materials absorbed similar volumes of water and for both materials, the largest volumes of water were expelled during the earlier compaction steps. Water was not expelled at each step.

The smectite clay in experiment 1 (MX80) absorbed 96.3 ml of ocean water but only 30 % of that volume was expelled during the compaction experiment. A total of 107.49 ml of water was absorbed in the marl porosity in experiment 2 (SSM) of which 52 % was expelled during compaction of the marl. For experiment 3 (MX80 no T) 109.9 ml of water was absorbed in the MX80 and only 13 % of the absorbed water was expelled during compaction.

Note that for all three experiments, two fluid samples could be collected during the compaction step at 65 MPa. A first and larger sample was collected shortly after increasing the pressure and temperature. Water continued to be expelled, and a second smaller sample was collected just before the pressure and temperature were increased to 85 MPa.

Table 4: Volumes of fluid absorbed and expelled during the experiment. For all three experiments, two fluid samples were collected during the compaction step at 65 MPa.

	Volumes of fluids absorbed and expelled					
	Experiment 1 MX80		**Experiment 2 SSM**		**Experiment 3 MX80**	
Volume of fluid absorbed	96.3 ml		107.49 ml		109.9 ml	
	Duration (days)	Volume expelled (ml)	Duration (days)	Volume expelled (ml)	Duration (days)	Volume expelled (ml)
Hydration phase	20		5		24	
Fluid circulation phase	70		43		42	
Step 0: 45MPa & ~20°C	26	2.8	14	-	7	-
					12	-
Step 1: 65 MPa & 30 °C	15	16.4 + 2.7	14	39.9 +3.9	6	2.5 + 2
					7	4.5
Step 2: 85 MPa & 60 °C	12	5.5	20	11.2	7	2.5
					42	1.1
Step 3: 105 MPa & 90 °C	17	-	7	1.24	7	-
					3	-
Step 4: 125 MPa & 120 °C	22	1.5	7	-	6	-
					7	-
Step 5: 150 MPa & 150 °C	18	-	22	-	21	2
Total	**200**	**28.9**	**132**	**56.3**	**189**	**14.6**

4.2.1- Cl and Br concentrations

The initial concentrations of Cl and Br in the ocean water used for the compaction experiments are 524 mmol.L^{-1} and 0.88 mmol.L^{-1} respectively. The Cl/Br molar ratio of the initial ocean water is 595 (Table 6). When the ocean water is first cycled through the clay under a minimum load of 1.5 MPa to obtain equilibrium between the clay and ocean water, the Cl concentration increases from 524 mmol.L^{-1} in the Bidart ocean water to 570.7 mmol.L^{-1} in the re-equilibrated pore water for experiment 1 (MX80). For experiment 2 (SSM) and experiment 3 (MX80 no T), the Cl concentration decreases to 506 mmol.L^{-1} and 507.65 mmol.L^{-1} respectively. The Br concentration increases from 0.88 mmol.L^{-1} in the Bidart ocean water to 0.97 mmol.L^{-1} in the re-equilibrated pore water for experiment 1 (MX80). For experiment 2 (SSM) and experiment 3 (MX80 no T), the Br concentration decreases to 0.78 mmol.L^{-1} and 0.81 mmol.L^{-1} respectively.

Table 5: Concentrations in the expelled fluid and concentrations calculated to remain in the compacted core. The ratio of enrichment for each element is given in brackets.

Experiment 1						
	Volume of sample (mL)	*Conc in expelled water (mmol.L^{-1})*	*Number of mmol in expelled water*	*Volume remaining in clay (mL)*	*Number of mmol remaining in clay*	*Conc remaining in clay (mmol.L^{-1})*
Cl^- (1.06)						
Bidart Ocean water		524				
Initial pore fluid*	96.31	**570.70**	54.96			**570.7**
Pore pressurization: 45.5 MPa	2.79	**738.64**	2.06	94	52.90	**565.7**
Step 1: 65 MPa & 30 °C	16.44	**497.79**	8.18	77	44.72	**580.2**
Step 1: 65 MPa & 30 °C	2.69	**514.61**	1.38	74	43.33	**582.5**
Step 2: 85 MPa & 60 °C	5.52	**436.26**	2.41	69	40.92	**594.3**
Step 4: 125 MPa & 120 °C	1.5	**238.17**	0.36	67	40.57	**602.2**
Br^- (1.06)						
Bidart Ocean water		0.88				
Initial pore fluid*	96.31	**0.97**	0.0932			**0.97**
Pore pressurization: 45.5 MPa	2.79	**1.24**	0.0034	94	0.0898	**0.96**
Step 1: 65 MPa & 30 °C	16.44	**0.81**	0.0134	77	0.0764	**0.99**
Step 1: 65 MPa & 30 °C	2.69	**0.83**	0.0022	74	0.0742	**1.00**
Step 2: 85 MPa & 60 °C	5.52	**0.71**	0.0039	69	0.0703	**1.02**
Step 4: 125 MPa & 120 °C	1.5	**0.38**	0.0006	67	0.0697	**1.03**
Na^+ (0.99)						
Bidart Ocean water		482				
Initial pore fluid*	96.31	**538.24**	51.83			**538.24**
Pore pressurization: 45.5 MPa	2.79	**649.53**	1.82	94	50.02	**534.92**
Step 1: 65 MPa & 30 °C	16.44	**548.63**	9.02	77	41.01	**531.99**
Step 1: 65 MPa & 30 °C	2.69	**576.16**	1.55	74	39.46	**530.40**
Step 2: 85 MPa & 60 °C	5.52	**501.46**	2.77	69	36.69	**532.72**
Step 4: 125 MPa & 120 °C	1.5	**296.55**	0.45	67	36.24	**537.98**

Experiment 1 (MX80) - continued						
	Volume of sample (mL)	*Conc in expelled water (mmol.L^{-1})*	*Number of mmol in expelled water*	*Volume remaining in clay (mL)*	*Number of mmol remaining in clay*	*Conc remaining in clay (mmol.L^{-1})*
K^+ (1.07)						
Bidart Ocean water		10.1				
Initial pore fluid*	96.31	**8.43**	0.812			**8.43**
Pore pressurization: 45.5 MPa	2.79	**13.90**	0.039	94	0.774	**8.27**
Step 1: 65 MPa & 30 °C	16.44	**6.48**	0.107	77	0.667	**8.65**
Step 1: 65 MPa & 30 °C	2.69	**5.49**	0.017	74	0.650	**8.73**
Step 2: 85 MPa & 60 °C	5.52	**4.48**	0.030	69	0.619	**8.99**
Step 4: 125 MPa & 120 °C	1.5	**2.38**	0.007	67	0.612	**9.09**
Ca^2 (1.23)$^+$						
Bidart Ocean water		10.7				
Initial pore fluid*	96.31	**17.73**	1.708			**17.73**
Pore pressurization: 45.5 MPa	2.79	**14.28**	0.040	94	1.67	**17.84**
Step 1: 65 MPa & 30 °C	16.44	**20.36**	0.335	77	1.33	**17.30**
Step 1: 65 MPa & 30 °C	2.69	**21.67**	0.058	74	1.23	**16.59**
Step 2: 85 MPa & 60 °C	5.52	**17.88**	0.099	69	1.22	**17.74**
Step 4: 125 MPa & 120 °C	1.5	**8.31**	0.012	67	1.22	**18.14**
Mg^{2+}(1.13)						
Bidart Ocean water		54.6				
Initial pore fluid*	96.31	**42.74**	4.116			**42.74**
Pore pressurization: 45.5 MPa	2.79	**75.27**	0.210	94	3.91	**41.77**
Step 1: 65 MPa & 30 °C	16.44	**27.92**	0.459	77	3.45	**44.72**
Step 1: 65 MPa & 30 °C	2.69	**24.73**	0.066	74	3.38	**45.45**
Step 2: 85 MPa & 60 °C	5.52	**20.34**	0.112	69	3.27	**47.46**
Step 4: 125 MPa & 120 °C	1.5	**9.36**	0.014	67	3.25	**48.31**

The pore pressurization (step 0) led to the consequent increase of the concentration of anions of the expelled solution for experiment 1 (MX80), and a decrease for experiment 2 (SSM). No fluid was expelled during step 0 for experiment 3 (MX80 no T). However, to be relevant, the concentrations have to be treated in terms of mass balance (Section 3.1.2- and Table 5). Figure 16 and Figure 17 give, for Cl and Br, the concentrations of the expelled water and the calculated concentration of the water that remains in the clay porosity. The good correlation between Cl and Br concentrations in the expelled water (Figure 18) as well as in the remaining water has to be highlighted. This implies that, within the accuracy of the analysis, no significant chemical partitioning occurs between Cl and Br.

The first increase in pressure, from 45 MPa to 65 MPa resulted in the largest volume of water expelled of all the steps and significant fractionation (see section 4.2.2-) in all three experiments. With progressive compaction, the Cl concentration in the expelled water generally decreases with each consecutive expulsion (Figure 16) for MX80 compaction, from 739 mmol.L^{-1} Cl in the first expelled water to 238 mmol.L^{-1} in the final expelled water for experiment 1(MX80),

and from 822 mmol.L^{-1} in the first expelled water to 580 mmol.L^{-1} in the final expelled water for experiment 3 (MX80 no T). For SSM compaction in experiment 2, the Cl concentrations slightly increase throughout progressive compaction, from 503 mmol.L^{-1} in the first expelled water to 541 mmol.L^{-1} in the final expelled water.

The corresponding calculated concentration of Cl for the pore water remaining in the compacted MX-80 clay slightly increases, from 565 mmol.L^{-1} initially to 602 mmol.L^{-1} in the final remaining pore water for Experiment 1 (MX80), and from 500 mmol.L^{-1} in the first compaction step to 482 mmol.L^{-1} in the last compaction step for Experiment 3 (MX80 no T). However, the concentration calculated for the remaining pore water during SSM compaction in Experiment 2, slightly decreases with progressive compaction, from 506 mmol.L^{-1} in the first expelled water to 495 mmol.L^{-1} in the last expelled water.

Table 6: Cl/Br in the pore fluid expelled and retained during the three compaction experiments.

Experiment 1 (MX80)			Experiment 2 (SSM)			Experiment 3 (MX80 no T)		
	Expelled water	**Remaining pore water**		**Expelled water**	**Remaining pore water**		**Expelled water**	**Remaining pore water**
Bidart Ocean water	597		Bidart Ocean water	597		Bidart Ocean water		
Re-equilibrated pore fluid*	589	**588**	Re-equilibrated pore fluid*	647	**649**	Initial pore fluid*	627	
Pore pressurization: 45.5 MPa	572	**589**	Step 1: 65 MPa & 30 °C	654	**649**	Step 2: 65 MPa & 27°C	600	**625**
Step 1: 65 MPa & 30 °C	598	**586**	Step 1: 65 MPa & 30 °C	653	**646**	Step 2: 65 MPa & 27°C	593	**626**
Step 1: 65 MPa & 30 °C	612	**583**	Step 2: 85 MPa & 60 °C	646	**644**	Step 3: 75 MPa & 27°C	608	**632**
Step 2: 85 MPa & 60 °C	621	**583**	Step 3: 105 MPa & 90 °C	646	**643**	Step 4: 85 MPa & 26°C	615	**628**
Step 4: 125 MPa & 120 °C	616	**585**	Water remaining in pore pressure pump	643	-	Step 5: 95 MPa & 26°C	624	**627**
Water remaining in pore pressure pump	623	-				Water remaining in pore pressure pump	-	

The same is seen for Br. The Br concentration in the water expelled decreases during the MX80 compaction (experiments 1 & 3) and slightly increases during the SSM compaction (experiment 2). For experiment 1 (MX80) the Br concentration decreases from 1.24 mmol.L^{-1} in the first expelled water to 0.38 mmol.L^{-1} in the final expelled water. For experiment 2 (SSM) the Br concentration slightly increases from 0.77 mmol.L^{-1} in the first expelled water to 0.84 mmol.L^{-1} in the last expelled water. For experiment 3 (MX80 no T) the Br concentration also slightly decreases during the compaction, from 1.37 mmol.L^{-1} in the first expelled water to 0.93 mmol.L^{-1} in the last sample.

The corresponding calculated concentration of Br for the pore water remaining in the compacted clay does not change significantly for any of the experiments and remains around 0.77 mg.L^{-1} ±1.

The Cl/Br for the pore water expelled from the compacted clays, increased from 588 in the re-equilibrated ocean water to 627 in the final expelled water for experiment 1 (MX80), barely changes for the pore water expelled from the SSM (647 to 643), and from 627 in the first expelled sample to 624 in the last sample for experiment 3 (MX80 no T).

To confirm if any back diffusion occured, the concentrations of Cl and Br of the ocean water remaining in the pore pressure generator pump (i.e. the "inflow" water) were analyzed at the end of each of the experiments. For Experiment 1 (MX80) Cl and Br concentration are 580 mmol.L^{-1} and 0.99 mmol.L^{-1} respectively, for Experiment 2 (SSM) concentrations are 501 mmol.L^{-1} Cl and 0.78 mmol.L^{-1} Br. These values are not significantly different from the original composition of the ocean water that is in equilibrium with the clay (see Tables 4, 6, and 7).It was not measured for experiment 3 (MX80 no T) due to the onset of the Covid 19 pandemic.

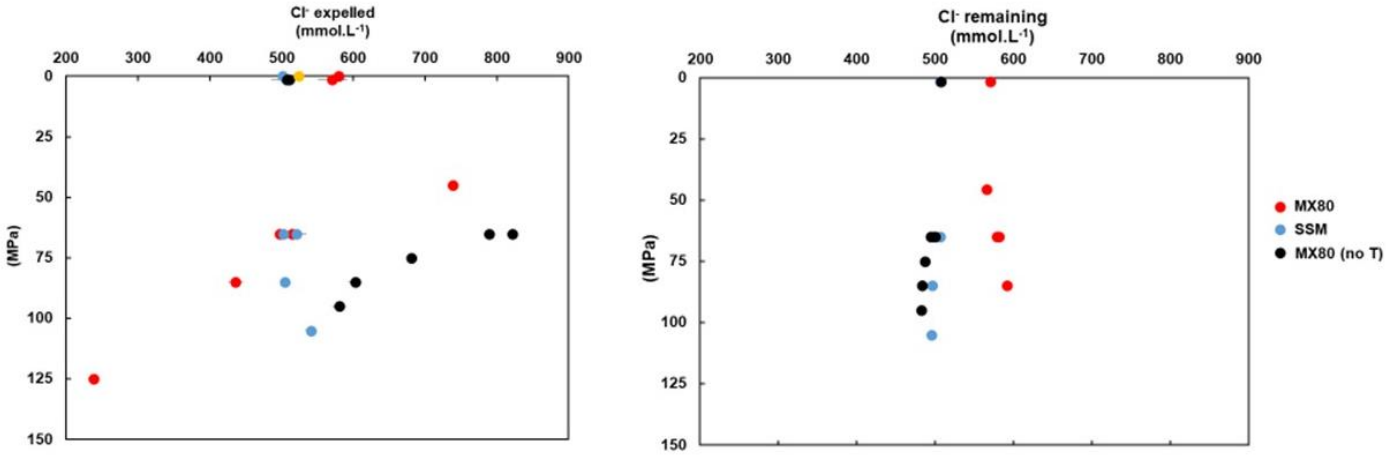


Figure 16 : Variation in concentration of Cl^- in the expelled water and in the water remaining in the compacted clay (from mass balance calculation, see section 3.4.2) as pressure and temperature increase. The Cl^- concentration of the original ocean water is shown in orange, Experiment 1, 2 and 3 are in red, blue and black respectively.

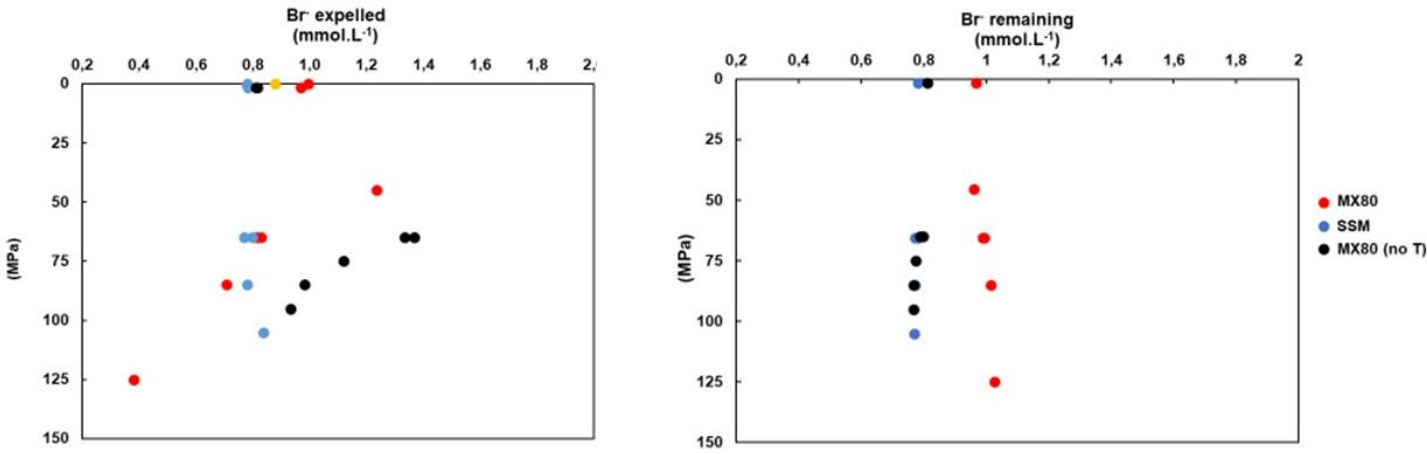


Figure 17 : Variation in concentration of Br^- in the expelled water and in the water remaining in the compacted clay (from mass balance calculation, see section 3.4.2) as pressure and temperature increase. The Br^- concentration of the original ocean water is shown in orange, Experiment 1, 2 and 3 are in red, blue and black respectively.

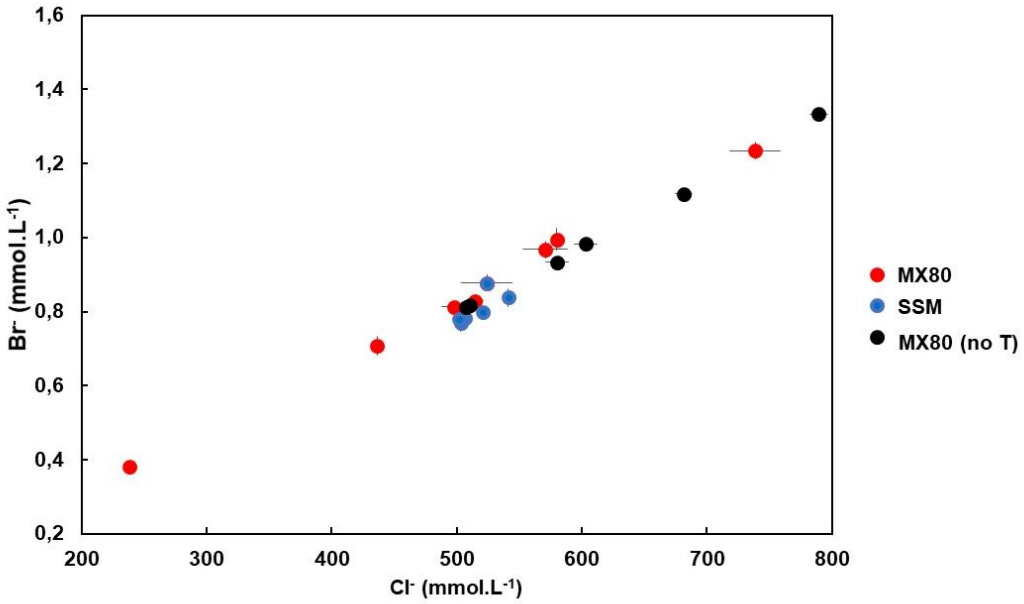


Figure 18: The Br vs Cl plot for the MX-80 compaction experiments and the Sainte-Suzanne marls. Experiment 1, 2 and 3 are in red, blue and black respectively.

Table 7: Concentrations in the expelled fluid and concentrations calculated to remain in the compacted core. The ratio of enrichment for each element is given in brackets.

Experiment 2 (SSM)						
	Volume of sample (mL)	*Conc in expelled water (mmol.L^{-1})*	*Number of mmol in expelled water*	*Volume remaining in clay (mL)*	*Number of mmol remaining in clay*	*Conc remaining in clay (mmol.L^{-1})*
Cl$^-$ (0.98)						
Bidart Ocean water		524				
Initial pore fluid*	107.49	**506.44**	54.44			**506.4**
Step 1: 65 MPa & 30 °C	3.87	**503.12**	1.95	104	52.49	**506.6**
Step 1: 65 MPa & 30 °C	39.99	**520.63**	20.82	64	31.67	**497.7**
Step 2: 85 MPa & 60 °C	11.2	**504.30**	5.65	52	26.02	**496.3**
Step 3: 105 MPa & 90 °C	1.24	**541.17**	0.67	51	25.35	**495.2**
Br$^-$ (0.98)						
Bidart Ocean water		0.88				
Initial pore fluid*	107.49	**0.78**	0.08			**0.78**
Step 1: 65 MPa & 30 °C	3.87	**0.77**	0.003	104	0.081	**0.78**
Step 1: 65 MPa & 30 °C	39.99	**0.80**	0.032	64	0.049	**0.77**
Step 2: 85 MPa & 60 °C	11.2	**0.78**	0.009	52	0.04	**0.77**
Step 3: 105 MPa & 90 °C	1.24	**0.84**	0.001	51	0.039	**0.77**
Na$^+$ (0.99)						
Bidart Ocean water		482				
Initial pore fluid*	107.49	**497.20**	53.44			**497.20**
Step 1: 65 MPa & 30 °C	3.87	**488.66**	1.89	104	51.55	**497.52**
Step 1: 65 MPa & 30 °C	39.99	**507.18**	20.28	64	31.27	**491.44**
Step 2: 85 MPa & 60 °C	11.2	**490.38**	5.49	52	25.78	**491.67**
Step 3: 105 MPa & 90 °C	1.24	**521.09**	0.65	51	25.13	**490.96**
K$^+$ (1.05)						
Bidart Ocean water		10.1				
Initial pore fluid*	107.49	**12.32**	1.32			**12.32**
Step 1: 65 MPa & 30 °C	3.87	**11.37**	0.04	104	1.28	**12.36**
Step 1: 65 MPa & 30 °C	39.99	**11.74**	0.47	64	0.81	**12.75**
Step 2: 85 MPa & 60 °C	11.2	**12.03**	0.13	52	0.68	**12.90**
Step 3: 105 MPa & 90 °C	1.24	**13.09**	0.02	51	0.66	**12.90**
Ca^{2+} (1.02)						
Bidart Ocean water		10.7				
Initial pore fluid*	107.49	**25.87**	2.78			**25.87**
Step 1: 65 MPa & 30 °C	3.87	**25.54**	0.10	104	2.68	**25.89**
Step 1: 65 MPa & 30 °C	39.99	**25.31**	1.01	64	1.67	**26.25**
Step 2: 85 MPa & 60 °C	11.2	**25.31**	0.28	52	1.39	**26.45**
Step 3: 105 MPa & 90 °C	1.24	**25.00**	0.03	51	1.36	**26.48**

Experiment 2 (SSM) - continued.						
	Volume of sample (mL)	*Conc in expelled water (mmol.L^{-1})*	*Number of mmol in expelled water*	*Volume remaining in clay (mL)*	*Number of mmol remaining in clay*	*Conc remaining in clay (mmol.L^{-1})*
Mg^{2+} (0.91)						
Bidart Ocean water		54.6				
Initial pore fluid*	107.49	**37.27**	4.01			**37.27**
Step 1: 65 MPa & 30 °C	3.87	**39.19**	0.15	104	3.85	**37.20**
Step 1: 65 MPa & 30 °C	39.99	**40.75**	1.63	64	2.23	**34.97**
Step 2: 85 MPa & 60 °C	11.2	**38.71**	0.43	52	1.79	**34.17**
Step 3: 105 MPa & 90 °C	1.24	**40.46**	0.05	51	1.74	**34.02**

Table 8: Concentrations in the expelled fluid and concentrations calculated to remain in the compacted core. The ratio of enrichment for each element is given in brackets.

Experiment 3 (MX80 no T)						
	Volume of sample (mL)	*Conc in expelled water (mmol.L^{-1})*	*Number of mmol in expelled water*	*Volume remaining in clay (mL)*	*Number of mmol remaining in clay*	*Conc remaining in clay (mmol.L^{-1})*
Cl^- (1.04)						
Bidart Ocean water		**524**				
Initial pore fluid*	109.9	**507.65**	55.79		55.79	
Step 1b: 65 MPa & 27°C	2.5	**821.66**	2.05	107.4	53.74	**500.34**
Step 1b: 65 MPa & 27°C	2	**789.42**	1.58	105.4	52.16	**494.85**
Step 3: 75 MPa & 27°C	4.5	**681.34**	3.07	100.9	49.09	**486.54**
Step 4: 85 MPa & 26°C	2.5	**602.79**	1.51	98.4	47.58	**483.58**
Step 5: 95 MPa & 26°C	1.1	**580.26**	0.64	97.3	46.95	**482.49**
Br^- (1.04)						
Bidart Ocean water		**0.88**				
Initial pore fluid*	109.9	**0.81**	0.089		0.089	
Step 2: 65 MPa & 27°C	2.5	**1.37**	0.003	107.4	0.086	**0.80**
Step 2: 65 MPa & 27°C	2	**1.33**	0.003	105.4	0.083	**0.79**
Step 3: 75 MPa & 27°C	4.5	**1.12**	0.005	100.9	0.078	**0.77**
Step 4: 85 MPa & 26°C	2.5	**0.98**	0.002	98.4	0.076	**0.77**
Step 5: 95 MPa & 26°C	1.1	**0.93**	0.001	97.3	0.075	**0.77**
Na^+ (1.06)						
Bidart Ocean water		**482**				
Initial pore fluid*	109.9	**451.43**	49.61		49.61	
Step 2: 65 MPa & 27°C	2.5	**799.56**	1.99	107.4	47.61	**443.33**
Step 2: 65 MPa & 27°C	2	**778.88**	1.56	105.4	46.06	**436.96**
Step 3: 75 MPa & 27°C	4.5	**689.57**	3.10	100.9	42.95	**425.70**
Step 4: 85 MPa & 26°C	2.5	**622.20**	1.56	98.4	41.40	**420.70**
Step 5: 95 MPa & 26°C	1.1	**600.02**	0.66	97.3	40.74	**418.67**

Experiment 3 (MX80 no T) - continued						
	Volume of sample (mL)	*Conc in expelled water (mmol.L^{-1})*	*Number of mmol in expelled water*	*Volume remaining in clay (mL)*	*Number of mmol remaining in clay*	*Conc remaining in clay (mmol.L^{-1})*
K^{+}(0.96)						
Bidart Ocean water		**10.1**				
Initial pore fluid*	109.9	**9.71**	1.07		1.07	
Step 2: 65 MPa & 27°C	2.5	**8.14**	0.02	107.4	1.05	**9.75**
Step 2: 65 MPa & 27°C	2	**6.99**	0.01	105.4	1.03	**9.80**
Step 3: 75 MPa & 27°C	4.5	**5.77**	0.03	100.9	1.01	**9.98**
Step 4: 85 MPa & 26°C	2.5	**4.92**	0.01	98.4	0.99	**10.11**
Step 5: 95 MPa & 26°C	1.1	**4.61**	0.01	97.3	0.99	**10.17**
Ca^{2+} (1.27)						
Bidart Ocean water		**10.7**				
Initial pore fluid*	109.9	**9.78**	1.07		1.07	
Step 2: 65 MPa & 27°C	2.5	**33.86**	0.08	107.4	0.99	**9.22**
Step 2: 65 MPa & 27°C	2	**33.09**	0.07	105.4	0.92	**8.76**
Step 3: 75 MPa & 27°C	4.5	**28.76**	0.13	100.9	0.79	**7.87**
Step 4: 85 MPa & 26°C	2.5	**24.80**	0.06	98.4	0.73	**7.44**
Step 5: 95 MPa & 26°C	1.1	**22.99**	0.02	97.3	0.71	**7.26**
Mg^{2+}(0.96)						
Bidart Ocean water		**54.6**				
Initial pore fluid*	109.9	**50.61**	5.56		5.56	
Step 2: 65 MPa & 27°C	2.5	**41.48**	0.10	107.4	5.46	**50.82**
Step 2: 65 MPa & 27°C	2	**35.59**	0.07	105.4	5.39	**51.11**
Step 3: 75 MPa & 27°C	4.5	**29.07**	0.13	100.9	5.26	**52.09**
Step 4: 85 MPa & 26°C	2.5	**25.13**	0.06	98.4	5.19	**52.78**
Step 5: 95 MPa & 26°C	1.1	**23.18**	0.02	97.3	5.17	**53.11**

4.2.1- Major elements

Similar depletion of major cations occurs in the water expelled from the MX80 compaction in experiments 1 and 3 (MX80 no T) with consequent enrichment in the remaining pore water (Figure 19). Cation concentration changes in the expelled water, correlate well with the Cl^- + Br^- concentrations (Figure 20). For SSM compaction in experiment 2 major cations in the water expelled from the marl compaction showed no significant change in concentration with increasing pressure and temperature.

With the initial pore pressurization from 1.5 MPa to 45 MPa (step 0) the Na^+, K^+, and Mg^{2+} concentrations increase in the first expelled water, while the Ca^{2+} concentration initially reacts opposite to the other cations caused by re-equilibration between the DDL and free pore water under the sudden increase in pressure.

The trend of decreasing concentration with increasing pressure and temperature is then assumed. For experiment 1 (MX80) the Na^+ concentration changes from 538 mmol.L^{-1} in the initial re-equilibrated ocean water to 295 mmol.L^{-1} in the final expelled water sample. The Na^+ concentration in the water remaining in the pore pressure pump after the experiment, has slightly increased to 557 mmol.L^{-1}. For K^+ concentration changes from 8.4 mmol.L^{-1} in the initial re-equilibrated ocean water to 2.4 mmol.L^{-1} in the final expelled water sample.

The K^+ concentration in the water remaining in the pore pressure generator pump after the experiment, is 8.8 mmol.L^{-1}. Mg^{2+} decreases from 42.7 mmol.L^{-1} in the initial re-equilibrated ocean water to 9.4 mmol.L^{-1} in the final expelled water sample. The Mg^{2+} concentration in the water remaining in the pore pressure generator pump after the experiment, is 44.3 mmol.L^{-1}. Ca^{2+} decreases from 17.7 mmol.L^{-1} in the initial re-equilibrated ocean water to a final concentration of 8.3 mmol.L^{-1} in the final expelled water sample. The Ca^{2+} concentration in the water remaining in the pore pressure pump after the experiment, is 18.6 mmol.L^{-1}.

For experiment 3 (MX80 no T) the Na^+ concentration changes from 451 mmol.L^{-1} in the initial re-equilibrated ocean water to 600 mmol.L^{-1} in the final expelled water sample at vertical stress of 150 MPa. For K^+ concentration was 9.7 mmol.L^{-1} in the initial re-equilibrated ocean water and 4.6 mmol.L^{-1} in the final expelled water sample. Mg^{2+} was 50.6 mmol.L^{-1} in the initial re-equilibrated ocean water and 23.18 mmol.L^{-1} in the final expelled water sample. Ca^{2+} was 9.8 mmol.L^{-1} in the initial re-equilibrated ocean water and 22.9 mmol.L^{-1} in the final expelled water sample.

For experiment 2 (SSM) it is different in that no significant change in concentrations of any major cations is observed, therefore no cation exchange or adsorption occurs due to the low CEC. For Na^+ the concentration changes from 497 mmol.L^{-1} in the initial re-equilibrated ocean water to 521 mmol.L^{-1} in the final expelled water sample. The Na^+ concentration in the water remaining in the pore pressure pump after the experiment was completed, was 501 mmol.L^{-1}. For K^+ concentration was 12.3 mmol.L^{-1} in the initial re-equilibrated ocean water and 13.1 mmol.L^{-1} in the final expelled water sample. The K^+ concentration in the water remaining in the pore pressure pump after the experiment, is 11.9 mmol.L^{-1}. Mg^{2+} was 37.3 mmol.L^{-1} in the initial re-equilibrated ocean water and 40.6 mmol.L^{-1} in the final expelled water sample. The Mg^{2+} concentration in the water remaining in the pore pressure pump after the experiment, is 38.4 mmol.L^{-1}. Ca^{2+} was 25.9 mmol.L^{-1} in the initial re-equilibrated ocean water and 25 mmol.L^{-1} in the final expelled water sample. The Ca^{2+} concentration in the water remaining in the pore pressure pump post experiment, is 25.8 mmol.L^{-1}.

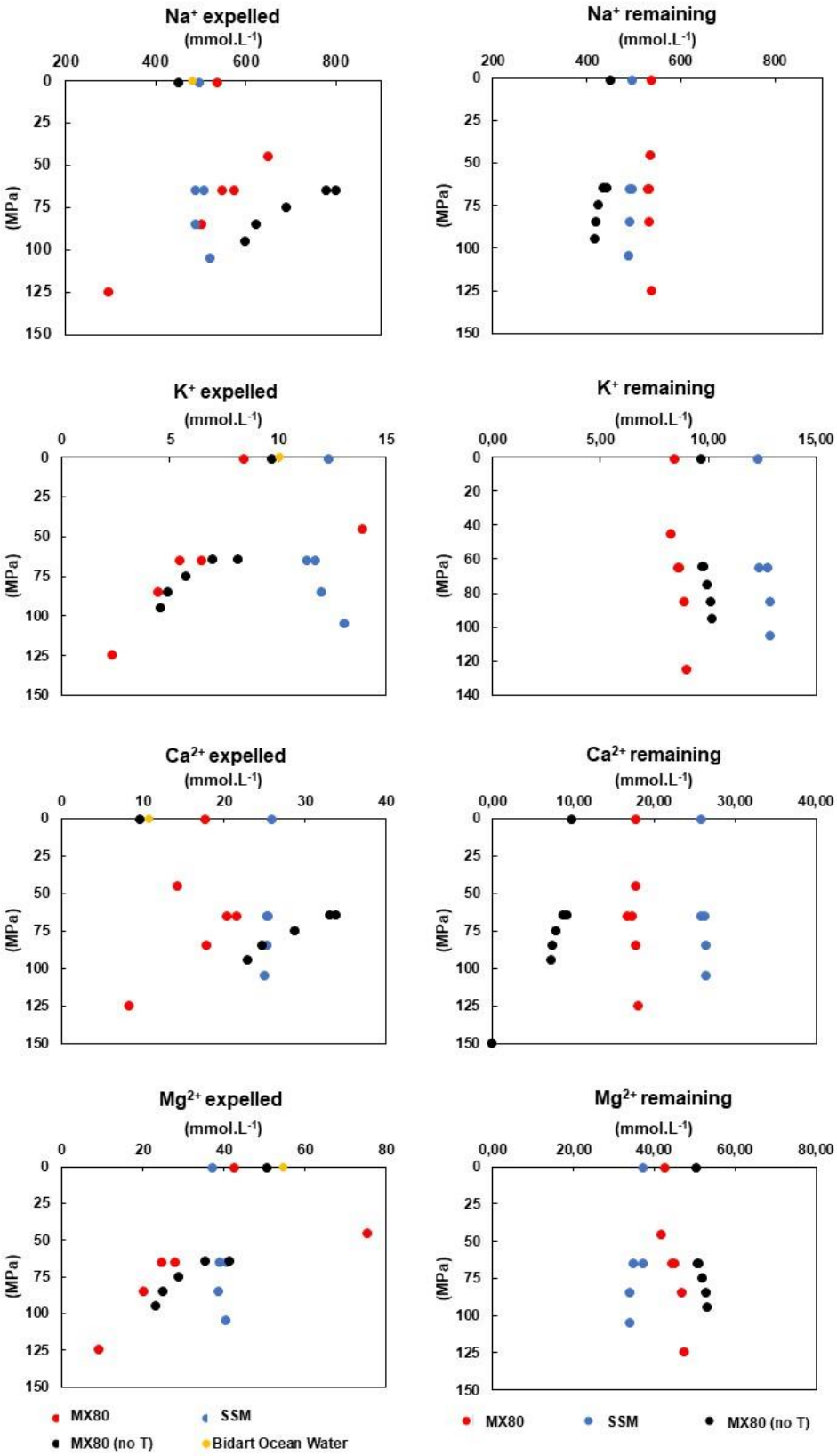


Figure 19: Variation in concentration of major cations in the expelled water and in the water remaining in the compacted clay (from mass balance calculation, see section 3.4.2) as pressure and temperature increase. The composition of the original ocean water is shown in orange, Experiment 1, 2 and 3 are in red, blue and black respectively.

Notice that the same mass balance presented for Cl and Br is also presented here for the major cations in Figure 19 and Table 5, Table 7 and Table 8. However since they are more sensitive to chemical reactions this calculated pore water composition will not be considered as part of the discussion.

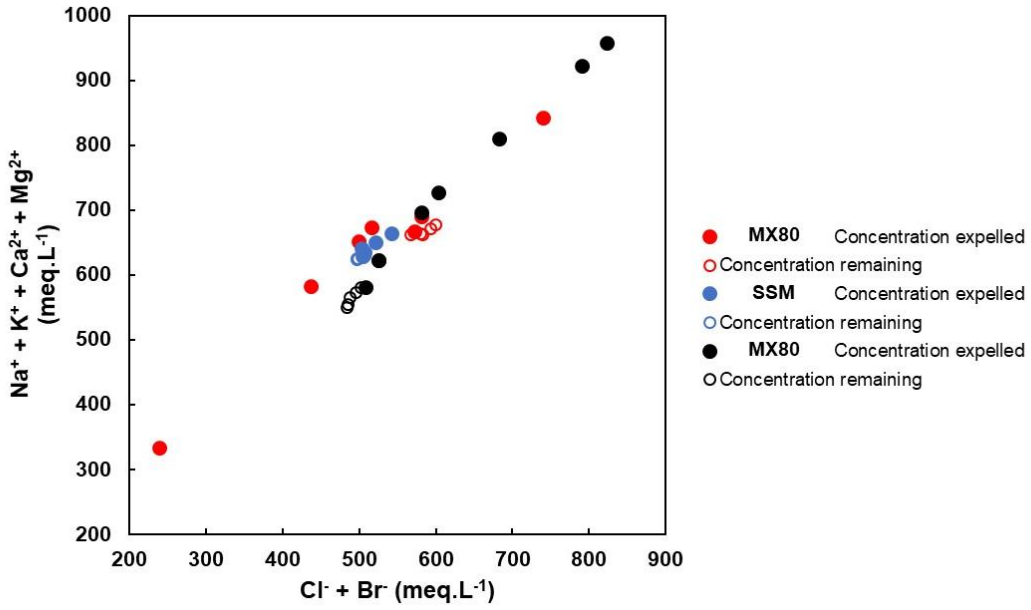


Figure 20 : Cation and corresponding anion concentrations of the water expelled during the three compaction experiments as well as for the calculated composition of the pore water remaining within the clay.

4.2.2- Cl and Br Isotopes

4.2.2.1- Chlorine

The range of isotope values obtained in the three compaction experiments falls within the expected range of values (Eggenkamp, 2014) as can be seen in Figure 21. $\delta^{37}Cl$ values are expected to fall, on average, within -8‰ to 1.5‰ and $\delta^{81}Br$ values are expected to fall between -1.5‰ and 4‰. From Figure 22 it is noteworthy that the lower the concentration of Cl is in the expelled water, the lower is the $\delta^{37}Cl$ value (this occurs for the higher vertical stresses).. The $\delta^{37}Cl$ of the initial Bidart ocean water is -0.12‰ (±0.02), not far from the standard mean ocean chlorides, or SMOC for at 0‰. After equilibration with the clays, the first notable Cl isotope fractionation occurred.

For experiment 1 (MX80) the $\delta^{37}Cl$ of the re-equilibrated ocean water has decreased to -0.2‰ (±0.01). For experiment 3 (MX80 no T) the $\delta^{37}Cl$ of the re-equilibrated ocean water has decreased to -0.06‰. Cl isotopes are not fractionated during compaction of the marl (experiment 2). The $\delta^{37}Cl$ values show little variation. It remains between 0.01 ‰ to -0.05 ‰.

The isotopic ratios calculated for Cl in the water remaining in the clay pores, slightly decrease during the MX80 compaction experiments (Table 10 and Table 16).

With pressurization to 45 MPa, $\delta^{37}Cl$ values reach 0.02‰ (±0.02) in the first water expelled during experiment 1 (MX80). The $\delta^{37}Cl$ values then decreased with increasing pressure and temperature. The fractionation that occurs at 65 MPa (step 1) is noteworthy in experiment 1 (MX80). As mentioned before, two samples were collected during this step. In the first water expelled at 65 MPa, the $\delta^{37}Cl$ was -0.24‰ (±0.03). After 14 days at the same pressure and temperature conditions, the $\delta^{37}Cl$ value has decreased to -0.45‰ (±0.03), as can be seen in Figure 24 Following the fractionation at 65 MPa and 30°C, no more significant fractionation occurred in the water expelled during experiment 1 (MX80).

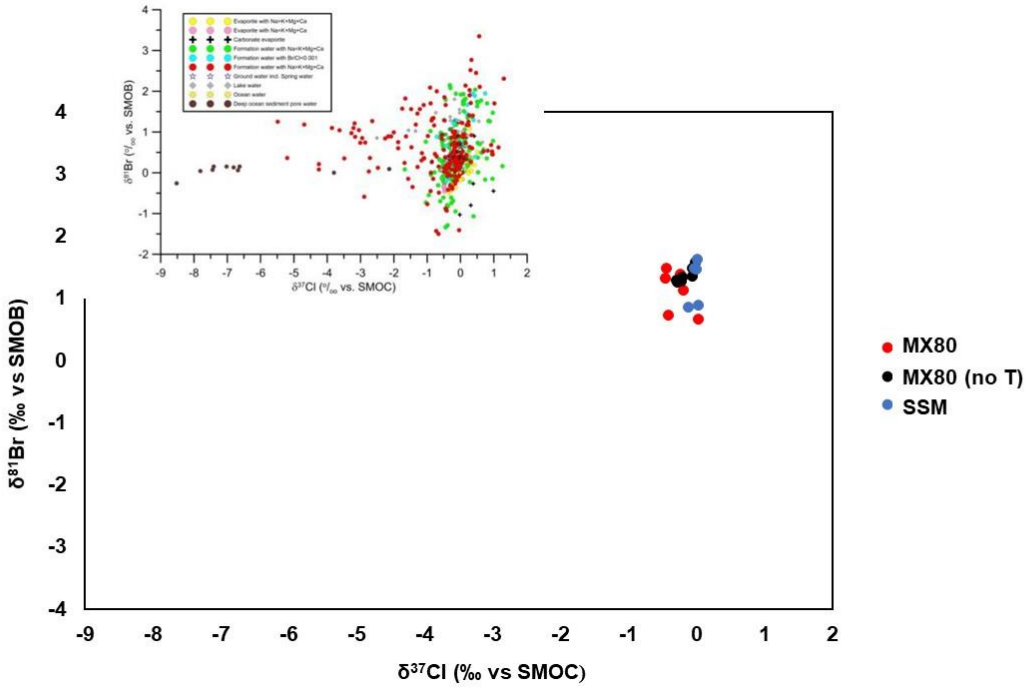


Figure 21: Values for the isotopes of Cl and Br plot within the expected range of values of -8‰ to 1.5‰ for $\delta^{37}Cl$ and -1.5‰ to 4‰ for $\delta^{81}Br$, as presented on the inserted figure from Eggenkamp (2014).

For experiment 3 (MX80 no T) the $\delta^{37}Cl$ values then decreased to 0.2‰ in the first expelled water when the vertical stress is increased to 65 MPa (step 1). Remember that two samples were also collected during step 1. After 3 days at the same pressure and temperature conditions, the $\delta^{37}Cl$ value at 0.2‰ has not changed (Figure 26 and Table 15). At 75 MPa, the $\delta^{37}Cl$ value further decreased to -0.3‰. With the increase in vertical stress to 85 MPa, the $\delta^{37}Cl$ value shifts to -0.06‰. Thereafter the value returns to -0.3 ‰ in the water expelled at 95 MPa.

The $\delta^{37}Cl$ value in the water remaining in the pore pressure pump after experiment 1 (MX80), was -0.24‰ (±0.01) (from -0.2‰). For experiments 2 and 3 the $\delta^{37}Cl$ value in the water remaining in the pore pressure pump after the experiment, are not known.

4.2.2.2- Bromine

Regarding Br isotopes, two important observations can be seen from Figure 24. Firstly, the range of Br fractionation observed, is larger than the range of fractionation of Cl and secondly, $\delta^{37}Cl$ values are negatively correlated with the $\delta^{81}Br$ (also see Figure 22 and Figure 23). However, during marl compaction, the range of Br isotope fractionation that occurs shows a similar range as observed during MX80 compactions (Figure 23 and Figure 25). Lastly, for experiment 3 (MX80 no T) the negative correlation between $\delta^{37}Cl$ and the $\delta^{81}Br$ observed in experiment 1, does not repeat (Figure 21).

The initial Bidart ocean water has a $\delta^{81}Br$ value of 0.86‰ (±0.07). As for Cl, the first significant fractionation of Br is also observed after the equilibration with the clays. The $\delta^{81}Br$ of the ocean water has increased to 1.14‰ (±0.01), meaning the fluid has become enriched in the heavier isotope, for Experiment 1. During the marl compaction (experiment 2), the $\delta^{81}Br$ value changes from 0.86‰ (±0.07) in the Bidart ocean water to 1.02‰ (±0.12) after it has been re-equilibrated with the clay. After the equilibration with MX80 in experiment 3, the first significant fractionation was observed. The $\delta^{81}Br$ of the ocean water has increased to 1.6‰ (±0.06).

With pressurization to 45 MPa in experiment 1, the $\delta^{81}Br$ measurement inversely shifts to 0.67‰ (±0.12). The significant fractionation of Cl isotopes that is observed for the two samples collected during the step at 65 MPa & 30°C in experiment 1, is not seen for Br. The $\delta^{81}Br$ value for the first sample at these conditions was 1.38‰ (±0.05) and for the next, 14 days later, was 1.33‰ (±0.14). When compaction of the MX80 progresses, the $\delta^{81}Br$ values continue to increase up to 1.5‰ (±0.01) at 85 MPa & 60°C before it decreases to 0.7‰ (±0.22) in the water expelled at 125 MPa & 120°C. The $\delta^{81}Br$ in the water remaining in the pore pressure generator pump at the end of experiment 1, was 1.1‰ (±0.04) (from 1.14‰).

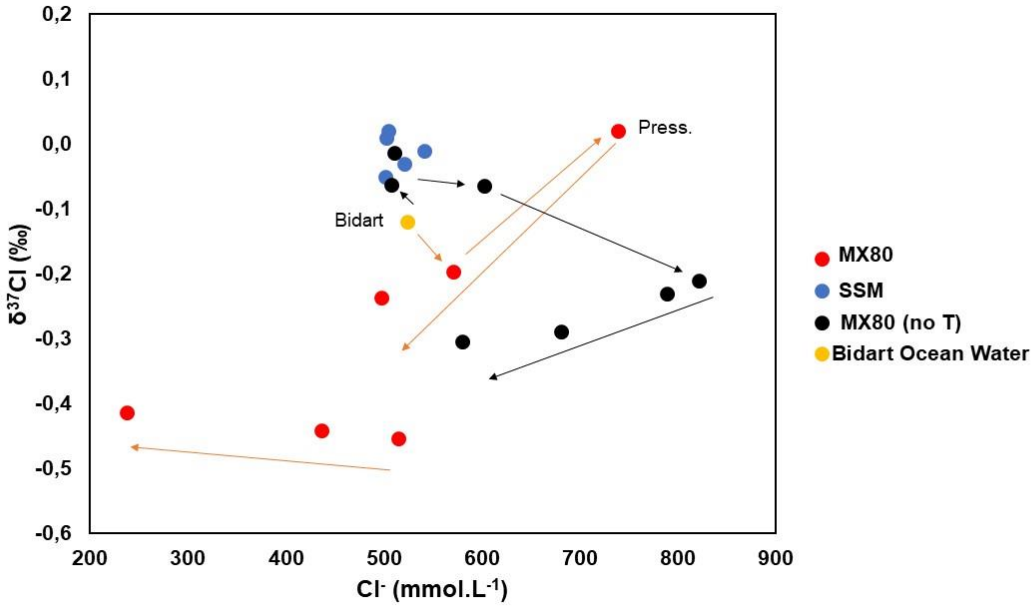


Figure 22 : The Cl isotope values plotted against the corresponding anion concentration for the water expelled during MX-80 (Experiment 1 & 3) and Sainte-Suzanne marl (Experiment 2) compaction.

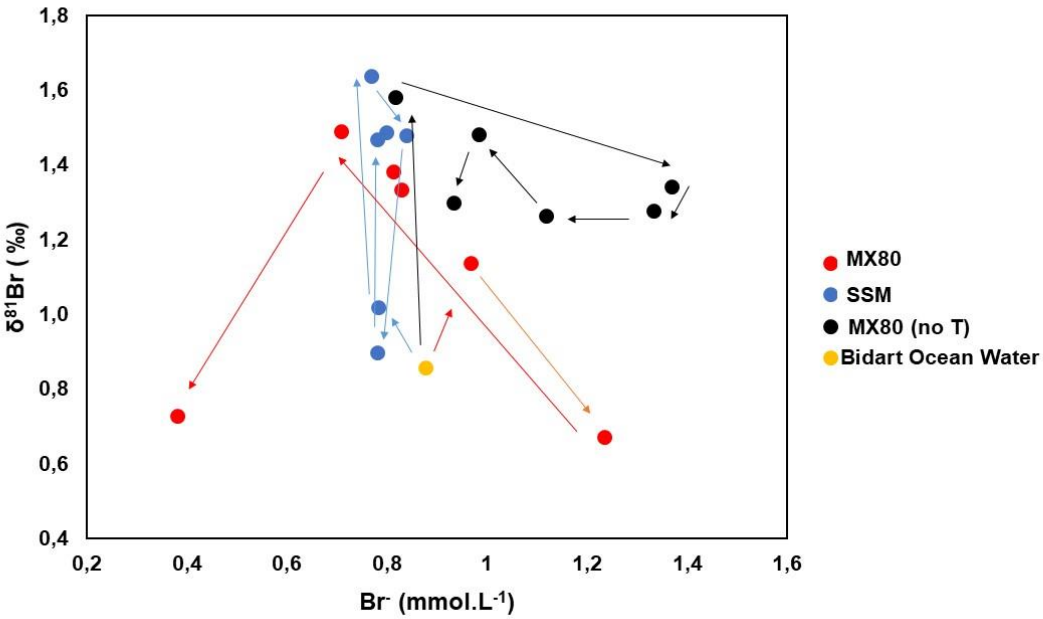


Figure 23: The Br isotope values plotted against the corresponding anion concentration for the water expelled during MX-80 (experiment 1 & 3) and Sainte-Suzanne marl (experiment 2) compaction.

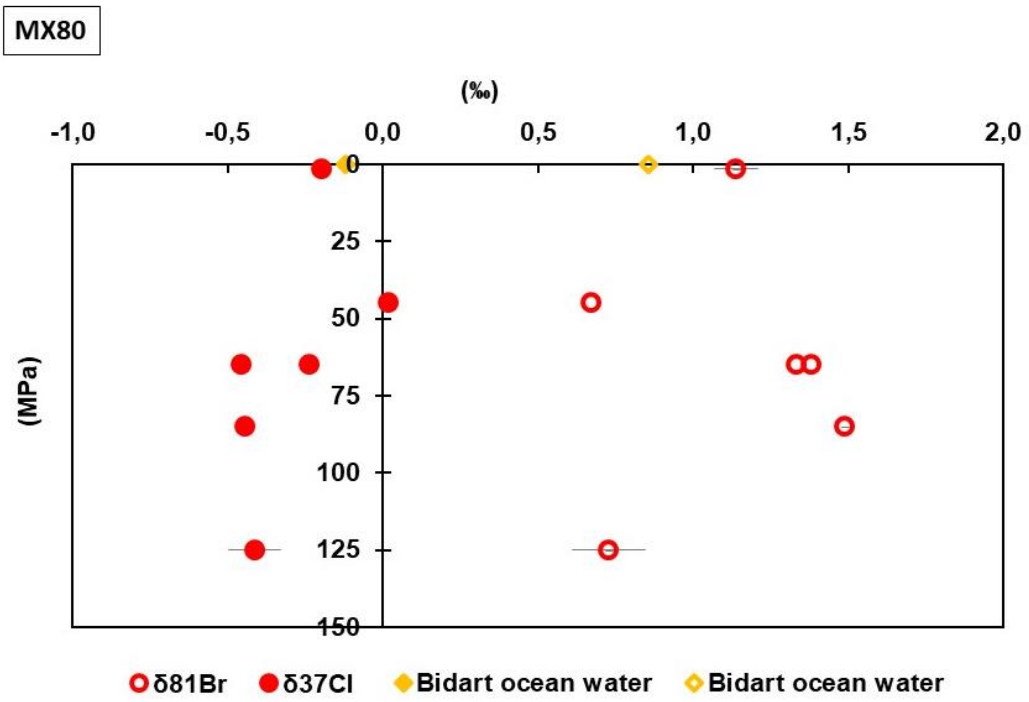


Figure 24: The range of Cl and Br isotopic fractionation observed in the water expelled during MX-80 compaction in Experiment 1. Colored circles represent $\delta^{37}Cl$ values and empty circles represent $\delta^{81}Br$ values. The colored and empty diamond represent the initial ocean water $\delta^{37}Cl$ and $\delta^{81}Br$ values respectively.

Table 9: Isotope values for the water expelled during Experiment 1.

	$\delta^{37}Cl$ (‰)	stdev	**$\delta^{81}Br$ (‰)**	stdev
Bidart ocean water	-0.12	0.02	0.86	0.07
Re-equilibrated water after circulation	-0.20	*	1.14	0.01
Pressurisation to 45.5 MPa	0.02	*	0.67	0.112
Step 1: Pressurisation to 65 MPa/30°C	-0.24	0.03	1.38	0.05
Step 1: Pressurisation to 65 MPa/30°C	-0.45	0.03	1.33	0.14
Step 2: Pressurisation to 85 MPa/60°C	-0.44	0.02	1.49	0.1
Step 4: Pressurisation to 125 MPa/120°C	-0.41	0.08	0.73	0.22
Water remaining in the pore pressure pump after experiment				

*In the case where only one sample could be measured and therefore no standard deviation determined either for technical reasons or not enough sample.

Table 10: Cl isotope mass balance to compute the isotopic composition of Cl trapped in MX-80 in Experiment 1.

	δ^{37}Cl (‰)	**Conc (mmol.L^{-1})**	**mmol expelled**	**35Cl expelled**	**37Cl expelled**	**35Cl remain**	**37Cl remain**	**δ^{37}Cl (‰) remain**	*Alpha (expelled-remaining)*
Bidart Ocean water	**-0.12**	570		433.21	136.79				
Re-equilibrated water	**-0.2**	570.70	54.96	41.77	13.19				
1st sample	**0.02**	738.64	2.06	1.57	0.49	40.21	12.69	**-0.21**	1.00001
2nd sample	**-0.24**	497.79	8.18	6.22	1.96	33.99	10.73	**-0.20**	1.00022
3rd sample	**-0.45**	514.61	1.38	1.05	0.33	32.94	10.40	**-0.19**	0.99995
4th sample	**-0.44**	436.26	2.41	1.83	0.58	31.10	9.82	**-0.18**	0.99973
5th sample	**-0.41**	238.17	0.36	0.27	0.09	30.83	9.74	**-0.18**	0.99974

Table 11: Br isotope mass balance to compute the isotopic composition of Cl trapped in MX-80 in Experiment 1.

	δ^{81}Br (‰)	**Conc (mmol.L^{-1})**	**mmol expelled**	**79Br expelled**	**81Br expelled**	**79Br remain**	**81Br remain**	**δ^{81}Br (‰) remain**	*Alpha (expelled-remaining)*
Bidart Ocean water	**0.86**	0.88		0.45	0.43				
Re-equilibrated water	**1.14**	0.97	0.0932	0.0475	0.0457				
1st sample	**0.67**	1.24	0.0034	0.0018	0.0017	0.046	0.0440	**1.16**	0.99998
2nd sample	**1.38**	0.81	0.0134	0.0068	0.0066	0.039	0.0375	**1.12**	0.99955
3rd sample	**1.33**	0.83	0.0022	0.0011	0.0011	0.038	0.0364	**1.11**	1.00027
4th sample	**1.49**	0.71	0.0039	0.0020	0.0019	0.036	0.0345	**1.09**	1.00024
5th sample	**0.73**	0.38	0.0006	0.0003	0.0003	0.036	0.0342	**1.09**	1.00039

For experiment 2 (SSM) a significant shift to 1.6 ‰ (±0.12) is observed in the water expelled at 65 MPa and 30°C. In the second sample collected at the same pressure and temperature conditions, 14 days later, the δ^{81}Br is 1.5‰ (±0.12). At 85 MP and 90°C, the δ^{81}Br value decreases suddenly to 0.9‰ (±0.07) before the value increases back to 1.5‰ (±0.10) in the last expelled water collected during Experiment 2 (SSM). Another important point to note from Table 12is the fractionation of Br that occurred in the ocean water that remained in the pore pressure generator pump after experiment 2 has been completed. The δ^{81}Br in the pore pressure generator pump increased to 1.5‰ (±0.11) (from 1.02‰).

For experiment 3 (MX80 no T), in the first water expelled with pressurization to 65 MPa the measurement does not change. After 3 more days at the same pressure and temperature conditions, the δ^{81}Br remains at 1.3‰ (±0.03). The δ^{81}Br value for the water expelled at 85MPa slightly increases to 1.5 ‰ (±0.2). A significant shift to 0.6‰ (±0.02) in δ^{81}Br value occurs in the water expelled under vertical stress of 150 MPa. The δ^{81}Br in the water remaining in the pore pressure generator pump at the end of experiment 3 (MX80 no T) was 0.6‰ (±0.02) (from 1.6‰).

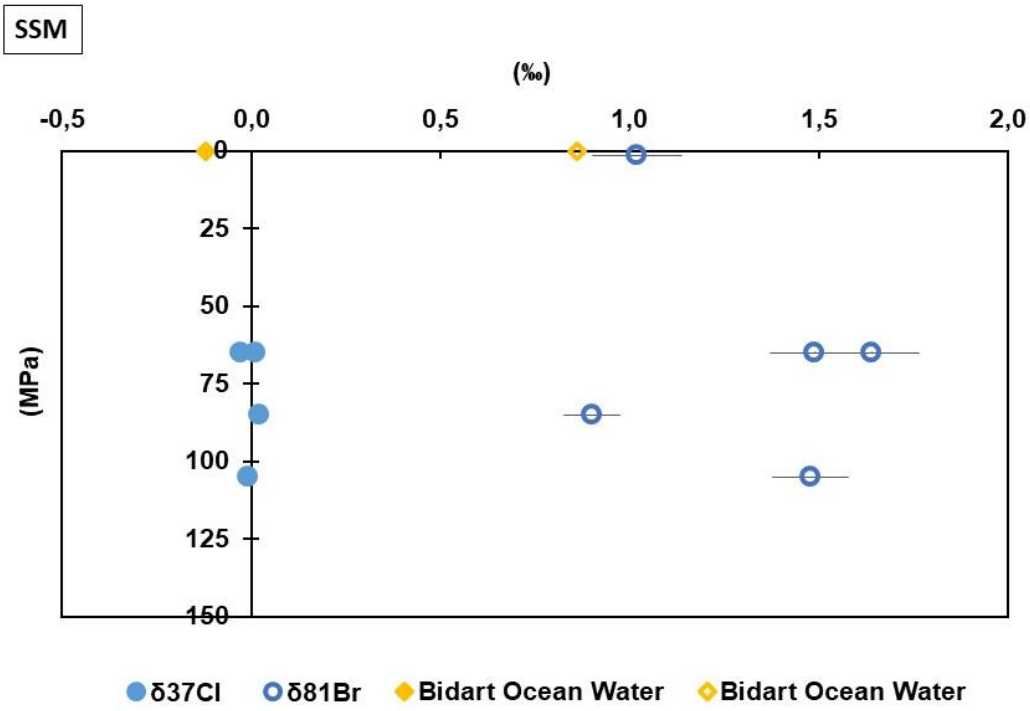


Figure 25: The range of Cl and Br isotopic fractionation observed in the water expelled during Sainte-Suzanne marl compaction in experiment 2. Colored circles represent δ37Cl values and empty circles represent δ81Br values. The colored and empty diamond represent the initial ocean water δ37Cl and δ81Br values respectively.

Table 12: Isotope values for the water expelled during Experiment 2 (SSM).

	$\delta^{37}Cl$	stdev	$\delta^{81}Br$	stdev
Bidart ocean water	-0.12		0.86	0.07
Re-equilibrated after circulation	-		1.02	0.12
Step 1 : 65 Mpa/30°C	0.01		1.64	0.12
Step 1 : 65 Mpa/30°C	-0.03		1.49	0.12
Step 2: 85 Mpa/60°C	0.02		0.90	0.07
Step 4 : 105 Mpa/120°C	-0.01		1.48	0.10
Water remaining in the pore pressure pump after experiment			1.5	

Table 13: Cl isotope mass balance to compute the isotopic composition of Cl trapped in Sainte-Suzanne marl in experiment 2.

	$\delta^{37}Cl$ (‰)	Conc ($mmol.L^{-1}$)	mmol expelled	35Cl expelled	37Cl expelled	35Cl remaining	37Cl remaining	$\delta^{37}Cl$ (‰) remaining	*Alpha (expelled-remaining)*
Bidart Ocean water	-0.12	570							
Re-equilibrated water	*	506.44	54.44						
1st sample	0.01	503.12	1.95						
2nd sample	-0.03	520.63	20.82						
3rd sample	0.02	504.30	5.65						
4th sample	-0.01	541.17	0.67						

***The $\delta^{37}Cl$ value of the re-equilibrated water could not be determined due to technical constraints, the $\delta^{37}Cl$ and α values for the remaining pore water could not be calculated.**

Table 14: Br isotope mass balance to compute the isotopic composition of Br trapped in Sainte-Suzanne marl in Experiment 2 (SSM).

	δ ^{81}Br (‰)	Conc (mmol.L^{-1})	mmol expelled	79Br expelled	81Br expelled	79Br remaining	81Br remaining	δ^{81}Br (‰) remaining	*Alpha (expelled-remaining)*
Bidart Ocean water	0.86	0.88		0.4486	0.4314				
Re-equilibrated water	1.02	0.782	0.084	0.0429	0.0412				
1st sample	1.64	0.769	0.003	0.0015	0.0015	0.0413	0.0398	1.00	1.0000227
2nd sample	1.49	0.798	0.032	0.0163	0.0156	0.0251	0.0241	0.68	1.0009616
3rd sample	0.9	0.781	0.009	0.0045	0.0043	0.0206	0.0198	0.63	1.0008597
4th sample	1.48	0.838	0.001	0.0005	0.0005	0.0201	0.0193	0.61	1.0002925

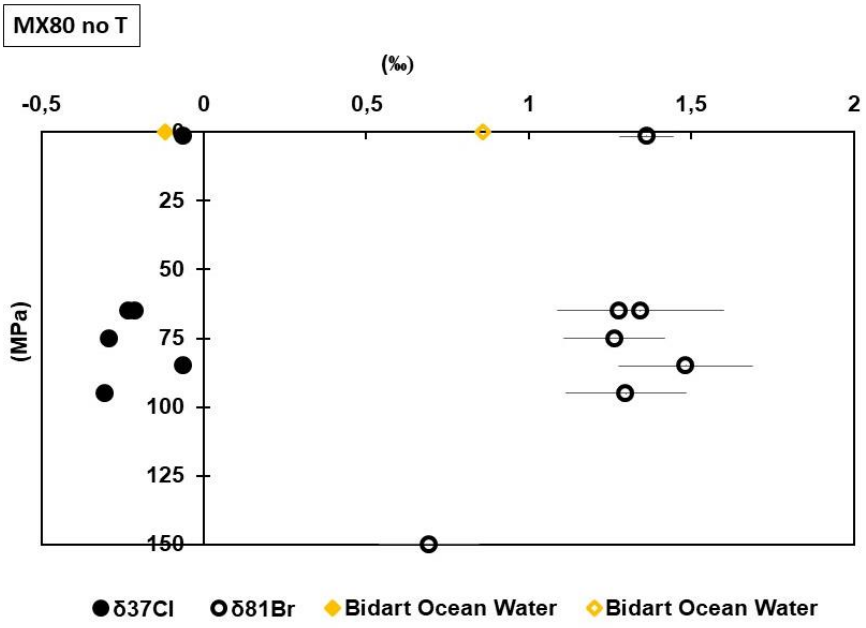


Figure 26 : The range of Cl and Br isotopic fractionation observed in the water expelled during Sainte-Suzanne marl compaction in experiment 2. Colored circles represent δ^{37}Cl values and empty circles represent δ^{81}Br values. The colored and empty diamond represent the initial ocean water δ^{37}Cl and δ^{81}Br values respectively.

Table 15: Isotope values for the water expelled during Experiment 3 (MX80 no T).

Experiment 3	**δ^{37}Cl**	stdev	**δ^{81}Br**	stdev
Bidart ocean water	-0.12		0.86	
Re-equilibrated after circulation	-0.013	0.02	1.58	0.06
Step 1: 65 MPa	-0.21		1.34	0.26
Step 1 : 65 MPa	-0.23		1.28	0.03
Step 2 :75 MPa	-0.30		1.26	0.16
Step 3 : 85 MPa	-0.06		1.48	0.21
Step 4 : 95 MPa	-0.31		1.30	0.18
Step 10 : 150 MPa			0.69	0.15
Water remaining in the pore pressure pump after experiment			0.61	0.02

Table 16: Cl isotope mass balance to compute the isotopic composition of Cl trapped in MX-80 in Experiment 3 (MX80 no T).

	$\delta^{37}Cl$ (‰)	Conc ($mmol.L^{-1}$)	mmol expelled	35Cl expelled	37Cl expelled	35Cl remaining	37Cl remaining	$\delta^{37}Cl$ (‰) remaining
Bidart Ocean water	-0.12	570		398.25	125.75			
Re-equilibrated water	-0.013	507.65	55.79	42.40	13.39			
1st sample	-0.21	821.66	2.05	1.56	0.49	40.84	12.90	-0.01
2nd sample	-0.23	789.42	1.58	1.20	0.38	39.64	12.52	0.00
3rd sample	-0.3	681.34	3.07	2.33	0.74	37.31	11.78	0.02
4th sample	-0.06	602.79	1.51	1.15	0.36	36.16	11.42	0.02
	-0.31	580.26	0.64	0.49	0.15	35.68	11.27	0.03

Table 17 : Br isotope mass balance to compute the isotopic composition of Br trapped in MX-80 in Experiment 3 (MX80 no T).

	$\delta^{81}Br$ (‰)	Conc ($mmol.L^{-1}$)	mmol expelled	79Br expelled	81Br expelled	79Br remaining	81Br remaining	$\delta^{81}Br$ (‰) remaining
Bidart Ocean water	0.86	0.88		0.4486	0.4314			
Re-equilibrated water	1.58	0.81	0.089	0.0454	0.0437	0.0437		
1st sample	1.34	1.37	0.003	0.0017	0.0017	0.0423	0.0421	1.59
2nd sample	1.28	1.33	0.003	0.0014	0.0013	0.0398	0.0408	1.60
3rd sample	1.26	1.12	0.005	0.0026	0.0025	0.0385	0.0383	1.62
4th sample	1.48	0.98	0.002	0.0013	0.0012	0.0380	0.0371	1.63
	1.3	0.93	0.001	0.0005	0.0005		0.0366	1.63
	0.69							

4.3- WATER CHEMISTRY MODELLING

4.3.1- PHREEQC

The geochemical modelling of the MX80 system shows the following mineralogical transformations: gypsum and phlogopite are entirely dissolved and 20% of the carbon disappears to reduce a few quantity of sulfates to give pyrite. The most important transformation concerns smectite with 27% being transformed in albite, kaolinite and montmorillonite high charge Na in the initial steps of the experiment. However, with increasing temperature, smectite tends to stabilize and the reactions are reversed. First, the pH decreases all along the experiment with the increase of T. Sulfur is immediately consumed to give pyrite, potassium is incorporated in microcline. The smectite dissolution liberates Na which is mostly incorporated in albite and montmorillonite. Calcium is controlled by the equilibrium with calcite. Magnesium incorporates the structure of montmorillonite. The last step at 150°C partially destabilizes the montomorillonite and the microcline to give smectite leading to an increasing concentration of potassium, calcium and magnesium and a drop of the sodium content.

The modeling of the SSM experiment shows very limited mineralogical transformation, even at 150°C. The only visible dissolution is that of anorthite with a resulting precipitation of small amounts of albite and clinochlore. The influence on the chemistry of the solution is marked through the sodium concentration which strongly decreases at low temperature, together with magnesium and potassium. Calcium content increases in the solution due to anorthite dissolution. The pH continuously decreases with the increase of temperature.

As expected, chlorine doesn’t play a role in the geochemical reactions of both experiments since no secondary mineral contains it.

The geochemical modelling of both MX80 and SSM experiments show that even if the mineralogical transformations are limited, a significant evolution of the chemical composition of the solution can occur especially for alkaline and alkaline-earth elements. As expected, the halogens, not incorporated in secondary minerals, are not impacted.

4.3.2- SURP

4.3.2.1- Water expelled due to smectite dehydration

The main result of the SURP modeling was to compute what proportion of the water expelled could be due to smectite mineral dehydration. The cumulative volume of water generated due to smectite dehydration was 7.6 ml. The modeled experiment shows that the largest amount of water released due to smectite dehydration occurred at the beginning of a compaction step followed by a period where no water was released or water was consumed.

During the pore pressurization step 0, 2.8 mL of pore fluid was expelled from the clay during the compaction experiment 1 (MX80). From the modeling, a total of 1.88 mL was was shown to be released due to smectite mineral dehydration. This volume comprised 1.82 mL that is immediately released and excessively small volumes of water, <0.001 mL, continuously released during the step. The water released and expelled at this step is likely the result of immediately reducing the number of adsorbed water layers through mechanical compaction. During the 15 days spent at 65 MPa & 30°C (step1), 19.1 mL of fluid was expelled from the clay, but only 0.57 mL was modeled to be due to thermodynamic mineral transformations. Increasing the pressure to 85 MPa and the temperature to 60 °C, 5.5 mL of fluid was expelled from the clay. According to the modeling, 2.17 mL was produced due to smectite dehydration during the 12 days at this step.

The dissolution of smectite and precipitation of illite normally occurs between 70 – 100°C. During step 3 (105 MPa & 90 °C for 17 days) the volume of water produced by thermodynamic transformations added up to 0.91 ml. An initial volume of 0.98 mL was produced but this was followed by consumption of excessively small volumes of water and then consequent release of excessively small volumes of water (<0.001 mL). However,during the experiment, no water was actually expelled from the clay during this step.

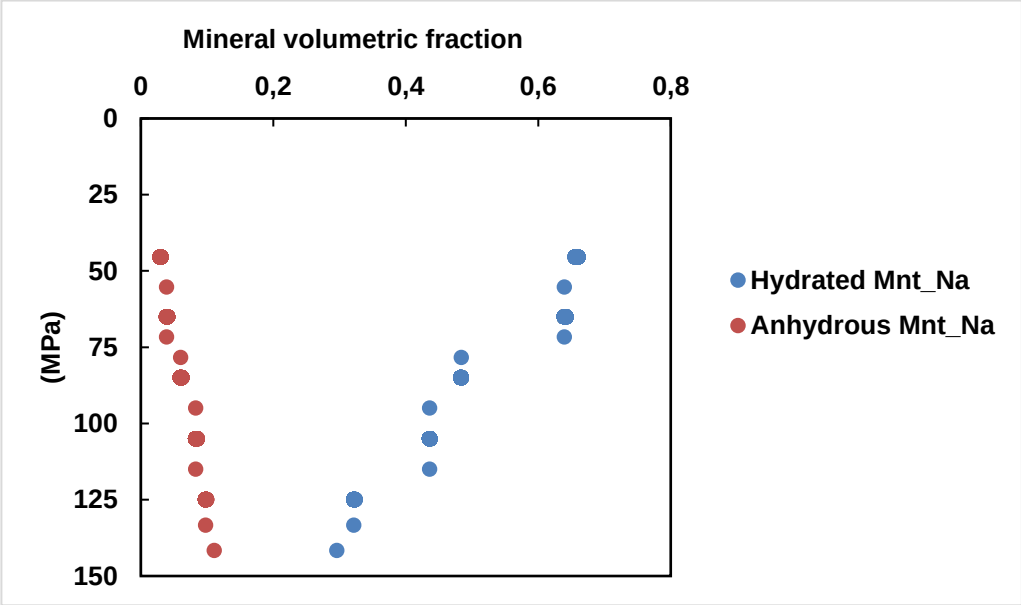


Figure 27: Simulate mineralogical profile showing hydrated Mnt Na (3w 2w or 1w Na montmorillonite) and anhydrous Na-Montmorillonite.

During step 4, with the pressure at 125 MPa and the temperature at 120°C for 22 days, the volume of water released as a result of smectite dehydration was 1.87 mL while 1.5 mL was expelled from the clay during the experiment. During the final experimental step 5 at 150 MPa and 150°C for 18 days, 0.003mL of water was actually consumed. It is expected that between 120 -140 °C, the

dissolution of kaolinite & K feldspar occurs as well as precipitation of illite and extensive quartz cementation.

Following 90 days of fluid circulation (step 0), it is assumed that that the smectite clay minerals are all fully hydrated at the start of the compaction experiment. We see that the volumetric proportion of hydrated smectite decreases with each compaction step (Figure 27). Simultaneously the volumetric proportion of anhydrous smectite increases steadily during the compaction experiment, fourfold. The hydrated proportion includes three, two and one adsorbed water layer. Only the dehydration of smectite is expressed through the SURP modeling. The transformation to illite is not expressed.

4.3.2.2- Anion inaccessible porosity

We calculated the proportion of pore space that would be affected by the anion exclusion effect. That is, the percentage pore size reduction due to anion exclusion. Step 1 was to calculate the hypothetical remaining pore water composition for each of the compaction steps. A mass-balance approach was used (Equation 1). The total moles input into the cell was then compared to the total moles that were collected during the experiment for each compaction step within the cell to estimate the composition of the remaining pore water.

(19)

$$\sum Moles_{In} - \sum Moles_{Out} = Remaining$$

From the ionic strength in mol/kg water (Equation 2) of the remaining pore water, the Debey length in nm (Equqtion 3) for each compaction step was calculated.

(20)

$$I = \frac{1}{2}\sum_{i} c_i z_i^2$$

Where c_i is the concentration of i^{th} species and z_i is the charge on the i^{th} species.

(21)

$$= \frac{0.304}{\sqrt{I}}$$

The average half distance between clay platelets (b), in Å, (i.e. pore throat diameter) can be calculated according to Equation 4 (Neuzil & Provost, 2009).

(22)

$$b = \frac{n}{A0\rho s(1-n)}$$

Where n is porosity and ρs is the mean solid grain density and A0 is the osmotic specific surface area in. A0 is an expression of the the measure of mineral surface area exerting control of solute transport (Neuzil & Provost, 2009; Neuzil, 2017) A0 can be considered invariant during compaction.

If we assume that all anions are excluded from the Debey layer, subtracting the Debey length from the half pore size, we end up with the free water proportion of the pore. That is the anion containing proportion, for one half of the total pore size.

Table 18: Calculated anion exclusion effect a percentage pore size reduction (proportion of pore size that is not available to anions).

Pressure Temperature	Ionic strength (mol/kgw)	Debey Length (nm)	Calculated (half) pore size (nm)	Freewater portion (half) (nm)	% pore size reduction due to anion exclusion
		(0.304/√I)	b=n/A0ρs(1-n)	(Anion containing portion)	
Bidart ocean water	6.20E-01	0.386	NA		
Re-equilibrated water	6.48E-01	0.376	9.43	9.06	4.00
45 MPa	6.43E-01	0.379	8.56	8.18	4.43
65 MPa & 30°C	6.53E-01	0.376	7.86	7.48	4.79
65 MPa & 30°C	6.53E-01	0.376	5.97	5.59	6.30
85 MPa & 60°C	6.65E-01	0.373	5.35	4.97	6.97
125 MPa & 120°C	6.74E-01	0.370	4.32	3.95	8.58

**In our compaction experiment, we see that the ionic strength of the pore water slightly increases with increasing compaction. However, the increasing ionic strength does not influence the Debey length noticeably (0.39 – 0.37nm). Decreasing the Debey length thickness can result in the effective anion available porosity increasing as thoroughly explained in Wigger & Van Loon (2017). What we do observe is that as the porosity decreases with increasing compaction, and the Debey length remains fairly constant, the proportion of the sore space that is unavailable to anions doubles through the compaction experiment.

4.3.2.3- Filtration efficiency

We also calculated the membrane efficiency for the MX80. That is how effectively the MX80 would filter out Cl and Br from the ocean water respectively . When *b*, the nominal half distance between clay surfaces (in Å) is known, the membrane efficiency (σ) of a clay-rich media can be determined through the Kemp-Bresler model (Figure 28) (Bresler, 1973; Neuzil & Provost, 2009; Neuzil and Person, 2017). This offers a way to characterize a clay medium's overall effectiveness as a filtration membrane for a particular chemical species. The σ is represented as a function of b√c of the relevant species, where c is its concentration in normality. If σ=1.0, the membrane is perfect and rejects all dissolved solutes. If σ=0, there is no solute rejection.

Table 19: Determining the membrane efficiency of MX-80 as filtration membrane.

	b√[Cl^-]	b√[Br^-]
Re-equilibrated ocean water	71.27	2.94
45 MPa	64.41	2.65
65 Mpa & 30°C	59.83	2.47
65 Mpa & 30°C	45.60	1.89
85 Mpa & 60°C	41.21	1.71
125 Mpa & 120°C	33.51	1.39

Considering the Kemp-Bresler model the membrane efficiency σ for Cl^- < 0.003 and the membrane efficiency (σ) for Br^- > 0.8. Br- is much more efficiently filtered by the MX-80 clay than Cl- due to the large difference in their respective concentrations. We see that with increasing compaction that the membrane efficiency increases for both Br^- and Cl^-.

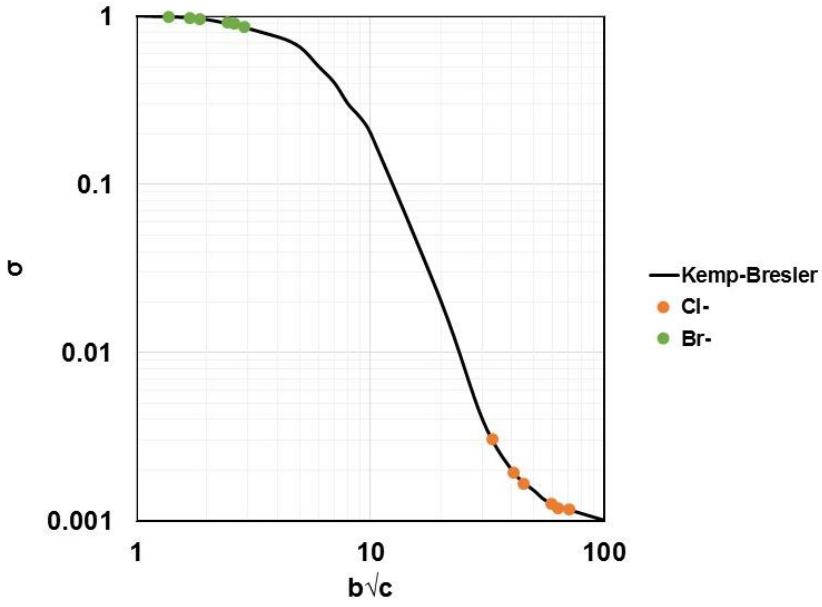


Figure 28: The membrane efficiency of compacting MX80 for Cl and Br respectively, according to the Kemp- Bresler model (Bresler, 1973).

4.4- THE SOLID MATERIAL CHARACTERIZATION OF THE COMPACTED CLAYS

4.4.1- Physical characterization

Due to a corrosion spot that developed during the first experiment, more material had to be used during the second and third experiments to ensure that the corrosion spot was covered by the volume of clay under maximum compaction. Because of different input mass and slightly different apparent density for the two clay materials, there is a significant difference in mass and height of the solidified core obtained from inside the compaction cell, after compaction. The weights after compaction, shown in Table 20, are due to some material that was lost as dust, from the process of drilling the core out of the compaction cell. No water was used to drill the cores out.

As the starting masses were not equal, the calculated bulk density is a better indicator of the degree of compaction. The heights, weights, percentage compaction, and bulk densities are in Table 20.

In both cases, the MX-80 was more densely compacted than the marl. During Experiment 1 (MX80) the bulk density increased from 1.02 g/cm^3 to 2.15 g/cm^3., and for Experiment 3 (MX80 no T) the clay was compacted to a bulk dry density of 2.09 g/cm^3. For the compaction of the marl in Experiment 2, a bulk dry density of 1.8 g/cm^3 was achieved due to the lower material density.

Table 20: Description of the materials for each of the experiments.

	Experiment 1 (MX80)		**Experiment 2 (SSM)**		**Experiment 3 (MX80 no T)**	
	Before	**After**	**Before**	**After**	**Before**	**After**
Mass (g)	450	354.9	550	414	500	318.88
Height (cm)	4.8	2.1	5.7	2.8	5.2	2.9
Bulk density (g/cm^3)	1.19	1.69	1.17	2.03	1.2	2.18
% Compaction		42		47		44
CEC (mEq.100g^{-1})	69.8	76.7	9.8	9.8	69.8	72.4

For the experiments with MX-80, an increase in CEC occurs. For Experiment 1 (MX80) the CEC increases from 69.8 mEq.100g^{-1} to 76.7 mEq.100g^{-1}. For Experiment 3 (MX80 no T) the CEC of the MX-80 increased as well, from 69.8 mEq.100g^{-1} to 72.4 mEq.100g^{-1}. This could indicate that there have been changes to the clay mineral surfaces. For the marl compaction, there was no change in the CEC.

4.4.2- Volumetric water content (Thermogravimetry)

For experiment 1 (MX80), the initial water content was 11% (wt) at the start of the experiment. After the compaction experiment the core had lost 7.5% of its weight due to the loss of water when heated to 65°C and at 350°C it sample had lost 13.3% of its weight. Following the experiment, the sample retained more moisture than was present in the original clay at the start of experiment 1 (13% (wt) vs 11% (wt). For experiment 2 (SSM) the initial water content at 65°C was 1.3% (wt). At 350°C it sample had lost 8.4% of its weight due to the loss of water. For Experiment 3 (MX80 no T), the compacted core sample lost 1.9% of its weight due to the loss of water when heated to 65°C and at 350°C the sample had lost 8.4% of its weight.

4.4.3- Porosity

4.4.3.1- MIP

After 200 days of compaction for experiment 1 (MX80) the mercury connected porosity, free porosity and trapped porosity of the post-experiment compacted cores were found to be 17%, 8%, and 9%, respectively (Figure 31). Then, a large proportion (53%) of the porosity is trapped. These are pores that no longer have a continuous path towards the sample surface. Intrusion of mercury into a cavity is controlled by the size of the pore throat radius while the radius of the cavity and its connectivity control the extrusion of mercury from the cavity.

The median pore radius for the compacted core is 0.007 μm. In Figure 29 the decrease in total porosity, calculated from the volumetric mass densities, is shown. During experiment 1 (MX80), the largest decrease in porosity occurs during the step where vertical stress is at 65 MPa and temperature at 30°C. This corresponds to the largest increase in bulk dry density (Figure 30). From the beginning to the end of the compaction experiment, the total porosity decreased from 55% to 22%. The discrepancy between the mercury porosity and calculated porosity is attributed to the initial presence of 11 wt % of water that was present at the beginning of the experiment. A proportion of 4% is contributed to structural water (Sauzéat et al., 2001), with the remainder being adsorbed water. From the beginning to the end of the compaction experiment, the bulk dry density increased from 1.2 $g.cm^{-3}$ to 1.7 $g.cm^{-3}$.

After 132 days of compaction of the marl in experiment 2, the mercury connected porosity, free porosity, and trapped porosity of the marl were found to be 8%, 4.4%, and 3.6%, respectively. In comparison to the MX80, a somewhat smaller proportion (44%) of the porosity is trapped. The median pore diameter for the marl is 0.009 μm. The largest decrease in total porosity (Figure 29**)** is also, as for MX80, during the pressure and stress increase from 45 MPa to 65 MPa and 30°C.

From the beginning of the compaction experiment, the total porosity decreased from 54% to 16%. From the beginning to the end of the compaction experiment, the bulk dry density increased from 1.2 $g.cm^{-3}$ to 2 $g.cm^{-3}$.

For experiment 3 (MX80 no T) the mercury connected porosity, free porosity, and trapped porosity were found to be 15%, 7%, and 8%, respectively, after 189 days of compaction. Again, a large proportion of the porosity (53%) is trapped. The median pore diameter is 0.007 µm. The largest decrease in total porosity (Figure 29**)** is during the pressure and stress increase from 85 MPa. From the beginning of the compaction experiment, the total porosity decreased from 43% to 18%. From the beginning to the end of the compaction experiment, the bulk dry density increased from 1.2 $g.cm^{-3}$ to 2.2 $g.cm^{-3}$.

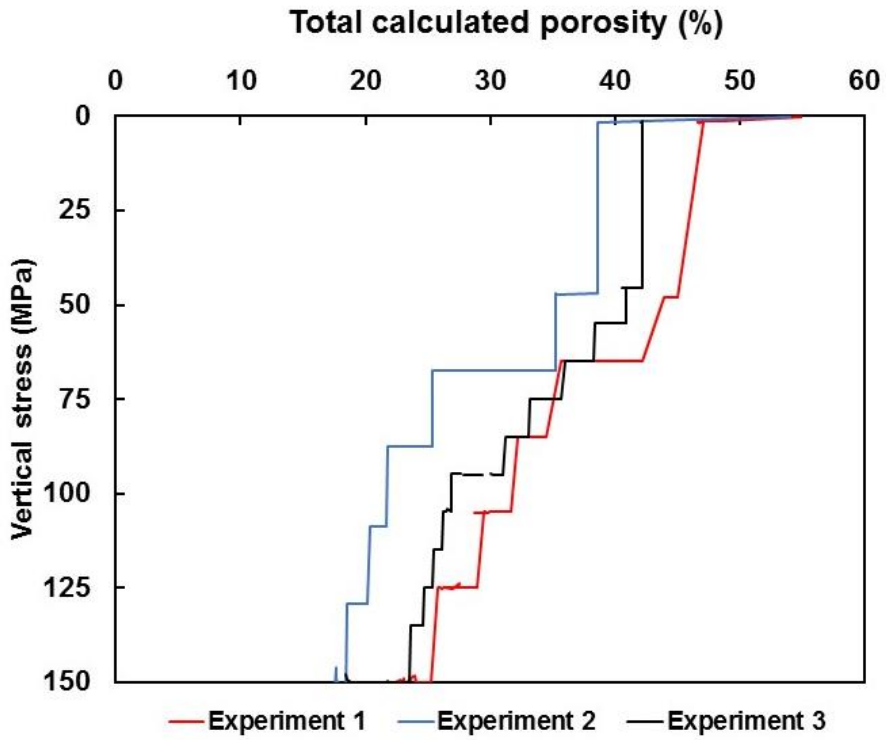


Figure 29: The total calculated percentage porosity with increasing vertical stress, for the three compaction experiments.

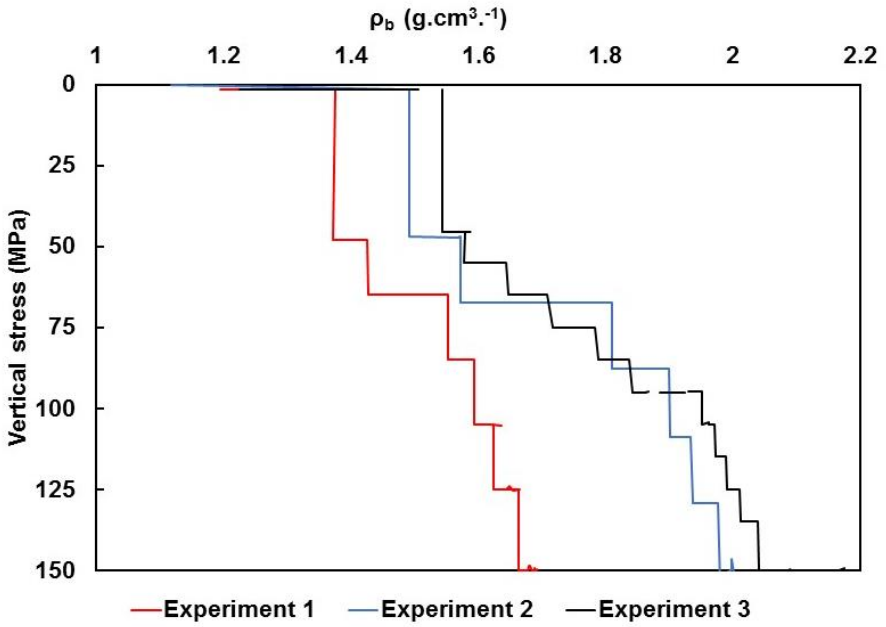


Figure 30: The calculated bulk dry density with increasing vertical stress for the three compaction experiments.

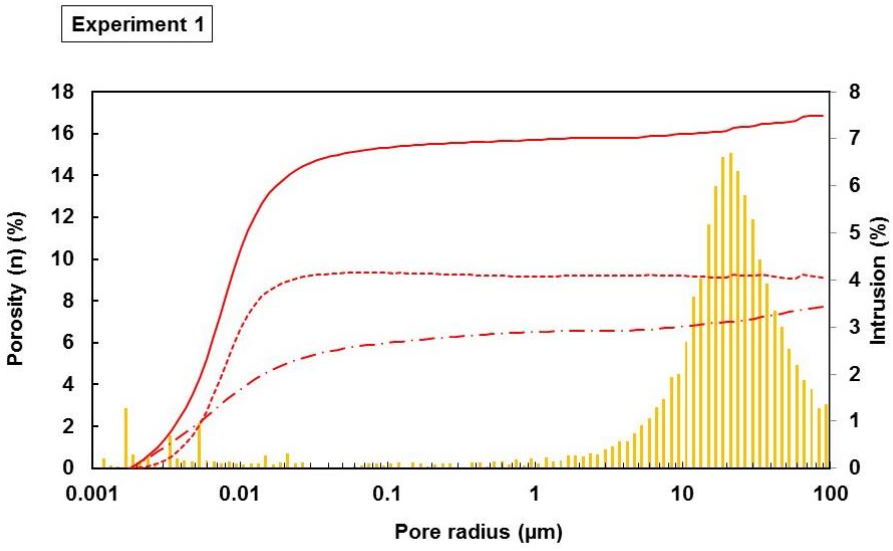


Figure 31: For Experiment 1 (MX80) the total mercury connected porosity (solid line), free (dashed line) and trapped porosity (dotted line) are plotted along with pore size radii.

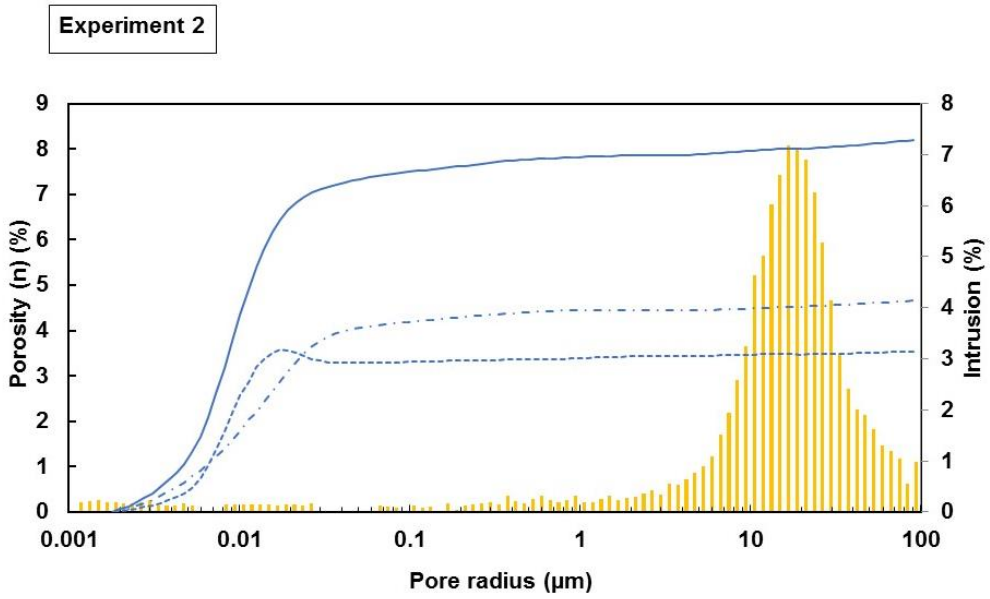


Figure 32 : For Experiment 2 (SSM) the total mercury connected porosity (solid line), free (dashed line) and trapped porosity (dotted line) are plotted along with pore size radii.

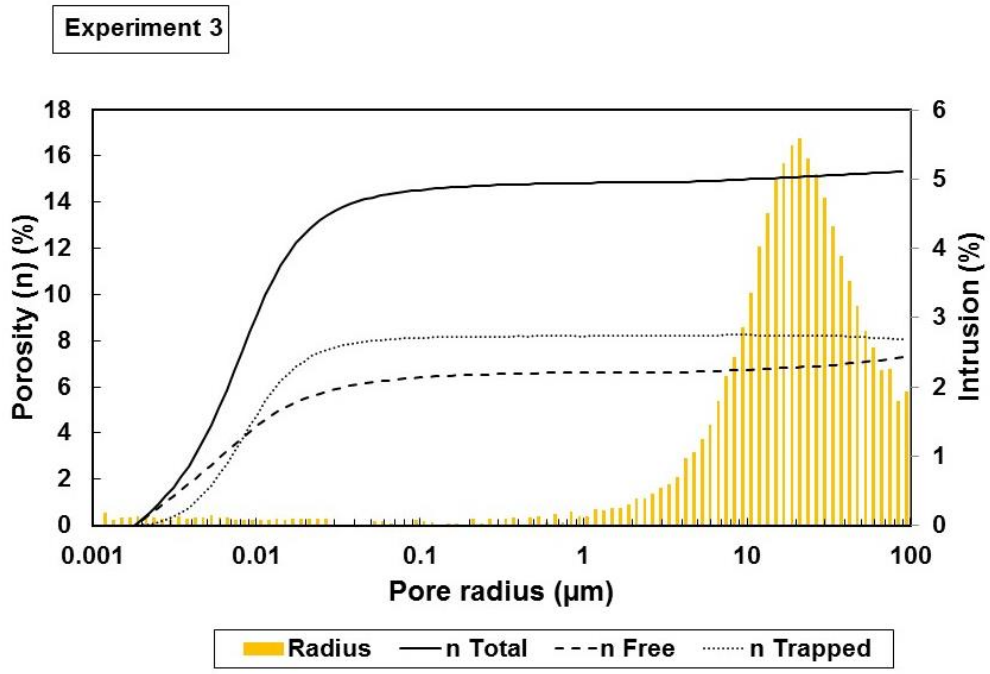


Figure 33: For Experiment 3 (MX80 no T) the total mercury connected porosity (solid line), free (dashed line) and trapped porosity (dotted line) are plotted along with pore size radii.

4.4.3.2- Nitrogen Adsorption

The shapes of adsorption/desorption isotherms are indicative of mesoporous materials, as hysteresis starts to occur for pores wider than ~ 4 nm. It can be seen in Figure 37, through BET treatment of the isotherms, that all three compacted cores contain mostly mesopores towards the lower end of the classification range. Mesopores range from 2-50 nm. Micropores are smaller than 2 nm and macropores are larger than 50 nm. The hysteresis loop for experiment 1 (MX80) and experiment 3 (MX80 no T) indicates complex pore structures and networks, for example, pore-blocking or narrowed pore necks. The desorption step is referred to as "cavitation". It results from a significant volume of mesopores that are blocked by micropores. Some molecules of N_2 are permanently trapped in the pores of the clay samples. For the marl compacted in experiment 2, the shape of the hysteresis loop is associated with the filling of micropores. The range of pore size distribution identified with this method, also as cylindrical theory, is showing a larger volume of smaller pore radii (< 10 nm) compared to what was observed with mercury intrusion porosimetry (Figure 31 to Figure 33).

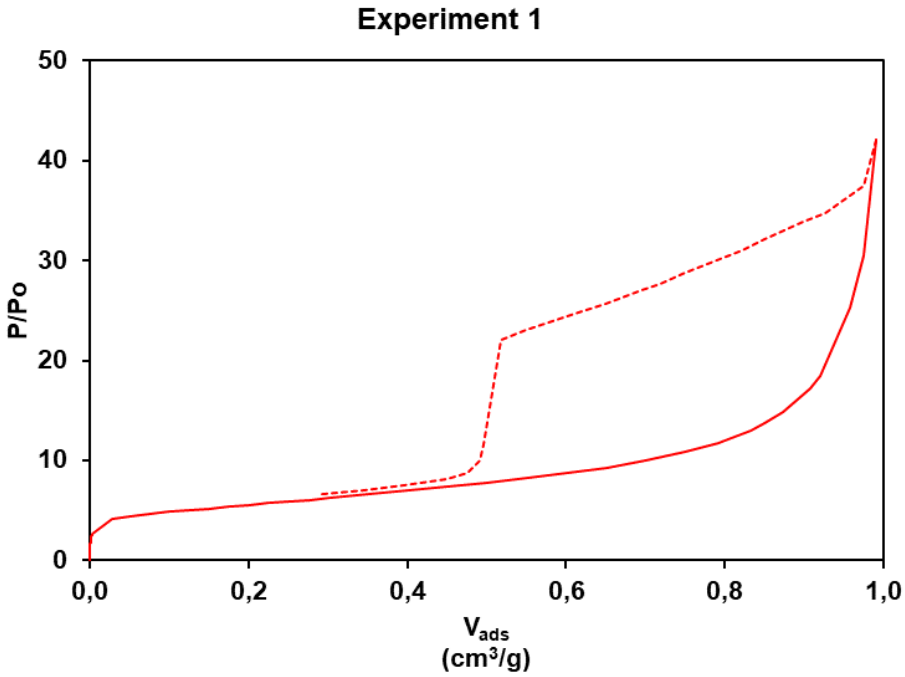


Figure 34 : N2 adsorption isotherme for MX80 after compaction Experiment 1. The adsorption curve is given in solid red and the desorption curve in dashed red.

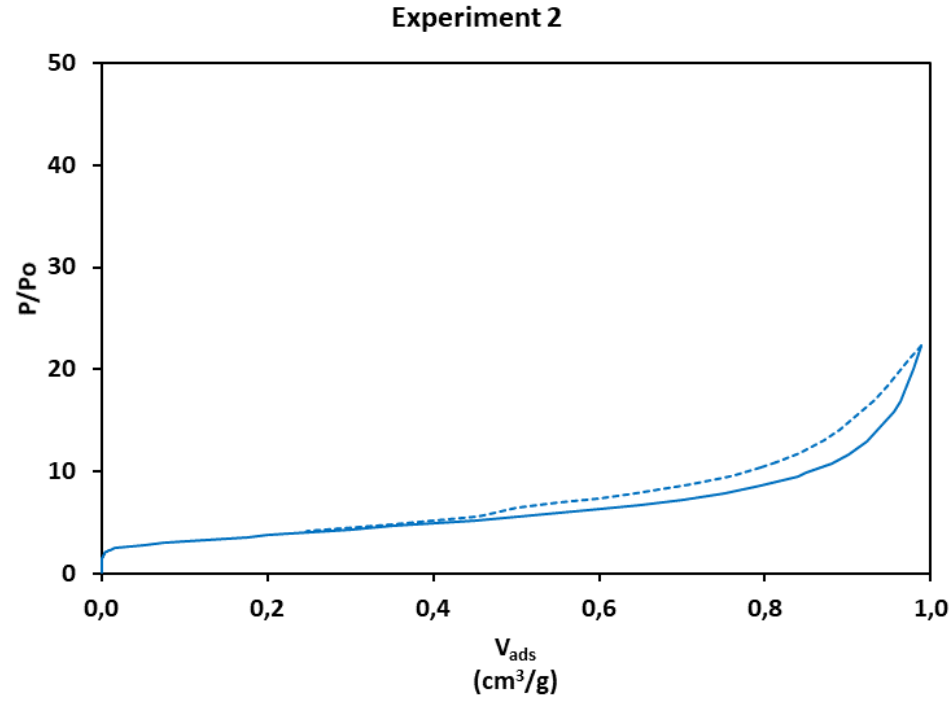


Figure 35 : Nitrogen adsorption/desorption isotherm for SSM after compaction Experiment 2. The adsorption curve is given in blue and the desorption curve in dashed blue.

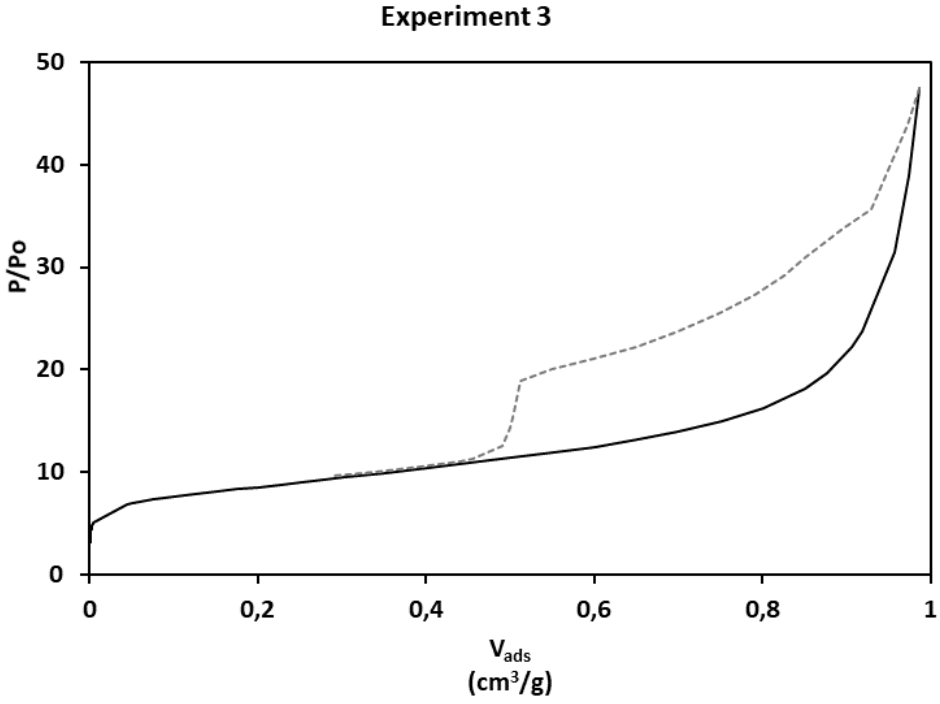


Figure 36 : Nitrogen adsorption/desorption isotherm for MX80 after compaction Experiment 3 (MX80 no T). The adsorption curve is given in black and the desorption curve in dashed grey.

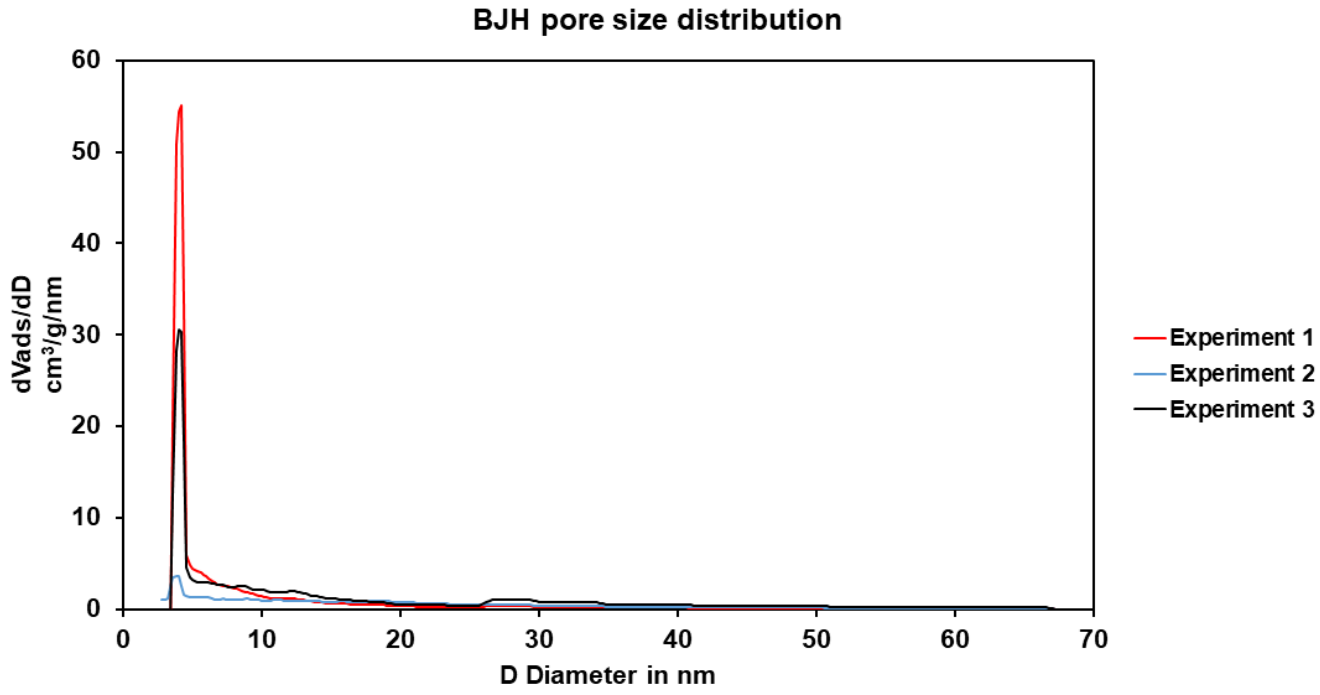


Figure 37: Pore size distribution profile after application of the BJH method on to the adsorption branches of the N_2 isotherms (assuming the cylindrical pore-shape model).

4.4.3.3- Porosity evolution with SURP modelling

The SURP modeling software calculated the evolution of porosity induced by individual contributions of mechanical compaction and diagenesis. We compare the experimental porosity evolution calculated from the vertical displacement measurements of compaction experiment 1 (MX80), with the SURP calculated porosity in Figure 38. An initial porosity of 55 % was applied in order to be comparable with the experimental data. The SURP calculated porosity and experimental porosity evolution correspond well. Figure 31 shows a relatively moderate reduction in porosity (from 55 % to 22 %) during the MX80 compaction. The SURP calculated diagenetic evolution is modeled assuming thermodynamic equilibrium between the pore water and the clay mineral assemblage.

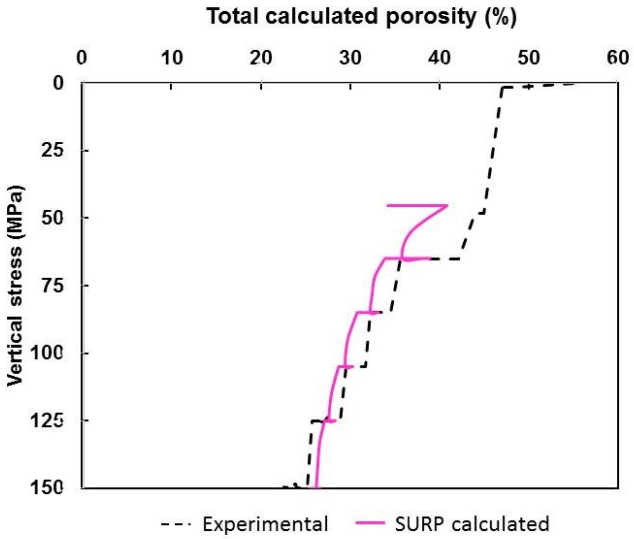


Figure 38 : The percentage total porosity with increasing vertical stress, for the compaction experiments (dashed black line) compared to the porosity evolution calculated with the SURP code (pink).

The evolution is driven by both the temperature changes and the pore water composition. Thus during the clay compaction, the porosity evolves both because of the mechanical compaction and because of potential mineral precipitations and dissolutions that occur. According to the SURP compaction model, the porosity decreases more pronounced during the first compaction steps. During the final compaction step (vertical stress > 125 MPa) the SURP calculated porosity is slightly lower than is experimentally observed. While the clay mineral transformation is minimal, the effect of potential cement precipitation (quartz or other) that could result in the loss of porosity and permeability is not investigated in this work (Hower et al, 1976; Foster and Custard, 1980).

A rise in temperature and above all, in pressure during burial/compaction expels water from the hydrated smectite interlayers. What follows is dehydration, absorption of alkali ions from concentrated porewater to replace water molecules, and a rearrangement within the lattice that occurs. Depending on the environment/system montmorillonite will be transformed by aggradation into chlorite, be degraded to kaolinite, or transition/transform to illite at a later stage. The threshold temperature required to initiate diagenesis to illite is about 70 °C. Smectite transformation is a rapid but progressive an irreversible reaction. In our work, the SURP modeling shows the continuous dehydration of the smectite from ~ 0.6 down to 0.2 mineral volume fraction hydrated smectite content (3 two or 1 water layers). However, the mineral volumetric fraction of anhydrous smectite only increases to ~0.18. That means, at the end of the experiment around 18 % of the total mineral content now constitutes anhydrous smectite. The remainder of the smectite remains to some extent hydrated. It is not distinguished which proportion contains 3 water layers, 2 water layers or 1 water layer. No transformation to illite is expressed with the SURP computation.

With the application of this code, water release by the smectite dehydration process was calculated by accounting for mechanical compaction and thermal effects. Smectite dehydration was simulated to be the cause of 26% of the total volume of water expelled during the laboratory clay compaction in the case this was accompanied by a ~10% reduction of porosity, as computed with the SURP code. This corresponds very well with what has been observed during the compaction experiment. The SURP calculated decrease in porosity is only slightly less than the experimental results. Later XRD and SEM analysis of the post compacted core did reveal an increase in Si content as well as the presence of chlorite clays, which was not expressed with the SURP calculation. Si cement precipitation and autogenic chlorite could contribute to the decreased porosity observed in the experiment vs with the SURP code.

4.4.4- Solid material chemical composition

The analysis of solid material after the MX80 compaction experiments shows a decrease in SiO_2, CaO, and K_2O while Al_2O_3 has slightly increased in experiment 3 (MX80 no T). The other major elements remain mostly constant for both MX80 experiments. For the marl compaction, there was a decrease in SiO_2, NaO, and CaO. The majority of major elements increase in the marl following the compaction, with a more pronounced enrichment for Al_2O_3. Table 21gives the major and trace elements in the pre-and post-compacted materials. In terms of trace elements, the large increases in Cr and Ni are due to corrosion of the metal plating in the cell during the long experiments.

Complementary whole rock chemistry analyses (ICP-OES) found that the Cl content of the MX-80 has increased from 110 to 550 ppm after experiment 1 (MX80). For the marl, the Cl content has increased from 105 to 560ppm after experiment 2. After experiment 3 (MX80 no T) the Cl content in the compacted MX-80 core has increased to 350 ppm.

4.4.5- Solid material mineralogical composition

Figure 39 and Figure 40 represent mineralogical characterization of the initial SSM rock before experimentation. The clay minerals illite (61%), kaolinite (7.1 %) and quartz, chlorite, was identified by XRD in the fractions smaller than 2 µm. The marl matrix also contains calcite and Fe-oxides. Furthermore, nodular pyrite, albeit and Ca & Fe carbonates were identified in the bulk SSM.

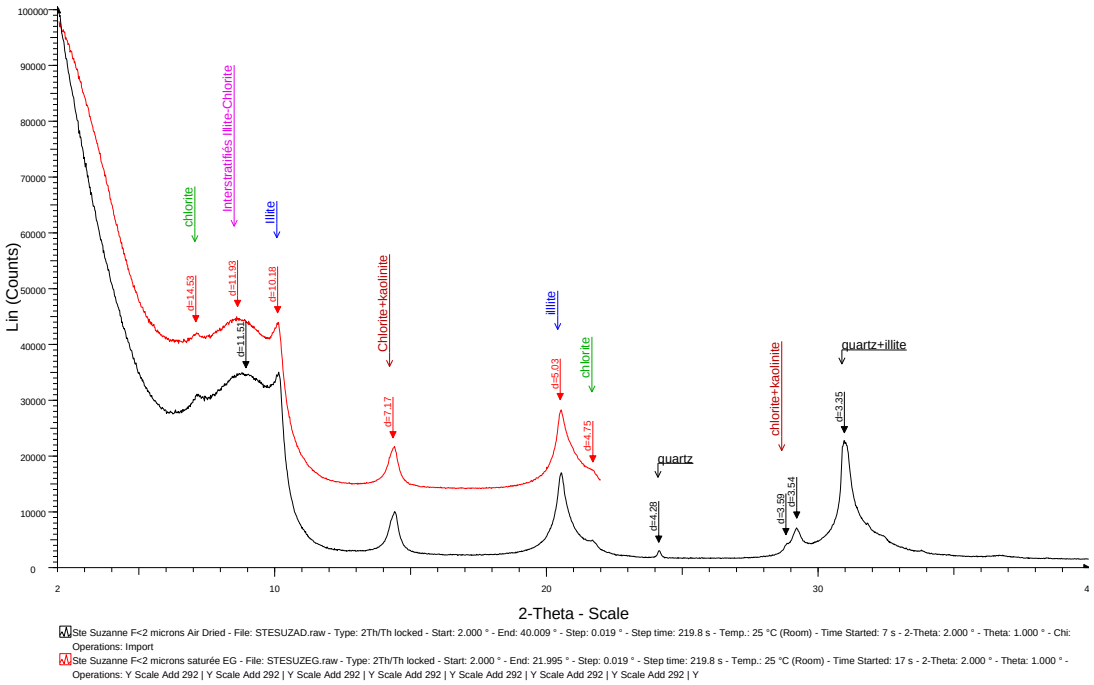


Figure 39: X-Ray diffractogram of the initial Sainte-Suzanne marl for fractions smaller than 2 µm.

Table 21: Chemical composition of MX-80 and Sainte Suzanne marl before and after compaction. Determination of major elements in percentage of oxides per ICP-MS iCapQ (SARM).

	MX-80 Initial composition	**MX-80** After compaction **Experiment 1**	**MX-80** After compaction **Experiment 3**	**Sainte-Suzanne marl** Initial composition	**Sainte-Suzanne marl** After compaction **Experiment 2**
Major elements in oxide percentages					
SiO_2	59.00	**58.75**	**60.41**	53.29	**49.65**
Al_2O_3	18.70	**18.78**	**19.21**	11.88	**14.66**
Fe_2O_3	4.20	**4.17**	**4.30**	3.79	**4.79**
MnO	0.042	**0.04**	**0.04**	0.040	**0.046**
MgO	2.22	**2.25**	**2.33**	1.42	**1.45**
CaO	1.99	**1.47**	**1.59**	10.71	**10.01**
Na_2O	2.28	**2.25**	**2.27**	1.00	**0.88**
K_2O	0.84	**0.75**	**0.73**	2.44	**2.89**
TiO_2	0.17	**0.14**	**0.15**	0.57	**0.65**
P_2O_5	0.19	**0.22**	**0.22**	0.10	**0.11**
Loss on Ignition	9.90	**11.47**	**7.90**	14.67	**14.27**
Total	99.51	**100.30**	**99.16**	99.89	**99.39**
Trace elements (ppm)					
As	14.9	15.05	12.5	9.32	9.73
Ba	348	342.5	337	336	378
Be	1.74	1.73	1.69	2.42	3.04
Bi	0.99	0.995	0.96	0.39	0.45
Cd	0.37	0.32	0.30	4.85	0.75
Co	2.16	1.6	1.41	18.5	46.8
Cr	43.7	605	46.3	67.2	608
Cs	0.79	0.53	0.43	8.41	9.79
Cu	5.4	5.55	5.1	21.2	31.6
Ga	28.4	28.5	29.2	16.5	20.7
Ge	0.86	0.855	0.81	1.47	1.56
Hf	8.03	7.765	8.01	4.96	4.70
In	0.08	0.08	0.09	0.05	0.06
Mo	4.75	4.29	4.47	1.32	1.68
Nb	26.4	26.7	26.3	11.1	12.2
Ni	6.8	141	539	32.0	56.3
Pb	48.4	48.8	48.1	20.8	22.2
Rb	22.4	17.3	16.6	122	142
Sb	1.58	1.555	1.55	1.13	0.93
Sc	6.02	5.85	6.28	9.83	13.49
Sn	12.2	12.55	8.87	6.09	6.89
Sr	346	316.5	340	540	472
Ta	3.47	3.5	3.65	1.19	1.34
Th	37.9	38.9	38.6	10.6	11.7
U	13.2	13.6	13.4	2.53	2.42
V	8.9	6.35	5.9	62.3	97.5
W	2.22	0	< L.D.	39.8	149
Y	42.3	42.75	44.3	22.2	24.5
Zn	106	105.5	98.8	75.7	97.3
Zr	210	198.5	189	179	172
La	48.6	49.15	48.7	28.1	32.2
Ce	103	105	107	58.8	66.8
Pr	12.0	12.05	12.6	6.66	7.77
Nd	44.6	44.95	46.8	25.1	29.5
Sm	10.1	10.3	10.6	5.04	5.86
Eu	0.757	0.735	0.746	0.936	1.13
Gd	8.64	8.785	9.09	4.20	4.86
Tb	1.40	1.425	1.46	0.665	0.747
Dy	8.53	8.645	8.86	4.04	4.55
Ho	1.68	1.7	1.75	0.819	0.927
Er	4.39	4.43	4.52	2.23	2.47
Tm	0.660	0.663	0.691	0.346	0.370
Yb	4.16	4.16	4.27	2.20	2.43

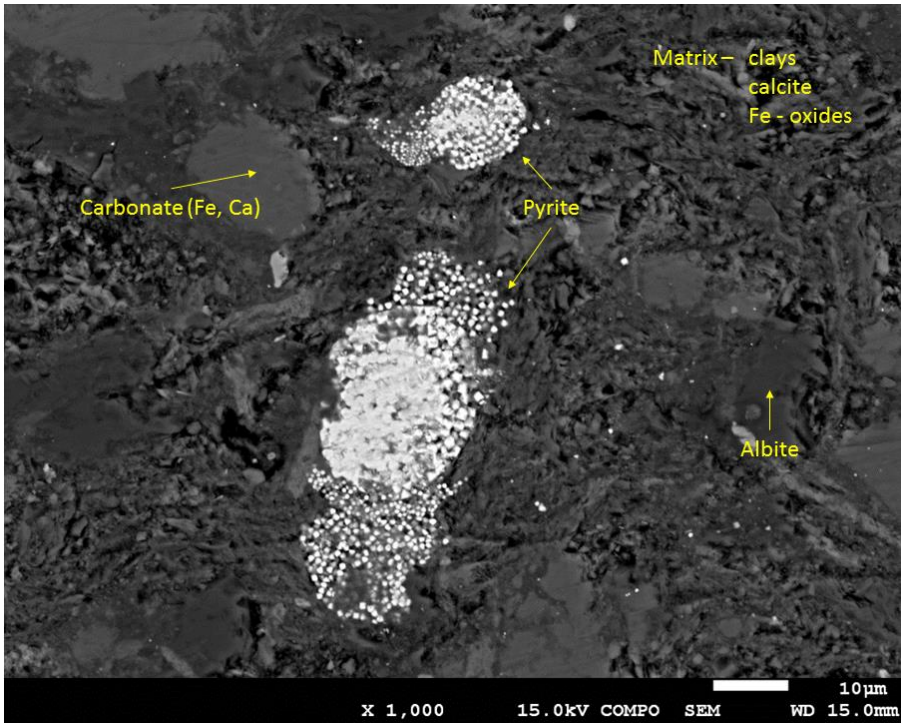


Figure 40: Scanning electron microscope image of the initial Sainte-Suzanne marl before experimentation.

The mineral compositions, identified with SEM, of the two materials post-compaction are represented in Figure 41 through Figure 46 Br and Cl are not likely to be influenced during mineral reactions in these conditions. The most likely influence that mineral reactions can have on the concentrations and isotope fractionation might be 1) on the pore fluid composition and 2) on diminishing porosity (therefore increasing turtuosity) due to mineral rearrangement and potential cement precipitation.

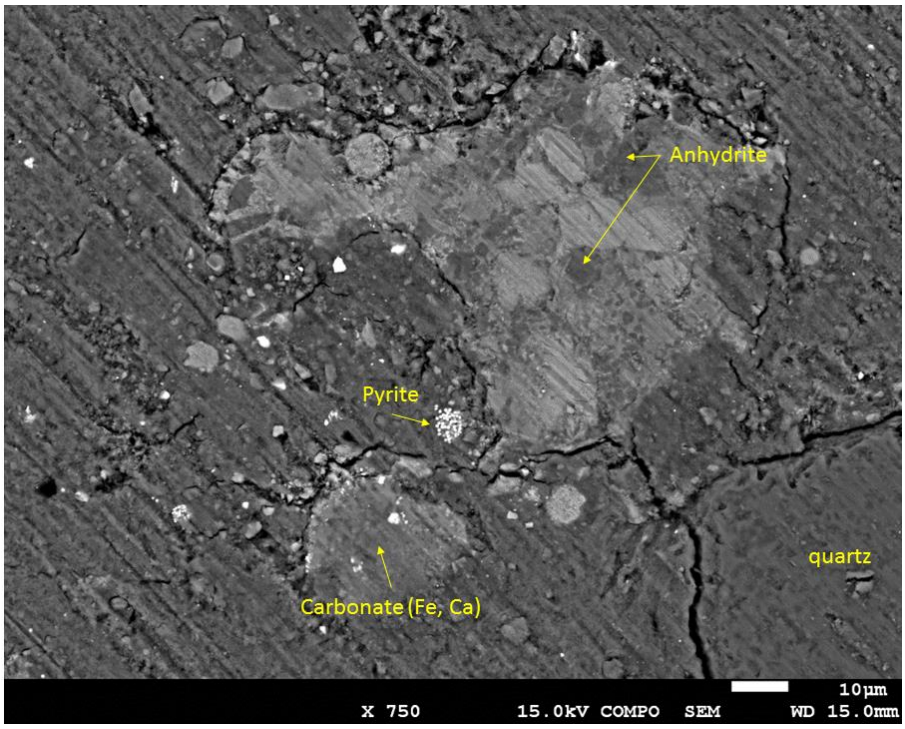


Figure 41: Scanning electron microscope image from a polished surface of the compacted MX-80 core from Experiment 1.

X-ray diffraction was performed after the experiments (Figure 43, Figure 45 , and Figure 47) to follow the possible mineral transformations during the experiments. Some modifications of the global mineralogical composition of solids have been observed. For MX80, the main transformation concerns the montmorillonite. Its interlayer composition changes after the experiment characterized by an enrichment in Na and K (shift of the (001) peak toward higher 2θ angles). Ca is expelled from the crystallographic structure. A possible but limited illitization could be envisaged. Phlogopite is likely altered if considering that the amount of quartz and calcite has not changed during the experiment (based on the comparison of the intensities of their peaks). Plagioclases crystallize (albite and anorthite). Peaks of gypsum are not observed on the diffractogram after experiment, it probably dissolves. Two peaks around 51.5°2θ and 62.6°2θ were difficult to attribute to the phases already identified. They could match with pyrrhotite.

For SSM, assuming that the quartz is not affected during the experiment (intensity of the main quartz peaks at 31 °2θ identical on the two diffractograms of Figure 45), a significant decrease in the intensity of kaolinite, illite and anorthite peaks can be attributed to a drop in the amounts of these three minerals during the experiment. Potentially the most altered mineral would be kaolinite. Low-intensity peaks of chlorite appear on the diffractogram of the sample after the experiment. Calcite and pyrite seem unaffected.

It has to be noticed that it is not possible to determine the moment when the mineralogical transformation occur during the experiment. It can be envisaged that the main transformations happen at higher temperatures thus rather at the end of an experiment, because kinetics are more favorable.

During the SEM study of compacted MX80 after experiment 1, it was discovered that Ca and Cl are present in larger quantities along the crack compared to the matrix and the visible feldspar mineral. This is seen in the EDS spectra along a crack on the edge of a feldspar crystal shown in Figure 42. Macro-pores will act as preferential flow paths and the observed increase can be due to the precipitation of salts during residual pore water evaporation. After experiment 2 (SSM) the minerals identified were quartz, fieldspar, calcite, pyrite and the clay minerals; illite, kaolinite and chlinochlore. The clay component of the marl after compaction (illite > kaolinite > chlorite) has decreased while the quartz content has markedly increased. Both SiO_2 and Al_2O_3 increases are also observed in the whole rock chemistry following the compaction experiment Table 21 After Experiment 3 (MX80 no T) the main difference from compaction experiment 1 seems that gypsum remain present and quartz crystallinity is not altered as it is in experiment 1 (MX80). The minerals identified after Experiment 3 (MX80 no T) are quartz, Na-Ca feldspar, K-fieldspar, apatite, calcite, gypsum , Fe-oxides/hydroxides and the clay minerals montmorillonite, illite have been identified by Scanning Electron microscope.

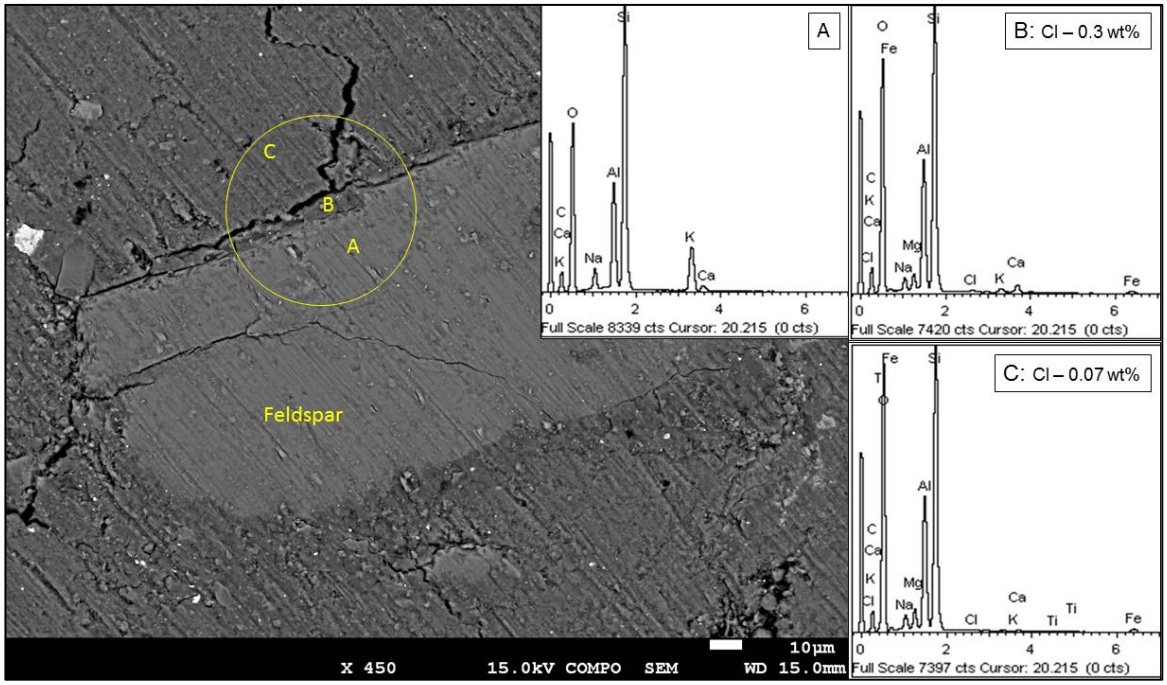


Figure 42: A crack along the border of feldspar grain observed in the compacted MX-80 core after Experiment 1. EDS spectra of the feldspar (A), the clay next to the crack (B) and the general clay matrix (C).

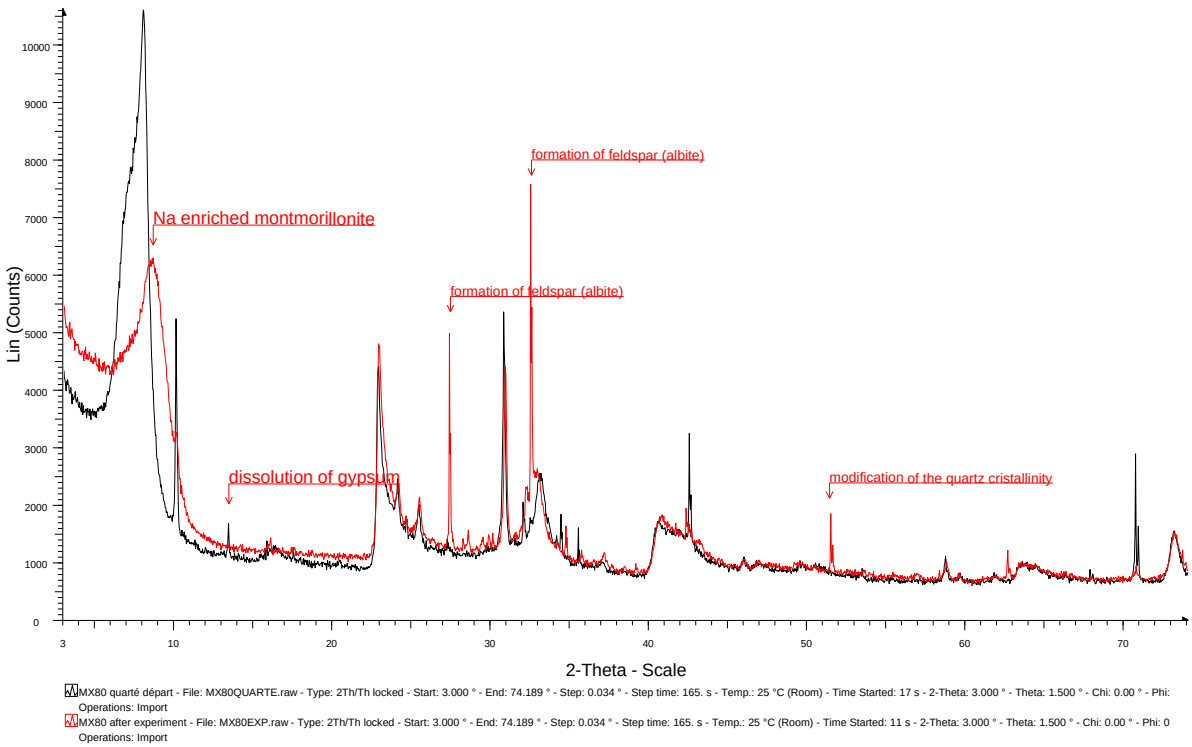


Figure 43: X-Ray diffractogram of the compacted MX-80 core after Experiment 1.

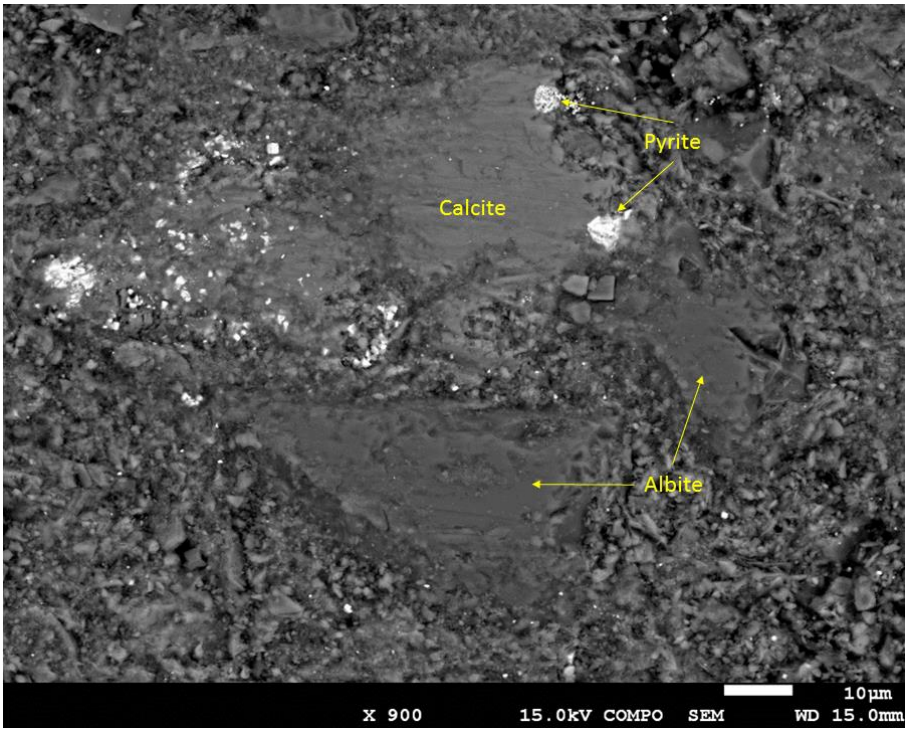


Figure 44: Scanning electron microscope image of the compacted Sainte-Suzanne marl core after Experiment 2.

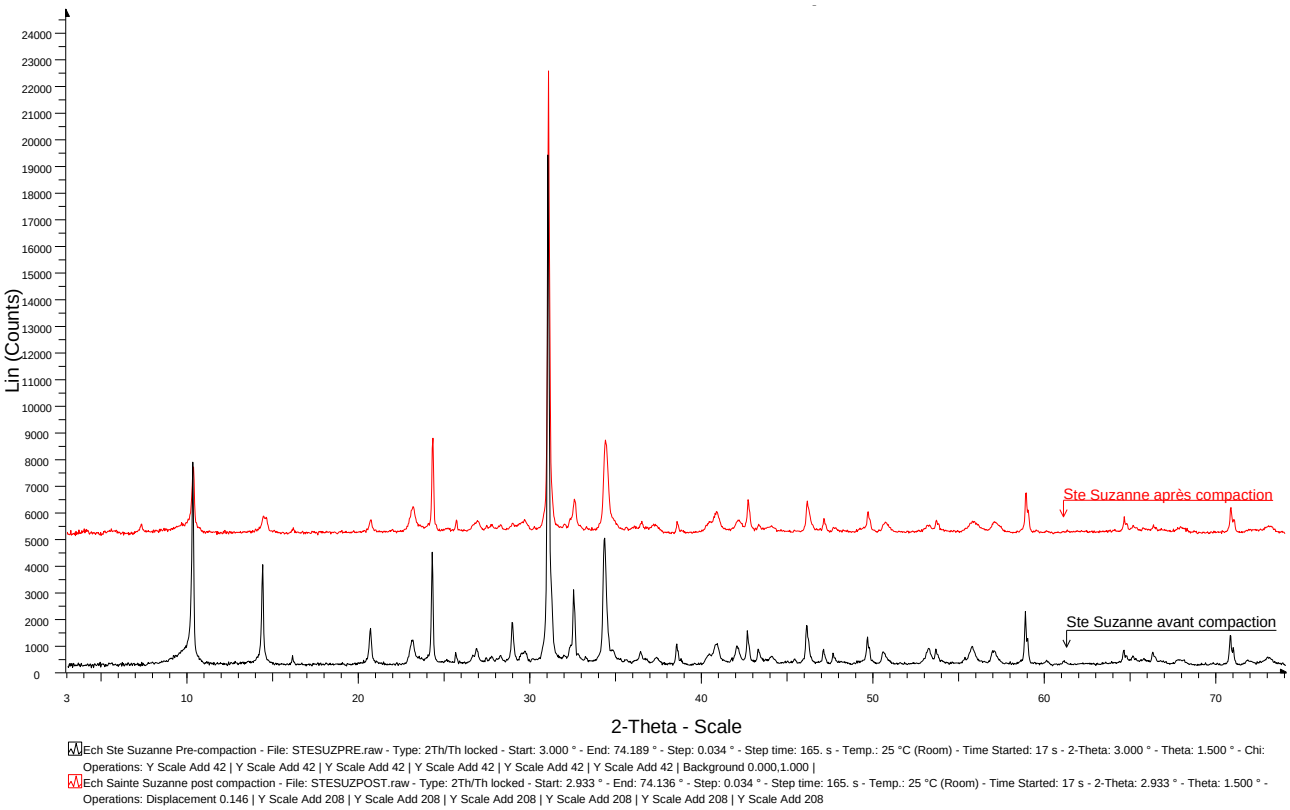


Figure 45: X-Ray diffractogram of the original Sainte Suzanne marl core (black line) and compacted core from Experiment 2 (red line).

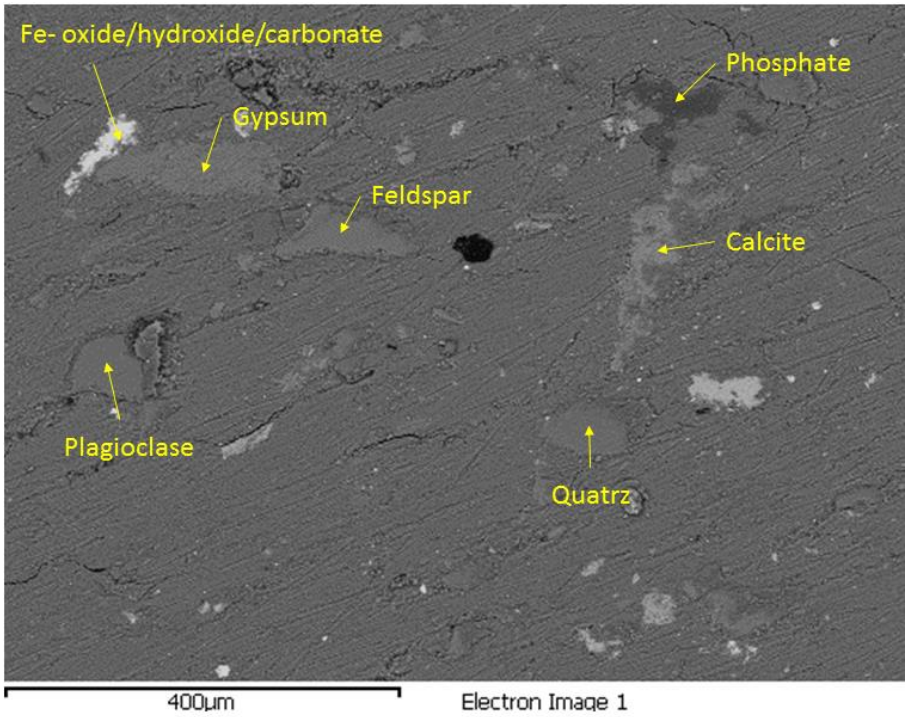


Figure 46: Scanning electron microscope image from a polished surface of the compacted MX-80 core from Experiment 3.

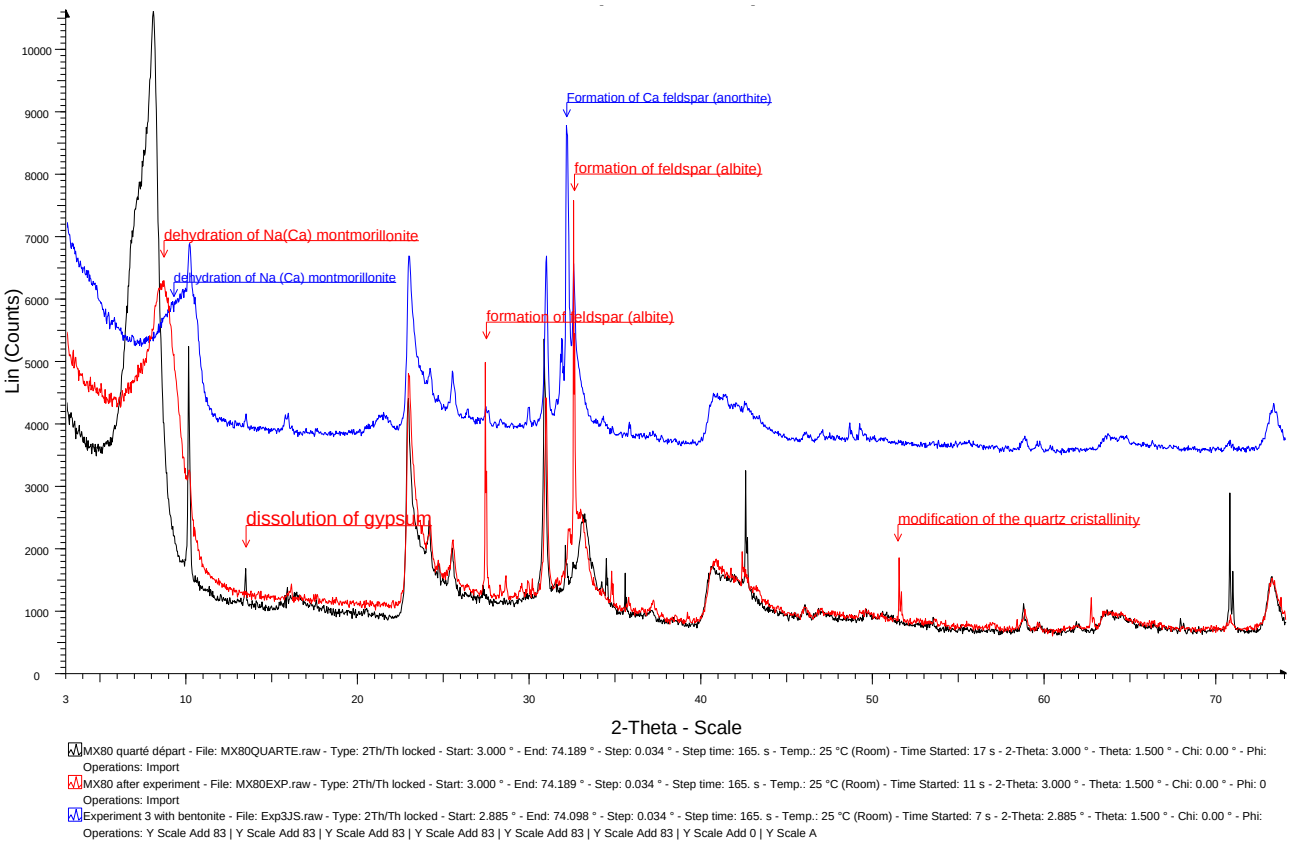


Figure 47: X-Ray diffractogram of the compacted MX80 core following experiment 3 (blue line) compared to experiment 1 (red) and the original MX80 (black lines).

Discussion

DISCUSSION

5.1- REACTIVITY OF THE SYSTEM

To interpret the results of the compaction experiments, we have to decipher the different mechanisms that are responsible for the chemical and mineralogical evolution of the system. It is worth noting that 1) the scale of the experiments remain minuscule compared to geological conditions and 2) the expelled volumes are small by comparison with the remaining water (several percent at each step).

XRD analyses show that the mineralogical transformations resulting from the three high pressure, high temperature compaction experiments remain limited. The main transformation concerns the MX-80 with a part of the smectite being transformed in sodic montmorillonite, kaolinite and albite in MX80 compaction (10 to 15% in experiment 1 and even less for experiment 3). Following the SSM compaction, experimental data predict an even weaker reactivity of the system. This is well confirmed by the chemistry of the expelled water that remains roughly constant whatever the experimental conditions applied for SSM compaction. Neither was any mineralogical transformation observed during SURP modelling of the MX80 compaction experiment1.

Thus, assuming limited mineralogical transformations during the compaction experiments, in terms of dissolution/precipitation processes, the mechanisms invoked for the evolution of the chemistry of the solution is a result of either adsorption/repulsion on the negatively charged surface of clay minerals (charge exclusion) and/or elemental mechanical trapping (pore size exclusion) due to the decrease of clay porosity under compaction.

Consequently, to better understand the behavior of elements, we largely look to the mass balance calculated to evaluate the bulk chemical composition of the pore water. Plotting the cations against anions in terms of charges (Figure 20), there is a relatively good correlation for the expelled water saying that electrical balance is more or less achieved. For the trapped water, the variation is weak and the electrical balance is less obvious. In this discussion, we will largely be focusing on the concentrations of halogens both in the expelled water and that calculated for the pore water. When looking at the variations of Cl and Br concentration in the pore water, they remain very very low by comparison with that of the expelled water (Figure 16 and Table 5, 7 and 8). That is to say that the chemical equilibrium between expelled water and pore water is never achieved in the experiment.

To understand the chemical and isotopic evolution of the system, special attention has to be paid to the different types of pore water in clays, to the anion exclusion effect and to the evolution of the porosity with compaction leading to a change of the dominated transport of solute.

When the negative electric potential in the interlayer space increases with increasing compaction and all anions are expelled from the interlayer porosity (Bolt and de Haan, 1982; Pusch et al., 1990; Wersin et al., 2004, Wigger and Van Loon, 2017), only the interparticle porosity remains available for anion transport. However, at high compaction rates, as in our experiments, interparticle porosity would have decreased dramatically/ having almost entirely disappeared (Bourg et al., 2006). In our experiments, we obtain porosity less than 20%, which is in line with material compacted to a depth of more than 5 km (Galan and Ferell, 2013). However, we do not achieve the force necessary (>250 MPa) to break the bond between the clay particle surface and the closest adsorbed water layers (Pusch et al., 1990: Sacchi et al., 2000). This is confirmed by the SURP modelling results (Figure 27) showing that after MX80 compaction, the anhydrous smectite only constitute a tenth of the mineral volumetric fraction compare to hydrated smectite (retaining 1, 2 or 3 adsorbed water layers). Therefore, in our experiments we succeed to expel only some of the interparticle freewater, not more.

In the case where the pore water solution is of high ionic strength (i.e. high salinity such as ocean water), the majority of experimental or modeling studies show that the accessible porosity for anions increases with increasing salinity. This is mainly explained by the fact that the volume of the DDL decreases due the high concentration of counterions in the solution able to counterbalance the mineral surface charge (Plecis et al., 2005). Applied to our study, the question arise if it could be the reason for the difference in fractionation behavior at the later compaction steps. For example, the continuous increasing trend for δ^{81}Br values in the MX80 compaction experiment is reversed when the pressurization is increased above 85MPa. However the expelled solution now contains more of the lighter ^{79}Br. Meaning the results does not fully support the proposition. This is also not well supported when we consider the calculated percentage of pore space lost due to the anion effect, we see that with increasing compaction, the calculated percentage of pore space lost, increased from 4 % to 8.6 % (Table 18).

But in addition to anion exclusion, anions can be trapped inside the diminishing pore spaces (Appelo et al., 2010; Alonso et al., 2011) as a function of the ion size. I.e. anion exclusion and size exclusion both hinders diffusion and result in exclusion enrichment effects. This anion trapping / retention can explain the high salinities that are observed in flowback waters produced within the shales after hydraulic fracturing in gas shale exploitations.This is especially applicable for elements such as halogens that are poorly incorporated into secondary minerals that could precipitate during the compaction (Alonso et al., 2019).

5.2- FLUID FLOW AND SOLUTE TRANSPORT IN COMPACTED CLAYS

In the fine-grained low-porosity compacted clays, diffusion will be the dominant transport mechanism. The mobility of ions is a function of the salinity (ionic strength) of the solution, its viscosity, the water content, the electrical charge of the clay surface, the temperature by the effect of Brownian movements, the pressure, the size and charge of the considered ions, the pore size of the medium, and its tortuosity for the main. To distinguish the impact of each of these parameters specifically, more work will be needed.

Electrostatic interactions increase with the salinity or the ionic strength of the solution resulting in slower diffusion of ions because the diffusion kinetics decreases when solution concentration increases (Schauble et al., 2003). Results from other diffusion experiments with clay-rich materials have shown that cation diffusion is normally enhanced compared to anion diffusion because cations can diffuse via the interlayer and DLL whereas anions are excluded from those areas (Shackelford and Daniel, 1991; Sato et al., 1992; Kozaki et al., 1998; Molera and Eriksen, 2002; Van Loon et al., 2004; Van Loon et al., 2007, Descostes et al., 2008).

But as we were only expelling freewater during our compaction experiments and not any of the interlayer or adsorbed water, the relative change in concentration of cations and anions in the expelled water, expressed as a filtration ration, remains in line with literature, up to a ratio of 6 for cations, and up to a ratio between 2 to 3 for anions, considering compaction experiment 1, the most reactive experiment. Filtration ratio refers to the concentration of an element that was sorbed/retarded/filtered (C_{final}) relative to its initial concentration ($C_{initial}$). For our experiments, the order of most - to least effectively filtered cations is $Mg^{2+} > K^{+} > Na^{+} > Ca^{2+}$. This result corresponds with the observations of Kharaka and Berry (1973). On average, half of the exchange sites of clays in equilibrium with seawater will be occupied with Na^{+} (Sayles and Mangelsdorf, 1977). Cation exchange, as filtration mechanism, would remove K^{+} and Na^{+} and increase concentrations of Ca^{2+} and Mg^{2+} (Yu et al., 2019, Davisson and Criss, 1996; Martel et al., 2001; Bagheri et al., 2014a; Liu et al., 2016). Additionaly the potential albitization of plagioclase that we observed, could decrease concentrations of Mg and Na, respectively, and both increase Ca concentration ((Davisson and Criss, 1996; Bagheri et al., 2014b). In turn, smectite illitisation could deplete K^{+}.

Considering anion filtration according to Kharaka and Berry's filtration ratio (1973), it is expected for Cl^{-} to be more effectively filtered than Br^{-}. In our results, this finding is not very pronounced (2.2 and 2.3 for Cl and Br respectively).However, when we extend the membrane efficiency evaluation to include/ also consider the natural abundance of the elements, according to the Kemp-Bresler model, the filtration efficiency of MX80 is certainly more pronounced for Br than it is for Cl (Figure 28).

In this case efficiency of a clay layer to act as a filtration membrane, is defined as a function of pore size diameter and pore water ionic strength (Neuzil and Person, 2017). The membranes filtration efficiency should improve with decreasing porosity. Due to physio-chemical characteristics of the clay materials, membrane filtration efficiency is also expected to be lower for more saline solutions. Due to the DDL being condensed for more saline solutions, it can potentially increase the available porosity. In correspondence with the findings of Kharaka and Berry (1973); Lavastre et al., (2005); Van Loon et al., (2007); and Nakata et al., (2016), if we evaluate the two different clay material in terms of filtration efficiency the results from this study emphasize that the surface chemistry of the clay is a key factor in the efficiency of the clay to act as a filtration membrane. Smectite rich MX-80, with a higher negative surface charge, was in general, a more efficient filtration membrane for both Cl and Br anions and had an overall larger effect on isotope fractionation (Figure 24 and Figure 26Figure 26) compared to the illite rich SSM (Figure 25), despite the SSM having been compacted to a much lower porosity than the MX-80 (Figure 29).

Although anions are less effectively filtered than cations by the negatively charged clay, diffusion coefficient for anions are generally lower than for the cations due to mechanical trapping and increased tortuosity (Alonso et al., 2011). For example, in all three experiments, some initial filtration is seen after ocean water was forced through the clay under minimum pressure- i.e. a small increase in concentration of solutes in the source water. Water flowing out on the other side had a lower salinity i.e. we see freshening. Flowing ocean water through the clay, also resulted in considerable storage of solutes as all the available adsorption site must become filled over time.

With the first compaction step, the water expelled from the MX80 is more saline than the original ocean water. More so for the first MX80 compaction experiment 1 that in the MX80 No T compaction experiment 3 – concentrated free water is expelled.

Then a general decrease in concentration was observed in the water expelled from both MX80 experiments, any concentration of the source water, can't be known due to the valve between inflow and the compaction cell having been closed. We could therefore not see any 'back flow' in our experiments. Only that freshening occurred as a result of water forced out of the clay while solutes remain inside the clay layer (in the case of MX80).

In our study we also see the influence of temperature changes, on the rate of out diffusion of the solutes. Better freshening was seen when increasing temperature increments were applied along with the increasing pressure incriments. At higher temperatures molecules vibrate at a higher tempo/faster. Faster random molecular vibration will result in slower/less overall flow. Therefore higher temperatures causes slower outflow of the solutes and we have more freshening and continuous decreasing concentrations of Cl and Br.

In the MX-80 no T compaction experiment 3, the Cl and Br concentrations never decreased below the level of the initial ocean water – therefore we do not achieve true freshening during the compaction. As was the case with the SSM compaction. No freshing was achieved during the SSM compaction.

We considered the possibility that we could potentially have dilution of pore water from extra water released due to smectite illitisation mineral transformation which can happen at temperature above 70°C. Applying the innovative SURP code to our dataset for MX80 compaction experiment 1, showed that 7% of the pore water volume, could be the result of smectite dehydration, but no water is produced due to illitisation during our experimental conditions.

5.3- ISOTOPE FRACTIONATION

Fractionation normally decreases with increasing temperature (Richet et al., 1977; Schauble et al., 2003; Balan et al., 2019) and stronger chemical bonds generally preferentially involve the heavier isotope (Schauble, 2004*)*. The fractionation in natural systems, such as in sediments, are dictated more by kinetics rather than equilibrium fractionations (solution and precipitation).

In order to assess element and isotopic fractionation during diffusion, there are three things that should be considered separately: (1) the relative atomic masses difference between Cl and Br, (2) the relative masses difference between ^{81}Br and ^{79}Br and (3) the relative mass difference between ^{37}Cl and ^{35}Cl.

The relationship between δ^{37}Cl and Cl- concentrations have previously been applied to interpret the source of salinity of formation waters. Formation waters originating from evaporated seawater, have been attributed to δ^{37}Cl values ranging from −0.9‰ to 0‰, while formation waters affected by the dissolution of halites typically have δ^{37}Cl values from 0‰ to +0.5‰ (Eggenkamp et al. 1995; Eastoe et al., 1999; Bagheri et al., 2014a). In the work of Yu et al. (2019), studies on δ^{81}Br values of formation waters attributed to sea water evaporation or halite dissolution is incorporated (Eggenkamp and Coleman, 2000; Shouakar-Stash et al., 2007a; Shouakar-Stash, 2008; Stotler et al., 2010;, Boschetti et al., 2011b and Bagheri et al., 2014a. This is illustrated in Figure 48.

Our work shows that while variation in δ^{37}Cl values resulting from clay filtration (ranging from -0.5‰ to -0.1‰) is more similar to the values resulting from evaporated seawater, distinctly higher δ^{81}Br values are observed as a result of clay filtration (ranging from 0.9‰ to 1.5‰).

Compaction of MX80 caused, in general, a decrease in δ^{37}Cl values with increasing compaction. This also corresponded to decreasing Cl concentration in the expelled fluid. Larger variation in δ^{37}Cl values (0.47‰) and lower δ^{37}Cl values (-0.45‰) are reached for the first MX80 compaction experiment 1 conducted at higher temperatures, than for the MX-80 no T compaction experiment 3 in which a δ^{37}Cl vatiation of 0.29‰ is observed and the lowest δ^{37}Cl value reached, is -0.3 ‰ (Figure 22). For the SSM compaction experiment, δ^{37}Cl values clustered around ocean water values.

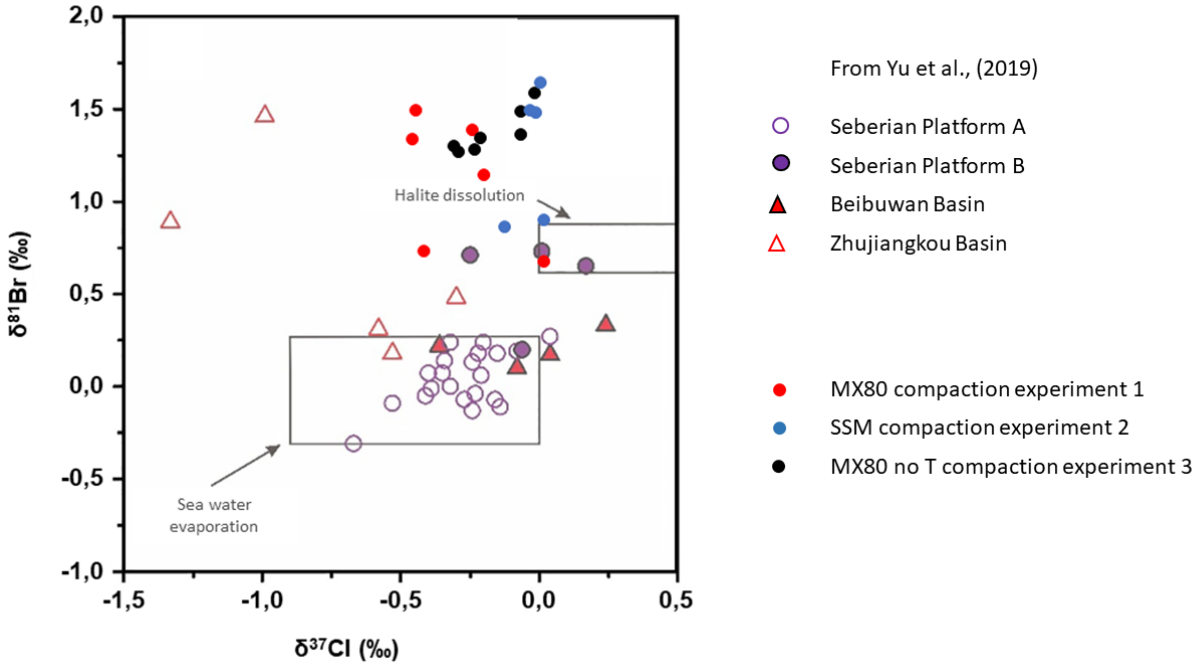


Figure 48: The relationship of $\delta^{81}Br$ and $\delta^{37}Cl$ in various source waters.

Our data supports the experimental data of Campbell (1985) and early model proposed by Phillips and Bentley (1987), that clay layers has the potential to, theoretically, fractionate chlorine stable isotopes because the negatively charged clay layers repel the negatively charged ^{35}Cl ion slightly more than the ^{37}Cl ion. Our data also confirms that fractionation effect was stronger for more negatively charged clays, as is seen for natural sediments. $\delta^{37}Cl$ values of pore waters from smectite rich clays are consistently lower (-8.5‰ & -6.8‰ in Agrinier et al., 2019; Underwood et al., 2013; Saito et al., 2010; Henry et al., 2012), than $\delta^{37}Cl$ values for pore waters from dominantly non-swelling clay rich sediment, such as kaolinite, chlorite and illite (-1.9‰ & -2.1‰ in Bonifacie et al,. 2007; Bonifacie et al.,2005; Elderfield et al., 1999; Underwood and Hoke, 2000).

However, our data shows that ^{35}Cl becomes enriched within the clay layer itself, and not before the clay layer (closed valve). Therefore, we can understand that the freshening observed is not only a result of retardation of dissolved solutes flowing through a clay layer (filtration) but in combination, a result of trapping of the solutes by the clay layer itself. This trapping of the solutes within the clay layer is a consquence of both physical and chemical interaction between the clay mineral surfaces and the pore fluid and the porosity.

From our data, it is most interesting to dicsuss Cl isotope fractionation considering the first MX80 compaction experiment 1.

Compaction of the MX80 clay caused isotope fractionation in Cl between the expelled fluid and the remaining pore fluid and the fluid remaining in the injection pump. The initial pressurisation to 45 MPa caused nearly equal proportions of ^{37}Cl and ^{35}Cl to be expelled ($\delta^{37}Cl$ of 0.02‰). The fluid expelled at 65 MPa & 30°C was depleted in ^{37}Cl, meaning more ^{35}Cl moved out of the clay compared to ^{37}Cl. After two more weeks at these same P/T conditions, the second sample was significantly depleted in ^{37}Cl relative to the first sample from this step. An even larger proportion of ^{35}Cl (relative to ^{37}Cl) has diffused out with the expelled solution. A variation of 0.2‰ is observed. In contrast, in experiment 3, MX80 compaction without temperature increase, no variation in Cl isotopic composiotion is observed in the two samples collected during 65 MPa step. Comparing the two MX80 compaction experiments, the temperature between the two experiments did not vary much, ~ 31˚C vs ~ 27 ˚C. However, the duration of the step differs, 15 days vs 6 days. Considering as Phillips and Bentley (1987) linked the efficiency of fractionation to the rate at which an isotope can diffuse away from a repulsive charge, resulted ^{35}Cl, with higher ionic mobility, being more effectively repulsed by the charge barrier than ^{37}Cl, as a consequence of longer duration of the step. This result suggest that time is therefore another factor that calls for further investigation.

It must also be taken into account that it is at this point where the mechanism of anion exclusion is expected to come into effect. The calculated bulk dry density achieved in both MX80 compaction experiments exceeds 1.4 $g.cm^{3}.^{-1}$. The calculated percentage pore spoce reduction due to the anion exclusion effect, increases from 4.7 % to 6.3% during this step (in experiment 1). Consequent longer diffusion routes (i.e. increased tortuosity) seems to have a noticeable effect in depleting the expelled solutions in ^{37}Cl. According to Celejewski et al., 2018, the heavier ^{37}Cl isotope should also be slower to diffuse out of the DDL into the free water when the anions are excluded during increasing compaction as theoretically, ^{37}Cl isotope associates more strongly with divalent cations which will preferentially remain sorbed (Schauble et al., 2003).

Steps 2 through 5, the expelled solution continues to be depleted in ^{37}Cl, but the proportion of ^{35}Cl to ^{37}Cl in each expelled sample remains the same. This may be due to the increasing temperatures as the experiment progresses that reduces Cl isotope fractionation.

Then, considering the Cl isotope composition computed from our data, for the chloride remaining in the clay. During the progress of the MX80 compaction, fractionation factors, $\alpha(^{37}Cl/^{35}Cl_{\text{expelled fluid - remaining fluid}})$, decreases from slightly above 1, 1.0002 ± 0.00009, at the beginning of the experiment (pressurization to 45 MPa), to around 1 for the first sample of step 1 and finally systematically below 1 for all the next compaction steps (≈ 0.99975 ± 0.00009). This relation shows that ^{37}Cl were more expelled than ^{35}Cl at the beginning of the compaction and then during further compaction, the opposite occurred.

In comparison, for Br, during all the steps of compaction, isotope fractionations between the expelled fluid and the remaining fluid, $\alpha(^{81}Br/^{79}Br_{\text{expelled fluid - remaining fluid}})$ values are ranging between 0.99984 and 0.99999. They are not distinguishable from 1 at the level of precision achieved here (± 0.0002).

Concerning the Bromine isotope evolution Kharaka and Berry (1973) found that Br is filtered more effectively by a thin clay membrane compared to Cl due to its higher hydrated ionic potential (a function of charge and radius). The repulsive force created by negatively charge barriers in clay under compaction, should generally be stronger on Br than on Cl (and so retardation/preferential expulsion will be more prevalent). In addition, due to the low concentration (natural abundance) of Br compared to Cl (in natural formation waters), any slight uptake or release of Br may significantly affect the bromide concentration (and in effect also the isotopic composition) as pointed out by Fontes and Matray (1993a). What we see here is that it translates into amplified isotope fractionation of Br. We found that calculating the Kemp-Bresler model for membrane efficiency (σ) for $Br^- > 0.8$ (closer to 1, i.e. perfect filtration, compared to $Cl^- < 0.003$).

In the initial increase in pore pressure in the MX80 compaction experiment 1 (up to 45 MPa), the isotopic fractionation of Br (in terms of δ value) is 2 times that of Cl (variation of 0.47‰ vs 0.22‰). Above 65 MPa & 30°C, isotopic fractionation for Br continues while isotopic fractionation for Cl does not.

5.4- **THE CASE OF Br**

Firstly, it has to be pointed out that a delta value of 0.86‰ is highly unlikely for ocean water. Preliminary data obtained from halite samples suggested that the values for the Br isotopes should not be higher than 0.5‰, the value of the reference standard from the IPGP (Eggenkamp et al., 2019). A possible bad distillation may have happened, but seems unlikely as to increase the value by 0.86‰ is so large that something very strange must have occurred during distillation that it could not have gone unnoticed. What however may be possible is that the high value is related to the sample location, which was along the coast: Br isotopes can change because of interaction with organic material, but how large that is, is also not known and has also never been studied in detail. The problem may be that the constancy of Br isotopes in ocean water has never been studied in much detail. What in fact is needed is a study as Godon et al (2004) but for Br isotopes (and perhaps preferentially for each sample measured by the old IRMS method and the new ICP-MS method). Little attention is given to this problem. The purpose of the study is after all to course the changes in isotope ratios due to compaction, and in principle for that study, the primary isotope ratio of the sample is not important, only the changes that occur during the experiments.

The range of Br fractionation achieved during the clay compaction experiments is smaller than what is measured in formation waters (up to 4‰ for δ^{81}Br (Eggenkamp, 2014)), likely due to the much smaller scale and shorter time of the compaction experiment.

What is most interesting to note is that the SSM compaction experiment caused Br isotope fractionation to the same extent as the MX80 compactions. Br isotopes fractionated significantly in the illite rich marl too. This result supports the idea that fractionation is a result of both diffusion and diminishing porosity. With a lesser/smaller influence from the the negative charge, it is possilbly the case that pore size reduction imposes sufficient size exclusion to explain the fractionation in Br isotopes, since they are double the atomic mass of both the Cl stable isotopes. Br also has lower mobility compared to both Cl isotopes. The fractionation of Br during compaction might be more sensitive to decreasing porosity than Cl. The role of pore size reduction is just as important as the negative surface charge in ultrafiltration processes.

When the original Bidart ocean water is first cycled through the marl, the re-equilibrated solution is already enriched in the heavier ^{81}Br, meaning a larger proportion of the lighter ^{79}Br has remained inside clay pore water fraction. During each of the following compaction steps, a larger proportion of ^{81}Br relative to ^{79}Br, is expelled. At the end of the experiment, the solution in the pore pressure generator pump, shows a significant fractionation (from 1.02 ‰ to 1.5‰) while there is no change from the initial Br concentration (0.78 mmol.L^{-1}), to the final Br concentration (0.78 mmol.L^{-1}).

Compaction of the SSM resulted in α ($^{37}Cl/^{35}Cl_{expelled\ fluid\ -\ remaining\ fluid}$) slightly and significantly above 1. They increase from 1.00013, for the two first steps of compaction, to larger values ≥ 1.00023 for the two final steps thus showing that ^{37}Cl were systematically more expelled than ^{35}Cl. For Br, α ($^{81}Br/^{79}Br_{expelled\ fluid\ -\ remaining\ fluid}$) increase from 0.9995 (± 0.0002) at the step 1, second sample, to values of ≈ 0.9998 ± 0.0002, i.e. not distinguishable from 1, for the next compaction steps.
As a summary, significant isotope fractionations were observed for Cl isotopes for compaction of the MX80 and the marl. Taking into account, the isotope fractionations between the expelled and the remaining fluids for the "mature" steps, i.e. above 65 MPa, during which isotope fractionations are established and constant, MX80 (smectite) and SSM (illite) behave the opposite way.

Another possible explanation that needs to be considered, can be the presence of organic matter in the marl. The organic matter/organic carbon content of the marl sample have not been determined. Gao and Liu (2021) found through first principles molecular dynamics modeling that the Br fractionation behavior, in gasses and aqueous environment, is related to the oxidation state of Br. The effect is larger when the Br/Cl ratio is larger. To consider this point, more work would be necessary.

Our study highlights the effect of the type of clay acting as geofilter. While the marl is more compactable, the negative charge of smectite clay is important, and the smectite can potentially dilute pore waters due to illitisation. From the work of Agrinier et al. (2019) the effect of ditution on $\delta^{37}Cl$ value variation, is certainly important when looking at natural sediments, but from our study there is not enough information available to deduce any impact of dilution from smectite clay mineral transformation. More work on to explore the influence of the thickness of the clay layer on Cl and Br isotopic fractionation might be very valuable.

5.5- **POROSITY**

Diagenetic processes affect the preservation of primary porosity and the development of secondary porosity during burial (in Hong et al 2020, Thyne et al., 2001; Bjørlykke and Jahren, 2012; Yuan et al., 2015; Liu et al., 2018; Oluwadebi et al., 2018). Mechanical compaction is generally the dominant porosity- reducing mechanism in all diagenetic facies types and can typically reduce porosity from 45% to 10% at a depth of 4000 m (Ramm and Bjørlykke, 1994).

The SSM was compacted to a lower final mercury connected porosity (8%) than the MX80 (17% in experiment 1, and 15% in experiment 3). However, the trapped porosity is larger for the MX80 (9% and 8%) than for the SSM (3.6%). Therefore, because of this trapped porosity, the effective network of porosity available for fluid flow or transport of solutes is greatly reduced in the MX80, which was found to be a more overall effective filtration membrane. In both the MX80 and SSM, the largest decreases in total porosity (calculated from the volumetric mass densities) correspond to significant fractionations. In the MX80 compaction experiment 1, the most prevalent decrease in calculated porosity (42% to 35.6%) during the step at 65MPa and 30°C corresponds to a significant fractionation for both Cl (-0.24‰ to -0.45‰ for δ^{37}Cl) and Br (1.38‰ to 1.33‰ for δ81Br). The next most prevalent decrease in porosity during the MX80 compaction occurred at 125 MPa and 120°C. The porosity was reduced by 4% (from 29 to 25 %). Significant fractionation is seen only for Br during this step (1.5‰ to 0.7‰ for δ^{81}Br). In the SSM compaction the largest loss of porosity (35% to 25%) also occurs at 65MPa and 30°C, which corresponds to a small fractionation in Br (from 1.65‰ to 1.5‰ for δ^{81}Br). However, the next most prevalent reduction in porosity (from 25% to 21%), at 85 MPa and 60°C, corresponds to significant fractionation of Br (from 1.5 to 0.9‰ for δ^{81}Br). For the two clay rocks, the reduction of porosity and its consequences on the isotope fractionations cannot be correlated with certainty. The fractionation of Br isotopes continues longer by comparison with Cl when the compaction increases. Potentially due to the larger size of the Br anions.

Although the two elements pass through the same filtration membrane with the same porosity, this large difference in filtration efficiency (σ), as presented in Figure 28, is likely due to concentration of Br^- being so much smaller than for Cl^-. If for example, we have a solution containing 2 Br molecules and 10 Cl molecules, and one of eace is filtered out when passing through a semi permeable membrane, that is 10% for Cl and 50% for Br. The effect on filtration is therefore remarkable. However, we have to keep in mind that anions are excluded from the DDL and therefore effectively a part of the pore size is lost to them. For our experiment, this has been found to be up to 9 % in the later compaction stages. As Br is the larger anion, the continuous reduction anion available porosity forces the ‘too large’ Br anions out, and we see the expelled water being enriched in the heavier Br

isotope. As Cl is significantly smaller, it is not affected in the same way. This could explain why we see Br isotopic fractionation in the SSM and not for the Cl. The same could be said for the MX80 compaction experiment 3 where no temperature is applied. The decreasing porosity drives isotopic fractionation and the extra retardation from higher temperature is not present, so less Cl isotopic fractionation is observed. As Br isotopic fractionation is much more subject to decreasing porosity, comparably similar ranges of isotopic fractionation are observed in all three compaction experiments.

Do note that, comparing the two MX80 compactions, experiment 3 was compacted do a somewhat lower porosity that experiment 1 in each of the compaction steps. This could be due to water being less compressible at higher temperatures, (normally accounted for as the thermal expansion coefficient). As water at higher temperatures is less compressible, it would rather be expelled. Therefore we see more pore water expelled in experiment 1 (temperature applied) compared to experiment 3 (no temperature applied) – 29 mL in total vs 15 mL in total).

5.6- POTENTIAL MECHANISMS DRIVING PORE WATER EVOLUTION

Since only a part of the total porosity is accessible for anion transport, the water sampled gives the chemistry of the free pore water. For both MX80 experiments 1 and 3, we see that without any pressure or temperature applied during the hydration phase of the experiments, the concentrations of Br and Cl increase, mainly due to the water uptake and adsorption by clay minerals. During the equilibrium phase, and because this phase lasted around three weeks, we can expect that diffusion processes could drive the isotopic fractionation observed for both Cl and Br. In our experiment, the outflowing water contains more of the lighter Cl isotope which is in agreement with the diffusion mechanism. However, because the heavier Br isotope is found in this same water, another mechanism has to be evoked. We can perhaps consider potential gravitational settlement of heavier Br isotopes. For example, it took a total of 90 days for the completion of the hydration and equilibration (fluid circulation) phase to be completed in experiment 1. Water was sampled at the end of the 90 days. During the fluid circulation phase, water was circulated from the pump connected at the top of the sample, to the pump connected at the bottom of the sample so that when compaction started, the expelled sample could be collected in the empty pump connected at the top of the clay sample. Therefore, the sample called 'initial water' came from the pump connected at the bottom of the clay. Gravitational isotopic fractionation is seen in columns of oil and gaz reservoirs, in hydrothermal fluids, in sediments and even trapped air (Bons and Gomaz Rivas, 2012; Shirdokar et al., 2003; Zang and Kroos, 2001, Guinta et al 2017; Agrinier, 2019). This might be the case for Br.

When compaction started, pore pressure was maintained with the full pump connected to the bottom of the clay, and the expelled samples were collected in the empty pump connected to the top of the clay. This could possibly explain the change in direction of the arrows on Figure 22 and Figure 23from 'initial' composition to 'pore pressure' composition, seen in experiment 1, 2 and 3. With the first pressurization, the free pore water is expelled.

The dominant mechanism of transport should be advection, so isotopic fractionation due to the pressurization should remain limited. This early compaction corresponds to the most significant decrease in porosity. As we reduced porosity, the composition of the free water, enriched in Cl and Br, can be attributed to the anion exclusion effect. The isotopic composition in Br and Cl is actually the composition enriched in heavier Cl and lighter Br, as a result of the inverse fractionation observed in the hydration step. The largest volumes of water are expelled during early compaction and the composition of the expelled water is supposed to be that of the free water.

As compaction continues pore size continues to decrease. The interparticle porosity will decrease first while the interlayer porosity will remain more or less constant (Muurinen et al., 2004). When the dry bulk density surpasses 1300 kg.m-3 (this is the case between 45 and 65 MPa), the interlayer porosity will also start to be affected and decrease (Van Loon et al., 2007). This further amplifies both the anion exclusion and trapping effect. The water expelled is different in composition from the trapped water. Cl and Br concentrations decrease in the water expelled at this point because they are trapped in the porosity by the anion exclusion effect. In addition to being forced to travel via longer transport routes through the clay layer, anions become trapped inside the diminishing pore spaces as a function of the ion size. Diffusion processes are more likely responsible for isotope fractionation implying that lighter isotopes move faster. This is valid for Cl. For Br it is the heavier (larger) isotope that is preferentially expelled. ^{35}Cl with higher ionic mobility would be more effectively repulsed by the charge barrier than ^{37}Cl. The heavier ^{37}Cl isotope is also slower to diffuse out of the DDL into the free water when the anions are excluded during increasing compaction as theoretically, ^{37}Cl isotope associates more strongly with divalent cations which will preferentially remain sorbed.

At the highest compaction steps, the effect of higher temperature has to be mentioned because this can lead to faster diffusion and potential mineral transformation. Cl and Br in the expelled water continue to decrease due to diminishing pore size, which can be enhanced by possible mineral precipitation at high temperature. In terms of isotopes the expelled water tends to be slightly enriched in heavier Cl isotope and more significantly enriched in lighter Br isotope. In correspondence to the findings of Kharaka and Berry (1973); Lavastre et al., (2005); Van Loon et al., (2007); and Nakata et al., (2016), the results from this study emphasize that the surface chemistry of the clay is a key factor in the efficiency of the clay to act as a filtration membrane. Smectite rich MX80, with a higher negative surface charge, was a more efficient filtration membrane for both Cl and Br anions compared to the illite-rich SSM, despite the SSM having been compacted to a much lower porosity than the MX-80.

Conclusion

CONCLUSION

Our study on the isotopes of Cl an Br in water expelled during experimental compaction of clays, shows that they can help to reveal the history of pore fluids through understanding the mechanisms that impact its composition. We experimentally showed the functioning of the same mechanisms as described in literature. There is much potential for further studies on the topic, especially concerning the thickness of a clay filtration layer, as well as the impact of organic matter on the fractionation of Br stable isotopes.

The aim of our work was to experimentally simulate the diagenetic processes of fluid and heat flow, mechanical compaction that are involved in the freshening of formation water from a saturated clay sample. With the novel large-scale oedometric compression cell we developed for the purpose of this study, our work highlights the effect of mechanical compaction, temperature and type of clay during ultrafiltration. The multi-disciplinary collaboration in this work contribute to a better understanding of Cl and Br behavior in geological processes. There are no similar multi-disciplinary large-scale experiments in the literature.

Our objective was to use the general water chemistry, as well as Cl and Br isotopic tracers to track the evolution of freshwater production with time. Our experiments showed effective freshening and fractionation of Cl and Br isotopes. The range of freshening and fractionation observed in our experiment is in line with, but smaller than what is measured in natural samples. This is due to the extremely short time of the experiments (compared to geological time) and small volume of expelled water produced during the compactions.

Continuously following the axial deformation, and monitoring the composition of the input and expelled water, it allowed for a water and chemical mass balance of the system. We could therefore calculate, what the remaining pore water composition should be, with each consecutive compaction step, to compare with the composition of the expelled water. Modeling one of the experiments with state of the art specialized SURP software confirmed/clarified that, under the experimental conditions applied, no true smectite illitisation is expected to occur and therefore potential dilution from water released during this mineral transformation, did not play a role in our experiments.

In conclusion, we suggest that:

1. Anion and isotope evolution during the compaction of clays is a function of both chemical and physical water-rock interactions. The surface chemistry of the clay in combination with decreasing porosity result in re-equilibration of compressed and overlapping diffuse double layers which, in large, drive the anion and isotope evolution, in accordance with well established diffusion theory.

2. The clay with more negative surface charge is more effective in ultrafiltration/freshening of water expelled during compaction irrespective of its degree of compaction.
3. More effective freshening is also achieved when temperature is incrementally increased along with pressure.
4. Reduction in porosity and the resulting charge barrier created due to overlapping of DDL's causes anions to become trapped in the clay layer. The retention effect is slightly more pronounced for Br than for Cl.
5. Longer transport routes did not have a significant effect on the concentration of anions in the expelled water but did have a significant effect on the isotope composition.
6. The range of isotopic fractionation observed for Br is larger than what is seen for Cl.
7. The charge barrier resulting from compaction of negatively charged clays caused preferential expulsion of the heavier isotope for Cl and the lighter isotope for Br.
8. Fractionation of Cl isotopes is more prevalent during the earlier compaction steps (lower pressures and temperatures) Fractionation of Br isotopes becomes more pronounced at the later compaction steps (higher pressures and temperatures).

LIST OF FIGURES

Figure 1: Profil minéralogique simulé montrant la Na-Montmorillonite hydratée (3, 2 ou 1 couches d'eau adsorbées) en orange et la Na-Montmorillonite anhydre en bleu en A. En B, la diminution de la porosité correspondante est représentée. 14

Figure 2: Concentrations en cations et en anions de l'eau expulsée au cours des trois expériences de compactage et composition calculée de l'eau interstitielle restant dans l'argile. 15

Figure 3: Gammes de fractionnement isotopique du Cl et du Br observées dans l'eau expulsée lors des trois expériences de compaction. Les formes pleines représentent les valeurs de δ37Cl et les formes vides représentent les valeurs de δ81Br. Les losanges jaunes colorés et vides représentent les valeurs initiales de l'eau océanique de $\delta^{37}Cl$ et $\delta^{81}Br$ respectivement. 16

Figure 4: An illustration of the influence of the negative charge of clay particles on the physical and chemical morphology of clay rock pore spaces showing progressive expulsion and trapping and of the Cl and Br anions during compaction of negatively charged stacks. *Red arrows represent the possible motions of ions in interlayer water and between free water and bound water* (Partly modified from Apello et al. 2010). 44

Figure 5: Cations in an electrolyte solution are attracted to the clay surface. As the pore is compacted, the double layers overlap, lowering the concentration of the anions in the pore solution, leading to anion exclusion (from Campbell 1985). 45

Figure 6 : Illustration of the experimental system showing the compaction (oedometric) cell [A] and various operation systems; the oil-pressure generator (for the axial stress) [B] and the fluid circulation system [C]; the control and data acquisition systems [D]; the system for heating control [E]. 55

Figure 7 : Schematic presentation of the pressure and temperature increments followed in the experiments. The pore pressure was maintained at 45 MPa while the axial stress was increased from 45.5 MPa to 150 MPa (maximal effective stress: 105 MPa) by increments not exceeding 25 MPa, and temperature increments of ~ 30°C. 57

Figure 8 : A photo of the experimental system showing the compaction (oedometric) cell [A] and various operation systems; the oil-pressure generator (for the axial stress) [B] and the fluid circulation system [C]; the control and data acquisition systems [D]; the system for heating control [E]. 58

Figure 9 : Gas column used for precipitation of silver chloride, preceding Cl isotope measurements. 60

Figure 10: Distillation of the ocean water to extract bromine. 61

Figure 11 : Diagram to illustrate the mass balance calculation between expelled and remaining pore water composition for a given element. 63

Figure 12 : Architecture of the calculations made by the SURP code, including the coupling of the thermo-hydro-mechanical calculations with Python language and the thermodynamic reactive calculations made using the IPHREEQC code (from Tremosa et al., 2020). 66

Figure 13: The compaction curve for the compaction of MX-80 in Experiment 1 that lasted from 22/11/2017 to 12/06/2018. 76

Figure 14: The compaction curve for the Sainte Suzanne marl in Experiment 2 that lasted from 16/07/2018 to 23/11/2018. 76

Figure 15 : The compaction curve for MX-80 in Experiment 3 that lasted from 02/04/2019 to 09/10/2019. 77

Figure 16 : Variation in concentration of Cl^- in the expelled water and in the water remaining in the compacted clay (from mass balance calculation, see section 3.4.2) as pressure and temperature increase. The Cl^- concentration of the original ocean water is shown in orange, Experiment 1, 2 and 3 are in red, blue and black respectively. 82

Figure 17 : Variation in concentration of Br^- in the expelled water and in the water remaining in the compacted clay (from mass balance calculation, see section 3.4.2) as pressure and temperature increase. The Br^- concentration of the original ocean water is shown in orange, Experiment 1, 2 and 3 are in red, blue and black respectively. 83

Figure 18: The Br vs Cl plot for the MX-80 compaction experiments and the Sainte-Suzanne marls. Experiment 1, 2 and 3 are in red, blue and black respectively. 83

Figure 19: Variation in concentration of major cations in the expelled water and in the water remaining in the compacted clay (from mass balance calculation, see section 3.4.2) as pressure and temperature increase. The composition of the original ocean water is shown in orange, Experiment 1, 2 and 3 are in red, blue and black respectively. 88

Figure 20 : Cation and corresponding anion concentrations of the water expelled during the three compaction experiments as well as for the calculated composition of the pore water remaining within the clay. 89

Figure 21: Values for the isotopes of Cl and Br plot within the expected range of values of -8‰ to 1.5‰ for $\delta^{37}Cl$ and -1.5‰ to 4‰ for $\delta^{81}Br$, as presented on the inserted figure from Eggenkamp (2014). 90

Figure 22 : The Cl isotope values plotted against the corresponding anion concentration for the water expelled during MX-80 (Experiment 1 & 3) and Sainte-Suzanne marl (Experiment 2) compaction. 92

Figure 23: The Br isotope values plotted against the corresponding anion concentration for the water expelled during MX-80 (experiment 1 & 3) and Sainte-Suzanne marl (experiment 2) compaction. 92

Figure 24: The range of Cl and Br isotopic fractionation observed in the water expelled during MX-80 compaction in Experiment 1. Colored circles represent $\delta^{37}Cl$ values and empty circles represent $\delta^{81}Br$ values. The colored and empty diamond represent the initial ocean water $\delta^{37}Cl$ and $\delta^{81}Br$ values respectively. 93

Figure 25: The range of Cl and Br isotopic fractionation observed in the water expelled during Sainte-Suzanne marl compaction in experiment 2. Colored circles represent δ37Cl values and empty circles represent δ81Br values. The colored and empty diamond represent the initial ocean water δ37Cl and δ81Br values respectively. 95

Figure 26 : The range of Cl and Br isotopic fractionation observed in the water expelled during Sainte-Suzanne marl compaction in experiment 2. Colored circles represent $\delta^{37}Cl$ values and empty circles represent $\delta^{81}Br$ values. The colored and empty diamond represent the initial ocean water $\delta^{37}Cl$ and $\delta^{81}Br$ values respectively. 96

Figure 27: Simulate mineralogical profile showing hydrated Mnt Na (3w 2w or 1w Na montmorillonite) and anhydrous Na-Montmorillonite. 99

Figure 28: The membrane efficiency of compacting MX80 for Cl and Br respectively, according to the Kemp- Bresler model (Bresler, 1973). 102

Figure 29: The total calculated percentage porosity with increasing vertical stress, for the three compaction experiments. 105

Figure 30: The calculated bulk dry density with increasing vertical stress for the three compaction experiments. 106

Figure 31: For Experiment 1 (MX80) the total mercury connected porosity (solid line), free (dashed line) and trapped porosity (dotted line) are plotted along with pore size radii. 106

Figure 32 : For Experiment 2 (SSM) the total mercury connected porosity (solid line), free (dashed line) and trapped porosity (dotted line) are plotted along with pore size radii. 107

Figure 33: For Experiment 3 (MX80 no T) the total mercury connected porosity (solid line), free (dashed line) and trapped porosity (dotted line) are plotted along with pore size radii. 107

Figure 34 : N2 adsorption isotherme for MX80 after compaction Experiment 1. The adsorption curve is given in solid red and the desorption curve in dashed red. 108

Figure 35 : Nitrogen adsorption/desorption isotherm for SSM after compaction Experiment 2. The adsorption curve is given in blue and the desorption curve in dashed blue. 109

Figure 36 : Nitrogen adsorption/desorption isotherm for MX80 after compaction Experiment 3 (MX80 no T). The adsorption curve is given in black and the desorption curve in dashed grey. 109

Figure 37: Pore size distribution profile after application of the BJH method on to the adsorption branches of the N_2 isotherms (assuming the cylindrical pore-shape model). 110

Figure 38 : The percentage total porosity with increasing vertical stress, for the compaction experiments (dashed black line) compared to the porosity evolution calculated with the SURP code (pink). 111

Figure 39: X-Ray diffractogram of the initial Sainte-Suzanne marl for fractions smaller than 2 µm. 113

Figure 40: Scanning electron microscope image of the initial Sainte-Suzanne marl before experimentation. 115

Figure 41: Scanning electron microscope image from a polished surface of the compacted MX-80 core from Experiment 1. 116

Figure 42: A crack along the border of feldspar grain observed in the compacted MX-80 core after Experiment 1. EDS spectra of the feldspar (A), the clay next to the crack (B) and the general clay matrix (C). 117

Figure 43: X-Ray diffractogram of the compacted MX-80 core after Experiment 1. 118

Figure 44: Scanning electron microscope image of the compacted Sainte-Suzanne marl core after Experiment 2. 118

Figure 45: X-Ray diffractogram of the original Sainte Suzanne marl core (black line) and compacted core from Experiment 2 (red line). 119

Figure 46: Scanning electron microscope image from a polished surface of the compacted MX-80 core from Experiment 3. 119

Figure 47: X-Ray diffractogram of the compacted MX80 core following experiment 3 (blue line) compared to experiment 1 (red) and the original MX80 (black lines). 120

Figure 48: The relationship of $\delta^{81}Br$ and $\delta^{37}Cl$ in various source waters. 129

LIST OF TABLES

Table 1: The total chemical composition for MX-80 and Sainte Suzanne marl as weight % of major elements oxides. MX-80 composition is from (Rapport caractérisation MX80, n.d.) and marl composition is determined by ICP-OES at SARM (Nancy). 52

Table 2: The initial chemical composition of the stock ocean water from Bidart, France, used in the three compaction experiments. 53

Table 3: Steps of compaction applied during the SURP during the geochemical modeling approach. 67

Table 4: Volumes of fluid absorbed and expelled during the experiment. For all three experiments, two fluid samples were collected during the compaction step at 65 MPa. 78

Table 5: Concentrations in the expelled fluid and concentrations calculated to remain in the compacted core. The ratio of enrichment for each element is given in brackets. 79

Table 6: Cl/Br in the pore fluid expelled and retained during the three compaction experiments. 81

Table 7: Concentrations in the expelled fluid and concentrations calculated to remain in the compacted core. The ratio of enrichment for each element is given in brackets. 84

Table 8: Concentrations in the expelled fluid and concentrations calculated to remain in the compacted core. The ratio of enrichment for each element is given in brackets. 85

Table 9: Isotope values for the water expelled during Experiment 1. 93

Table 10: Cl isotope mass balance to compute the isotopic composition of Cl trapped in MX-80 in Experiment 1. 94

Table 11: Br isotope mass balance to compute the isotopic composition of Cl trapped in MX-80 in Experiment 1. 94

Table 12: Isotope values for the water expelled during Experiment 2 (SSM). 95

Table 13: Cl isotope mass balance to compute the isotopic composition of Cl trapped in Sainte-Suzanne marl in experiment 2. 95

Table 14: Br isotope mass balance to compute the isotopic composition of Br trapped in Sainte-Suzanne marl in Experiment 2 (SSM). 96

Table 15: Isotope values for the water expelled during Experiment 3 (MX80 no T). 96

Table 16: Cl isotope mass balance to compute the isotopic composition of Cl trapped in MX-80 in Experiment 3 (MX80 no T). 97

Table 17 : Br isotope mass balance to compute the isotopic composition of Br trapped in MX-80 in Experiment 3 (MX80 no T). 97

Table 18: Calculated anion exclusion effect a percentage pore size reduction (proportion of pore size that is not available to anions). 101

Table 19: Determining the membrane efficiency of MX-80 as filtration membrane. 102

Table 20: Description of the materials for each of the experiments. 103

Table 21: Chemical composition of MX-80 and Sainte Suzanne marl before and after compaction. Determination of major elements in percentage of oxides per ICP-MS iCapQ (SARM). 114

REFERENCES

Ab'Saber, A. N. (1961). AMERICAN GEOLOGICAL INSTITUTE," Glossary of Geology and Sciences"(Book Review). *Revista Geográfica*, *29*(55), 139.

Ader, M., Coleman, M. L., Doyle, S. P., Stroud, M., & Wakelin, D. (2001). Methods for the stable isotopic analysis of chlorine in chlorate and perchlorate compounds. *Analytical Chemistry*, *73*(20), 4946-4950.

Agrinier, P., Bardoux, G., Giunta, T., Bonifacie, M., Destrigneville, C., Lucazeau, F., ... & Eggenkamp, H. (2018, October). Chlorine stable isotope ratios (35Cl/37Cl) of chlorides of fluids produced in low permeability clay-rich sediments: the potential role ion filtration. In *Second EAGE Workshop on Geochemistry in Petroleum Operations and Production* (pp. cp-581). European Association of Geoscientists & Engineers.

Agrinier, P., Destrigneville, C., Giunta, T., Bonifacie, M., Bardoux, G., Andre, J., & Lucazeau, F. (2019). Strong impact of ion filtration on the isotopic composition of chlorine in young clay-rich oceanic sediment pore fluids. *Geochimica et Cosmochimica Acta*, *245*, 525-541.

Alcalá, F. J., & Custodio, E. (2008). Using the Cl/Br ratio as a tracer to identify the origin of salinity in aquifers in Spain and Portugal. *Journal of Hydrology*, *359*(1-2), 189-207.

Alonso, U., Missana, T., Garcia-Gutierrez, M., Patelli, A., Albarran, N., & Rigato, V. (2011). Colloid diffusion coefficients in compacted and consolidated clay barriers: Compaction density and colloid size effects. *Physics and Chemistry of the Earth, Parts A/B/C*, *36*(17-18), 1700-1707.

Altaner, S. P., & Ylagan, R. F. (1997). Comparison of structural models of mixed-layer illite/smectite and reaction mechanisms of smectite illitization.

Appelo, C. A. J., Van Loon, L. R., & Wersin, P. (2010). Multicomponent diffusion of a suite of tracers (HTO, Cl, Br, I, Na, Sr, Cs) in a single sample of Opalinus Clay. Geochimica et Cosmochimica Acta, 74(4), 1201-1219.

Aran, D., Maul, A., & Masfaraud, J. F. (2008). A spectrophotometric measurement of soil cation exchange capacity based on cobaltihexamine chloride absorbance. *Comptes Rendus Geoscience*, *340*(12), 865-871.

Arndt, S., Jørgensen, B. B., LaRowe, D. E., Middelburg, J. J., Pancost, R. D., & Regnier, P. (2013). Quantifying the degradation of organic matter in marine sediments: a review and synthesis. Earth-science reviews, 123, 53-86.

Audet, D. M. (1995). Modelling of porosity evolution and mechanical compaction of calcareous sediments. Sedimentology, 42(2), 355-373.

Bagheri, R., Nadri, A., Raeisi, E., Eggenkamp, H. G. M., Kazemi, G. A., & Montaseri, A. (2014). Hydrochemical and isotopic (δ18O, δ2H, 87Sr/86Sr, δ37Cl and δ81Br) evidence for the origin of saline formation water in a gas reservoir. *Chemical Geology*, *384*, 62-75.

Bagheri, R., Nadri, A., Raeisi, E., Kazemi, G. A., Eggenkamp, H. G. M., & Montaseri, A. (2014a). Origin of brine in the Kangan gasfield: isotopic and hydrogeochemical approaches. *Environmental Earth Sciences*, *72*(4), 1055-1072.

Bahnan, A. E., Carpentier, C., Pironon, J., Ford, M., Ducoux, M., Barré, G., ... & Gaucher, E. C. (2020). Impact of geodynamics on fluid circulation and diagenesis of carbonate reservoirs in a foreland basin: Example of the Upper Lacq reservoir (Aquitaine basin, SW France). *Marine and Petroleum Geology*, *111*, 676-694.

Balan, E., Créon, L., Sanloup, C., Aléon, J., Blanchard, M., Paulatto, L., & Bureau, H. (2019). First-principles modeling of chlorine isotope fractionation between chloride-bearing molecules and minerals. *Chemical Geology*, *525*, 424-434.

Beekman, H. E., Eggenkamp, H. G. M., & Appelo, C. A. J. (2011). An integrated modelling approach to reconstruct complex solute transport mechanisms–Cl and δ37Cl in pore water of sediments from a former brackish lagoon in The Netherlands. *Applied geochemistry*, *26*(3), 257-268.

Benzel, W. M., & Graf, D. L. (1984). Studies of smectite membrane behavior: Importance of layer thickness and fabric in experiments at 20 C. *Geochimica et Cosmochimica Acta*, *48*(9), 1769-1778.

Benzel, W. M., & Graf, D. L. (1984). Studies of smectite membrane behavior: Importance of layer thickness and fabric in experiments at 20 C. Geochimica et Cosmochimica Acta, 48(9), 1769-1778.

Bernachot, I., Garcia, B., Ader, M., Peysson, Y., Rosenberg, E., Bardoux, G., & Agrinier, P. (2017). Solute transport in porous media during drying: The chlorine isotopes point of view. *Chemical Geology*, *466*, 102-115.

Berry, F. A. (1969). Relative factors influencing membrane filtration effects in geologic environments. *Chemical geology*, *4*(1-2), 295-301.

Berry, F. A. F., & Hanshaw, B. B. (1960). Geologic evidence suggesting membrane properties of shales: 21st Internal. *Geol. Cong.(Copenhagen 1960), Abstract Volume*, 209.

Bethke, C. M., & Altaner, S. P. (1986). Layer-by-layer mechanism of smectite illitization and application to a new rate law. *CLAYS CLAY MINER. Clays Clay Miner.*, *34*(2), 136.

Bethke, C. M., & Marshak, S. (1990). Brine migrations across North America—The plate tectonics of groundwater. *Annual Review of Earth and Planetary Sciences*, *18*(1), 287-315.

Bjørlykke, K. (1999). Principal aspects of compaction and fluid flow in mudstones. *Geological Society, London, Special Publications*, *158*(1), 73-78.

Bjørlykke, K., & Jahren, J. (2012). Open or closed geochemical systems during diagenesis in sedimentary basins: Constraints on mass transfer during diagenesis and the prediction of porosity in sandstone and carbonate reservoirs. *AAPG bulletin*, *96*(12), 2193-2214.

Boles, J. R., & Franks, S. G. (1979). Clay diagenesis in Wilcox sandstones of Southwest Texas; implications of smectite diagenesis on sandstone cementation. Journal of Sedimentary Research, 49(1), 55-70.

Bolt, G. H., & De Haan, F. A. M. (1979). Anion exclusion in soil. In *Developments in Soil Science* (Vol. 5, pp. 233-257). Elsevier.

Bonifacie, M., Charlou, J. L., Jendrzejewski, N., Agrinier, P., & Donval, J. P. (2005). Chlorine isotopic compositions of high temperature hydrothermal vent fluids over ridge axes. *Chemical Geology*, *221*(3-4), 279-288.

Bonifacie, M., Monnin, C., Jendrzejewski, N., Agrinier, P., & Javoy, M. (2007). Chlorine stable isotopic composition of basement fluids of the eastern flank of the Juan de Fuca Ridge (ODP Leg 168). *Earth and Planetary Science Letters*, *260*(1-2), 10-22.

Boschetti, G., Nancey, S., Sardi, F., Roblin, X., Flourié, B., & Kaiserlian, D. (2011). Therapy with anti-TNFα antibody enhances number and function of Foxp3+ regulatory T cells in inflammatory bowel diseases. *Inflammatory bowel diseases*, *17*(1), 160-170.

Boschetti, T., Toscani, L., Shouakar-Stash, O., Iacumin, P., Venturelli, G., Mucchino, C., & Frape, S. K. (2011b). Salt waters of the Northern Apennine Foredeep Basin (Italy): origin and evolution. *Aquatic Geochemistry*, *17*(1), 71-108.

Bourg, I. C., Bourg, A. C., & Sposito, G. (2003). Modeling diffusion and adsorption in compacted bentonite: a critical review. *Journal of Contaminant Hydrology*, *61*(1-4), 293-302.

Brady, N. C., & Weil, R. R. (2008). *The Nature and Properties of Soils, 15th ed Pearson Prentice Hall, New Jersey and Ohio*.

Bredehoeft, J. D., Blyth, C. R., White, W. A., & Maxey, G. B. (1963). Possible mechanism for concentration of brines in subsurface formations. AAPG Bulletin, 47(2), 257-269.

Bredehoeft, J. D., Neuzil, C. E., & Milly, P. C. D. (1983). Regional flow in the Dakota aquifer: A study of the role of confining layers (Vol. 2237). US Government Printing Office.

Bresler, E. (1973). Anion exclusion and coupling effects in nonsteady transport through unsaturated soils: I. Theory. *Soil Science Society of America Journal*, *37*(5), 663-669.

Campbell, D. J. (1985). FRACTIONATION OF STABLE CHLORINE ISOTOPES DURING TRANSPORT THROUGH SEMIPERMEABLE MEMBRANES (Doctoral dissertation, The University of Arizona).

Carrizo, D., Unger, M., Holmstrand, H., Andersson, P., Gustafsson, Ö., Sylva, S. P., & Reddy, C. M. (2011). Compound-specific bromine isotope compositions of one natural and six industrially synthesised organobromine substances. *Environmental Chemistry*, *8*(2), 127-132.

Cazanacli, D., Paola, C., & Parker, G. (2002). Experimental steep, braided flow: application to flooding risk on fans. *Journal of Hydraulic Engineering*, *128*(3), 322-330.

Celejewski, M., Barton, D., & Al, T. (2018). Measurement of Cl−: Br− Ratios in the Porewater of Clay-Rich Rocks—A Comparison of the Crush-and-Leach and the Paper-Absorption Methods. *Geofluids*, *2018*.

Christidis, G. E. (1995). Mechanism of illitization of bentonites in the geothermal field of Milos Island Greece: Evidence based on mineralogy, chemistry, particle thickness and morphology. Clays and Clay Minerals, 43(5), 569-585.

Clauer, N., Liewig, N., & Bobos, I. (2010). K-Ar, δ 18 O and REE constraints on the genesis of ammonium illite from the Harghita Bai hydrothermal system, Romania. Clay Minerals, 45(3), 393-411.

Clauer, N., Środoń, J., Francu, J., & Šucha, V. (1997). K-Ar dating of illite fundamental particles separated from illite-smectite. Clay minerals, 32(2), 181-196.

Coleman, M. L. (1992). Water composition variation within one formation. In *International symposium on water-rock interaction* (pp. 1109-1112).

Conin, M., Henry, P., Bourlange, S., Raimbourg, H., & Reuschlé, T. (2011). Interpretation of porosity and LWD resistivity from the Nankai accretionary wedge in light of clay physicochemical properties: Evidence for erosion and local overpressuring. *Geochemistry, Geophysics, Geosystems*, *12*(3).

Coplen, T. B., & Hanshaw, B. B. (1973). Ultrafiltration by a compacted clay membrane—I. Oxygen and hydrogen isotopic fractionation. *Geochimica et Cosmochimica Acta*, *37*(10), 2295-2310.

Cuisinier, O., & Laloui, L. (2004). Fabric evolution during hydromechanical loading of a compacted silt. *International Journal for Numerical and Analytical Methods in Geomechanics*, *28*(6), 483-499.

Davis, S. N., Whittemore, D. O., & Fabryka-Martin, J. (1998). Uses of chloride/bromide ratios in studies of potable water. *Groundwater*, *36*(2), 338-350.

Davisson, M. L., & Criss, R. E. (1996). Na-Ca-Cl relations in basinal fluids. *Geochimica et Cosmochimica Acta*, *60*(15), 2743-2752.

De Sitter, L. U. (1947). Diagenesis of oil-field brines. *AAPG Bulletin*, *31*(11), 2030-2040.

Desaulniers, D. E., Kaufmann, R. S., Cherry, J. A., & Bentley, H. W. (1986). 37Cl-35Cl variations in a diffusion-controlled groundwater system. *Geochimica et Cosmochimica Acta*, *50*(8), 1757-1764.

Descostes, M., Blin, V., Bazer-Bachi, F., Meier, P., Grenut, B., Radwan, J., ... & Tevissen, E. (2008). Diffusion of anionic species in Callovo-Oxfordian argillites and Oxfordian limestones (Meuse/Haute–Marne, France). *Applied Geochemistry*, *23*(4), 655-677.

Drever, J. I. (1997). The geochemistry of natural waters Prentice Hall. *Englewood Cliffs, New Jersey*.

Düppenbecker, S. J., Dohmen, L., & Welte, D. H. (1991). Numerical modelling of petroleum expulsion in two areas of the Lower Saxony Basin, Northern Germany. Geological Society, London, Special Publications, 59(1), 47-64.

Eastoe, C. J., Long, A., & Knauth, L. P. (1999). Stable chlorine isotopes in the Palo Duro Basin, Texas: evidence for preservation of Permian evaporite brines. *Geochimica et Cosmochimica Acta*, *63*(9), 1375-1382.

Eastoe, C. J., Long, A., Land, L. S., & Kyle, J. R. (2001). Stable chlorine isotopes in halite and brine from the Gulf Coast Basin: brine genesis and evolution. *Chemical Geology*, *176*(1-4), 343-360.

Eberl, D. D., & Srodon, J. (1988). Ostwald ripening and interparticle-diffraction effects for illite crystals. American Mineralogist, 73(11-12), 1335-1345.

Eggenkamp, H. (2014). *The geochemistry of stable chlorine and bromine isotopes* . Berlin: Springer.

Eggenkamp, H. G. M. (1994). δ37Cl: The geochemistry of chlorine isotopes (Ph. D. thesis, Utrecht, Universiteit Utrecht).

Eggenkamp, H. G. M. (2014a). A closer look at chlorine and bromine isotopes; An approach to understand the similarities and differences. *Journal of Biology and Earth Sciences*, *4*(3 Suppl. 1).

Eggenkamp, H. G. M., & Coleman, M. L. (2000). Rediscovery of classical methods and their application to the measurement of stable bromine isotopes in natural samples. *Chemical Geology*, *167*(3-4), 393-402.

Eggenkamp, H. G. M., & Coleman, M. L. (2009). The effect of aqueous diffusion on the fractionation of chlorine and bromine stable isotopes. *Geochimica et Cosmochimica Acta*, *73*(12), 3539-3548.

Eggenkamp, H. G. M., & Louvat, P. (2018). A simple distillation method to extract bromine from natural water and salt samples for isotope analysis by multi-collector inductively coupled plasma mass spectrometry. *Rapid Communications in Mass Spectrometry*, *32*(8), 612-618.

Eggenkamp, H. G. M., Bonifacie, M., Ader, M., & Agrinier, P. (2016). Experimental determination of stable chlorine and bromine isotope fractionation during precipitation of salt from a saturated solution. *Chemical Geology*, *433*, 46-56.

Eggenkamp, H. G. M., Kreulen, R., & Van Groos, A. K. (1995). Chlorine stable isotope fractionation in evaporites. *Geochimica et Cosmochimica Acta*, *59*(24), 5169-5175.

Eggenkamp, H. G. M., Louvat, P., Agrinier, P., Bonifacie, M., Bekker, A., Krupenik, V., ... & Bagheri, R. (2019). The bromine and chlorine isotope composition of primary halite deposits and their significance for the secular isotope composition of seawater. *Geochimica et Cosmochimica Acta*, *264*, 13-29.

Eisenman, G. (1962). Cation selective glass electrodes and their mode of operation. *Biophysical journal*, *2*(2 Pt 2), 259.

Elderfield, H., Wheat, C. G., Mottl, M. J., Monnin, C., & Spiro, B. (1999). Fluid and geochemical transport through oceanic crust: a transect across the eastern flank of the Juan de Fuca Ridge. *Earth and Planetary Science Letters*, *172*(1-2), 151-165.

Emerson, S., & Hedges, J. I. (1988). Processes controlling the organic carbon content of open ocean sediments. Paleoceanography, 3(5), 621-634.

Everdingen, R. V. (1968). Mobility of main ion species in reverse osmosis and the modification of subsurface brines. *Canadian Journal of Earth Sciences*, *5*(5), 1253-1260.

Fick A (1855) Über Diffusion. Ann Phys 170, 59–86.

Fontes, J. C., & Matray, J. M. (1993a). Geochemistry and origin of formation brines from the Paris Basin, France: 1. Brines associated with Triassic salts. *Chemical Geology*, *109*(1-4), 149-175.

Fontes, J. C., & Matray, J. M. (1993b). Geochemistry and origin of formation brines from the Paris Basin, France: 2. Saline solutions associated with oil fields. *Chemical Geology*, *109*(1-4), 177-200.

Foster, W.R. & Custard, H.C. 1980. Smectite–illite transformation-role in generating and maintaining geopressure. *AAPG Bulletin*, **64**, 708–708

Fritz, S. J. (1986). Ideality of clay membranes in osmotic processes: a review. Clays and clay minerals, 34(2), 214-223.

Fritz, S. J., & Whitworth, T. M. (1994). Hyperfiltration-induced fractionation of lithium isotopes: Ramifications relating to representativeness of aquifer sampling. *Water Resources Research*, *30*(2), 225-235.

Galán, E., & Ferrell, R. E. (2013). Genesis of clay minerals. In Developments in clay science (Vol. 5, pp. 83-126). Elsevier.

Gao, C., & Liu, Y. (2021). First-principles calculations of equilibrium bromine isotope fractionations. Geochimica et Cosmochimica Acta, 297, 65-81

Garven, G., (1995) Continental-scale fluid flow and geologic processes. Annu. Rev. Earth Planet. Sci. 24, 89–117.

Giunta, T., Devauchelle, O., Ader, M., Locke, R., Louvat, P., Bonifacie, M., ... & Agrinier, P. (2017). The gravitas of gravitational isotope fractionation revealed in an isolated aquifer. *Geochem Persp Lett*, *4*, 53-58.

Giunta, T., Devauchelle, O., Ader, M., Locke, R., Louvat, P., Bonifacie, M., ... & Agrinier, P. (2017). The gravitas of gravitational isotope fractionation revealed in an isolated aquifer. Geochemical Perspectives Letters, 4, 53-58.

Godon, A., Jendrzejewski, N., Eggenkamp, H. G., Banks, D. A., Ader, M., Coleman, M. L., & Pineau, F. (2004). A cross-calibration of chlorine isotopic measurements and suitability of seawater as the international reference material. *Chemical Geology*, *207*(1-2), 1-12.

Grgic, D., Giraud, A., & Schoumacker, L. (2019). Dynamic anisotropic elastic properties of a claystone under variable loading direction and saturation. *Geophysical Journal International*, *216*(1), 148-163.

Gribble, G. W. (1999). The diversity of naturally occurring organobromine compounds. *Chemical Society Reviews*, *28*(5), 335-346.

Gribble, G.W. (1998). Naturally occurring organohalogen compounds. Accounts of Chemical Research 31, 141e152.

Gribble, G.W. (2010). Naturally occurring organohalogen compounds e a comprehensive update. Progress in the Chemistry of Organic Natural Products 91. Springle Wien New York, ISBN 978-3-211-99322-4.

Guggenheim, S., & Martin, R. T. (1995). Definition of clay and clay mineral: joint report of the AIPEA nomenclature and CMS nomenclature committees. Clays and clay minerals, 43(2), 255-256.

Hanor, J. S. (1987). Origin and migration of subsurface sedimentary brines (No. 21). Sepm Society for Sedimentary.

Hanor, J. S. (1994). Physical and chemical controls on the composition of waters in sedimentary basins. *Marine and petroleum geology*, *11*(1), 31-45.

Hart, M. (2013). Low-head hyperfiltration through Jurassic-Cretaceous metamorphic Darrington Phyllite discs (from the Northwest Cascades of Washington State, USA). *Hydrogeology Journal*, *21*(2), 481-489.

Hendry, M. J., Wassenaar, L. I., & Kotzer, T. (2000). Chloride and chlorine isotopes (36Cl and δ37Cl) as tracers of solute migration in a thick, clay-rich aquitard system. *Water Resources Research*, *36*(1), 285-296.

Henry, P. (1997). Relationship between porosity, electrical conductivity, and cation exchange capacity in Barbados wedge sediments. In PROCEEDINGS-OCEAN DRILLING PROGRAM SCIENTIFIC RESULTS (pp. 137-150). NATIONAL SCIENCE FOUNDATION.

Henry, P., Kanamatsu, T., Moe, K. T., & Strasser, M. (2012). IODP expedition 333: return to Nankai Trough subduction inputs sites and coring of mass transport deposits. *Scientific drilling*, *14*, 4-17.

Hesse, R., Egeberg, P. K., & Frape, S. K. (2006). Chlorine stable isotope ratios as tracer for pore-water advection rates in a submarine gas-hydrate field: implication for hydrate concentration. *Geofluids*, *6*(1), 1-7.

Hong, D., Cao, J., Wu, T., Dang, S., Hu, W., & Yao, S. (2020). Authigenic clay minerals and calcite dissolution influence reservoir quality in tight sandstones: Insights from the central Junggar Basin, NW China. *Energy Geoscience*, *1*(1-2), 8-19.

Horseman, S. T., Higgo, J. J. W., Alexander, J., & Harrington, J. F. (1996). Water, gas and solute movement through argillaceous media. *Nuclear Energy Agency Rep. CC-96/1. OECD, Paris*.

Horst A, Thornton BJ, Holmstrand H, Andersson P, Crill PM, Gustafsson Ö (2013) Stable bromine isotopic composition of atmospheric CH3Br. Tellus Ser B— Chem Phys Meteor 65, no 21040.

Horst, A., Holmstrand, H., Andersson, P., Thornton, B. F., Wishkerman, A., Keppler, F., & Gustafsson, Ö. (2014). Stable bromine isotopic composition of methyl bromide released from plant matter. *Geochimica et Cosmochimica Acta*, *125*, 186-195.

Hower, J., Eslinger, E. V., Hower, M. E., & Perry, E. A. (1976). Mechanism of burial metamorphism of argillaceous sediment: 1. Mineralogical and chemical evidence. *Geological Society of America Bulletin*, *87*(5), 725-737.

Inoue, A., & Kitagawa, R. (1994). Morphological characteristics of illitic clay minerals from a hydrothermal system. *American Mineralogist*, *79*(7-8), 700-711.

Inoue, A., Kohyama, N., Kitagawa, R., & Watanabe, T. (1987). Chemical and morphological evidence for the conversion of smectite to illite. Clays and Clay Minerals, 35(2), 111-120.

Inoue, A., Velde, B., Meunier, A., & Touchard, G. (1988). Mechanism of illite formation during smectite-to-illite conversion in a hydrothermal system. American Mineralogist, 73(11-12), 1325-1334.

Karnland, O., Olsson, S., Nilsson, U. and Sellin, P. (2007) Experimentally determined swelling pressures and geochemical interactions of compacted Wyoming bentonite with highly alkaline solutions. Phys. Chem. Earth 32, 275–286.

Kaufmann, R., Long, A., Bentley, H., & Davis, S. (1984). Natural chlorine isotope variations. *Nature*, *309*(5966), 338-340.

Kemper, W. D. (1961). Movement of water as effected by free energy and pressure gradients: I. Application of classic equations for viscous and diffusive movements to the liquid phase in finely porous media. *Soil Science Society of America Journal*, *25*(4), 255-260.

Kemper, W. D., & Maasland, D. E. L. (1964). Reduction in salt content of solution on passing through thin films adjacent to charged surfaces. *Soil Science Society of America Journal*, *28*(3), 318-323.

Kendrick, M. A., Phillips, D., Wallace, M., & Miller, J. M. (2011). Halogens and noble gases in sedimentary formation waters and Zn–Pb deposits: A case study from the Lennard Shelf, Australia. *Applied Geochemistry*, *26*(12), 2089-2100.

Kharaka, Y. K., & Berry, F. A. (1973). Simultaneous flow of water and solutes through geological membranes—I. Experimental investigation. Geochimica et Cosmochimica Acta, 37(12), 2577-2603.

Kharaka, Y. K., & Berry, F. A. (1973). Simultaneous flow of water and solutes through geological membranes—I. Experimental investigation. Geochimica et Cosmochimica Acta, 37(12), 2577-2603.

Kharaka, Y. K., & Hanor, J. S. (2003). Deep fluids in the continents: I. Sedimentary basins. *Treatise on geochemistry*, *5*, 605.

Kharaka, Y. K., & Hanor, J. S. (2003). Deep fluids in the continents: I. Sedimentary basins. Treatise on geochemistry, 5, 605.

Komada, T., Anderson, M. R., & Dorfmeier, C. L. (2008). Carbonate removal from coastal sediments for the determination of organic carbon and its isotopic signatures, δ13C and Δ14C: comparison of fumigation and direct acidification by hydrochloric acid. *Limnology and Oceanography: Methods*, *6*(6), 254-262.

Kozaki, T., Saito, N., Fujishima, A., Sato, S., & Ohashi, H. (1998). Activation energy for diffusion of chloride ions in compacted sodium montmorillonite. *Journal of Contaminant Hydrology*, *35*(1-3), 67-75.

Langmuir, I. (1918). The adsorption of gases on plane surfaces of glass, mica and platinum. *Journal of the American Chemical society*, *40*(9), 1361-1403.

Lanson, B., Sakharov, B. A., Claret, F., & Drits, V. A. (2009). Diagenetic smectite-to-illite transition in clay-rich sediments: A reappraisal of X-ray diffraction results using the multi-specimen method. American Journal of Science, 309(6), 476-516.

Lavastre, V., Jendrzejewski, N., Agrinier, P., Javoy, M., & Evrard, M. (2005). Chlorine transfer out of a very low permeability clay sequence (Paris Basin, France): 35Cl and 37Cl evidence. *Geochimica et Cosmochimica Acta*, *69*(21), 4949-4961.

Le Gallo, Y., Bildstein, O., & Brosse, E. (1998). Coupled reaction-flow modeling of diagenetic changes in reservoir permeability, porosity and mineral compositions. *Journal of Hydrology*, *209*(1-4), 366-388.

Letey, J., Kemper, W. D., & Noonan, L. (1969). The effect of osmotic pressure gradients on water movement in unsaturated soil. *Soil Science Society of America Journal*, *33*(1), 15-18.

Liu, J., Chen, Z., Wang, L., Zhang, Y., Li, Z., Xu, J., & Peng, Y. (2016). Chemical and isotopic constrains on the origin of brine and saline groundwater in Hetao plain, Inner Mongolia. *Environmental Science and Pollution Research*, *23*(15), 15003-15014.

Liu, Y., Hu, W., Cao, J., Wang, X., Tang, Q., Wu, H., & Kang, X. (2018). Diagenetic constraints on the heterogeneity of tight sandstone reservoirs: A case study on the Upper Triassic Xujiahe Formation in the Sichuan Basin, southwest China. *Marine and Petroleum Geology*, *92*, 650-669.

Louvat, P., Bonifacie, M., Giunta, T., Michel, A., & Coleman, M. (2016). Determination of bromine stable isotope ratios from saline solutions by “wet plasma” MC-ICPMS Including a comparison between high-and low-resolution modes, and three introduction systems. *Analytical chemistry*, *88*(7), 3891-3898.

Luo, C., Xiao, Y., Wen, H., Ma, H., Ma, Y., Zhang, Y., ... & He, M. (2014). Stable isotope fractionation of chlorine during the precipitation of single chloride minerals. *Applied geochemistry*, *47*, 141-149.

Mann, U. (1994). An integrated approach to the study of primary petroleum migration. Geological Society, London, Special Publications, 78(1), 233-260.

Martel, A. T., Gibling, M. R., & Nguyen, M. (2001). Brines in the Carboniferous Sydney Coalfield, Atlantic Canada. *Applied Geochemistry*, *16*(1), 35-55.

Martin, R. B. (1964). Introduction to biophysical chemistry. *Academic Medicine*, *39*(9), 867.

Maurice, P. A., Namjesnik-Dejanovic, K., Lower, S. K., Pullin, M. J., Chin, Y. P., & Aiken, G. R. (1998). Sorption and fractionation of natural organic matter on kaolinite and goethite. *Water-Rock Interaction IX. Balkema, Rotterdam*, 109-113.Mazurek, M., Alt-Epping, P., Bath, A., Gimmi, T., Waber, H. N., Buschaert, S., ... & Wouters, L. (2011). Natural tracer profiles across argillaceous formations. *Applied Geochemistry*, *26*(7), 1035-1064.

McKelvey, J. G., & Milne, I. H. (1962). The flow of salt solutions through compacted clay. In Clays and clay minerals (pp. 248-259). Pergamon.

Melkior, T., Gaucher, E. C., Brouard, C., Yahiaoui, S., Thoby, D., Clinard, C., ... & Coelho, D. (2009). Na+ and HTO diffusion in compacted bentonite: Effect of surface chemistry and related texture. *Journal of Hydrology*, *370*(1-4), 9-20.

Merriman, R. J. (2005). Clay minerals and sedimentary basin history. European Journal of Mineralogy, 17(1), 7-20.

Molera, M., & Eriksen, T. (2002). Diffusion of 22Na+, 85Sr2+, 134Cs+ and 57Co2+ in bentonite clay compacted to different densities: experiments and modeling. *Radiochimica Acta*, *90*(9-11), 753-760.

Mondol, N. H., Bjørlykke, K., Jahren, J., & Høeg, K. (2007). Experimental mechanical compaction of clay mineral aggregates—Changes in physical properties of mudstones during burial. Marine and petroleum geology, 24(5), 289-311.

Mondol, N. H., Bjørlykke, K., Jahren, J., & Høeg, K. (2007). Experimental mechanical compaction of clay mineral aggregates—Changes in physical properties of mudstones during burial. *Marine and petroleum geology*, *24*(5), 289-311.

Mondol, N. H., Fawad, M., Jahren, J., & Bjørlykke, K. (2008). Synthetic mudstone compaction trends and their use in pore pressure prediction. first break, 26(12).

Musashi, M., Oi, T., & Eggenkamp, H. G. (2004). Experimental determination of chlorine isotope separation factor by anion-exchange chromatography. *Analytica chimica acta*, *508*(1), 37-40.

Muurinen, A., Karnland, O., & Lehikoinen, J. (2004). Ion concentration caused by an external solution into the porewater of compacted bentonite. Physics and Chemistry of the Earth, Parts A/B/C, 29(1), 119-127.

Nadeau, P. H. (2011). Earth's energy “Golden Zone”: a synthesis from mineralogical research. Clay Minerals, 46(1), 1-24.

Neaman, A., Pelletier, M., & Villieras, F. (2003). The effects of exchanged cation, compression, heating and hydration on textural properties of bulk bentonite and its corresponding purified montmorillonite. *Applied Clay Science*, *22*(4), 153-168.

Neuzil, C. E. (1995). Abnormal pressures as hydrodynamic phenomena. American journal of Science, 295(6), 742-786.

Neuzil, C. E., & Person, M. (2017). Reexamining ultrafiltration and solute transport in groundwater. *Water Resources Research*, *53*(6), 4922-4941.

Neuzil, C. E., & Provost, A. M. (2009). Recent experimental data may point to a greater role for osmotic pressures in the subsurface. *Water Resources Research, 45*(3).

Nieto, F., Ortega-Huertas, M., Peacor, D. R., & Arostegui, J. (1996). Evolution of illite/smectite from early diagenesis through incipient metamorphism in sediments of the Basque-Cantabrian Basin.

Nygård, R., Gutierrez, M., Gautam, R., & Høeg, K. (2004). Compaction behavior of argillaceous sediments as function of diagenesis. *Marine and Petroleum Geology, 21*(3), 349-362.

Oluwadebi, A. G., Taylor, K. G., & Dowey, P. J. (2018). Diagenetic controls on the reservoir quality of the tight gas Collyhurst sandstone formation, lower Permian, east Irish Sea basin, United Kingdom. *Sedimentary Geology, 371*, 55-74.

Osborne, M. J., & Swarbrick, R. E. (1997). Mechanisms for generating overpressure in sedimentary basins: A reevaluation. AAPG bulletin, 81(6), 1023-1041.

Parkhurst, D. L., & Appelo, C. A. J. (1999). User's guide to PHREEQC (Version 2): A computer program for speciation, batch-reaction, one-dimensional transport, and inverse geochemical calculations. *Water-resources investigations report, 99*(4259), 312.

Person, M., Raffensperger, J. P., Ge, S., & Garven, G. (1996). Basin-scale hydrogeologic modeling. *Reviews of Geophysics, 34*(1), 61-87.

Phillips, F. M., & Bentley, H. W. (1987). Isotopic fractionation during ion filtration: I. Theory. *Geochimica et Cosmochimica Acta, 51*(3), 683-695.

Plecis, A., Schoch, R. B., & Renaud, P. (2005). Ionic transport phenomena in nanofluidics: experimental and theoretical study of the exclusion-enrichment effect on a chip. *Nano letters*, *5*(6), 1147-1155.

Poelchau, H. S., Baker, D. R., Hantschel, T., Horsfield, B., & Wygrala, B. (1997). Basin simulation and the design of the conceptual basin model. In Petroleum and basin evolution (pp. 3-70). Springer, Berlin, Heidelberg.

Pusch, R., Karnland, O., & Hökmark, H. (1990). *GMM-a general microstructural model for qualitative and quantitative studies of smectite clays* (No. SKB-TR--90-43). Swedish Nuclear Fuel and Waste Management Co..

Ramm, M., & Bjørlykke, K. (1994). Porosity/depth trends in reservoir sandstones: Assessing the quantitative effects of varying pore-pressure, temperature history and mineralogy, Norwegian Shelf data. *Clay minerals, 29*(4), 475-490.

Reeve, A.S. 2002. The migration of a sodium bromide tracer in a large Maine peatland. Geological Society of America Abstracts with Programs 34, no. 6: 420.

Richet, P., Bottinga, Y., & Javoy, M. (1977). A review of hydrogen, carbon, nitrogen, oxygen, sulphur, and chlorine stable isotope fractionation among gaseous molecules. *Annual Review of Earth and Planetary Sciences*, *5*(1), 65-110.

Rotenberg, B., Marry, V., Dufrêche, J. F., Malikova, N., Giffaut, E., & Turq, P. (2007). Modelling water and ion diffusion in clays: A multiscale approach. *Comptes Rendus Chimie*, *10*(10-11), 1108-1116.

Rudkiewicz, J.L., Vear, A.and Brigaud, F. (1999) Mechanisms for high pressures and high temperatures in the Central North Sea Graben. Sciences Géologiques, bulletins et mémoires. pp. 127-128.

Russell, W. L. (1933). Subsurface concentration of chloride brines. AAPG Bulletin, 17(10), 1213-1228.

Sacci, E., Michelot, J-L. & Pitsch, H. 2000. Porewater extraction from argillaceous rocks for geochemical characterization. Methods and interpretation. France: AEN/OECD, 185 p. ISBN 92-64-17181-9.

Saito S. (2010a) Expedition 322 Scientists. Site C0012. In Proc. IODP, 322 (eds. S. Saito, M. B. Underwood and Y. Kubo), and the Expedition 322 Scientists. Integrated Ocean Drilling Program Management International, Inc., Tokyo, doi:10.2204/iodp.proc.322.104.2010.

Sato, H., Ashida, T., Kohara, Y., Yui, M., & Sasaki, N. (1992). Effect of dry density on diffusion of some radionuclides in compacted sodium bentonite. *Journal of Nuclear Science and Technology*, *29*(9), 873-882.

Sauzeat, E. Guillaume, D. Villiéras, F. Dubessy, J. Francois, M. Pfeiffert, C. Pelletier, M. Ruck, R. Barrès, O. Yvon, J. Cathelineau, M. (2001) Caractérisation minéralogique, cristallochimique et texturale de l'argile MX-80. Ref ANDRA : C RP 0LEM 01-001.

Sauzéat, E., Guillaume, D., Neaman, A., Dubessy, J., François, M., Pfeiffert, C., ... & Cathelineau, M. (2001). Caractérisation fine de l'argile brute MX-80: Caractérisation minéralogique, cristallochimique et texturale de l'argile MX-80. *ANDRA C RP 1ENG*, 01-001.

Sayles, F. L., & Mangelsdorf Jr, P. C. (1977). The equilibration of clay minerals with sea water: exchange reactions. *Geochimica et Cosmochimica Acta*, *41*(7), 951-960.

Schauble, E. A. (2004). Applying stable isotope fractionation theory to new systems. *Reviews in mineralogy and geochemistry*, *55*(1), 65-111.

Schauble, E. A., Rossman, G. R., & Taylor Jr, H. P. (2003). Theoretical estimates of equilibrium chlorine-isotope fractionations. *Geochimica et Cosmochimica Acta*, *67*(17), 3267-3281.

Shackelford, C. D., & Daniel, D. E. (1991). Diffusion in saturated soil. II: Results for compacted clay. *Journal of Geotechnical Engineering*, *117*(3), 485-506.

Shouakar-Stash, O. (2008). Evaluation of stable chlorine and bromine isotopes in sedimentary formation fluids.

Shouakar-Stash, O., Alexeev, S. V., Frape, S. K., Alexeeva, L. P., & Drimmie, R. J. (2007). Geochemistry and stable isotopic signatures, including chlorine and bromine isotopes, of the deep groundwaters of the Siberian Platform, Russia. *Applied geochemistry*, *22*(3), 589-605.

Sofer, Z., & Gat, J. R. (1972). Activities and concentrations of oxygen-18 in concentrated aqueous salt solutions: analytical and geophysical implications. Earth and Planetary Science Letters, 15(3), 232-238.

Sofer, Z., & Gat, J. R. (1975). The isotope composition of evaporating brines: effect of the isotopic activity ratio in saline solutions. *Earth and Planetary Science Letters*, *26*(2), 179-186.

Solley, W. B., & Chase, E. B. (1983). Estimated use of water in the United States in 1980.

Sparks, D. L. (2003). Environmental soil chemistry: An overview. *Environmental soil chemistry, 2nd edn. Academic Press, New York*, 1-42.

Środoń, J. (1999). Use of clay minerals in reconstructing geological processes: recent advances and some perspectives. Clay Minerals, 34(1), 27-37.

Środoń, J., (2010) Evolution of mixed-layer clay minerals in prograde alteration systems. In: Fiore, S., Cuadros, J., Huertas, F.J. (Eds.), Interstratified Clay Minerals. Origin, Characteristics and Geochemical Significance. AIPEA Educational Series, vol. 1. Digilabs, Bari, Italy, pp. 114–175.

Środoń, J., Drits, V. A., McCarty, D. K., Hsieh, J. C., & Eberl, D. D. (2001). Quantitative X-ray diffraction analysis of clay-bearing rocks from random preparations. Clays and Clay Minerals, 49(6), 514-528.

Srodon, J., Eberl, D. D., & Drits, V. A. (2000). Evolution of fundamental-particle size during illitization of smectite and implications for reaction mechanism. Clays and Clay Minerals, 48(4), 446-458.

Stern, O. (1924) "Zur Theorie der Elektrolytischen Doppelschicht". Zeitschrift für Elektrochemie. 30: 508.

Stotler, R. L., Frape, S. K., & Shouakar-Stash, O. (2010). An isotopic survey of δ81Br and δ37Cl of dissolved halides in the Canadian and Fennoscandian Shields. *Chemical Geology*, *274*(1-2), 38-55.

Swarbrick, R. E., & Osborne, M. J. (1998). Memoir 70, Chapter 2: Mechanisms that Generate Abnormal Pressures: an Overview.

Tanikawa, W., Shimamoto, T., Wey, S. K., Lin, C. W., & Lai, W. C. (2008). Stratigraphic variation of transport properties and overpressure development in the Western Foothills, Taiwan. Journal of Geophysical Research: Solid Earth, 113(B12).

Taylor, T. R., Giles, M. R., Hathon, L. A., Diggs, T. N., Braunsdorf, N. R., Birbiglia, G. V., ... & Espejo, I. S. (2010). Sandstone diagenesis and reservoir quality prediction: Models, myths, and reality. *AAPG bulletin*, *94*(8), 1093-1132.

Theng, B. K. G. (1972). Formation, properties, and practical applications of clay—organic complexes. *Journal of the Royal Society of New Zealand*, *2*(4), 437-457.

Thyberg, B., & Jahren, J. (2011). Quartz cementation in mudstones: sheet-like quartz cement from clay mineral reactions during burial. Petroleum Geoscience, 17(1), 53-63.

Thyne, G., Boudreau, B. P., Ramm, M., & Midtbø, R. E. (2001). Simulation of potassium feldspar dissolution and illitization in the Statfjord Formation, North Sea. *AAPG bulletin*, *85*(4), 621-635.

Tissot, B. P., & Welte, D. H. (1984). Diagenesis, catagenesis and metagenesis of organic matter. In Petroleum formation and occurrence (pp. 69-73). Springer, Berlin, Heidelberg.

Tournassat, C., & Appelo, C. A. J. (2011). Modelling approaches for anion-exclusion in compacted Na-bentonite. *Geochimica et Cosmochimica Acta*, *75*(13), 3698-3710.

Tremosa, J., Gailhanou, H., Chiaberge, C., Castilla, R., Gaucher, E. C., Lassin, A., ... & Claret, F. (2020). Effects of smectite dehydration and illitisation on overpressures in sedimentary basins: A coupled chemical and thermo-hydro-mechanical modelling approach. *Marine and Petroleum Geology*, *111*, 166-178.

Underwood M. B. and Hoke K. D. (2000). In Proceedings of the Ocean Drilling Program, Scientific Results, 168 (eds. A. Fisher, E. E. Davis and C. Escutia), pp. 51–65.

Underwood, M. B., Guo, J., Saito, S., & Kubo, Y. (2013). Data report: Clay mineral assemblages in the Shikoku Basin, NanTroSEIZE subduction inputs, IODP Sites C0011 and C0012. In *Proceedings of the Integrated Ocean Drilling Program* (Vol. 322, pp. 2-34).

Ungerer, P., Béhar, E. and Discamps, D., Eds. (1983) Tentative Calculation of the Overall Volume Expansion of Organic Matter During Hydrocarbon Genesis from Geochemistry Data. Implications for Primary Migration. Advances in Organic Geochemistry, 1981, Wiley.

Urey, H. C. (1947). The thermodynamic properties of isotopic substances. *Journal of the Chemical Society (Resumed)*, 562-581.

Van Everdingen, R.O. (1968). Studies of formation waters in western Canada: Geochemistry and hydrodynamics. Canadian Journal of Earth Sciences, 5(3), 523-543.

Van Loon L.R., Glaus, M.A. and Müller W (2007) Anion exclusion effects in compacted bentonites: Towards a better understanding of anion diffusion. Appl. Geochemistry 22, 2536–2552.

Van Loon, L. R., Soler, J. M., Müller, W., & Bradbury, M. H. (2004). Anisotropic diffusion in layered argillaceous rocks: a case study with Opalinus Clay. Environmental science & technology, 38(21), 5721-5728.

Van Olphen, H. (1964). An introduction to clay colloid chemistry. Soil Science, 97(4), 290.

Vidal, O., & Dubacq, B. (2009). Thermodynamic modelling of clay dehydration, stability and compositional evolution with temperature, pressure and H2O activity. Geochimica et Cosmochimica Acta, 73(21), 6544-6564.

Wangen, M. (2001). A quantitative comparison of some mechanisms generating overpressure in sedimentary basins. Tectonophysics, 334(3-4), 211-234.

Welte, D. H., & Tissot, P. B. (1984). Petroleum formation and occurrence. Springer-verlag.

Wenk, H. R., & Bulakh, A. (2004). Minerals. Minerals, 668.

Wersin, P., Curti, E., & Appelo, C. A. J. (2004). Modelling bentonite–water interactions at high solid/liquid ratios: swelling and diffuse double layer effects. *Applied Clay Science*, *26*(1-4), 249-257.

Whitney, G. (1990). Role of water in the smectite-to-illite reaction. Clays and Clay Minerals, 38(4), 343-350.

Whitworth, T. M., & Fritz, S. J. (1994). Electrolyte-induced solute permeability effects in compacted smectite membranes. *Applied Geochemistry*, *9*(5), 533-546.

Wigger, C., & Van Loon, L. R. (2017). Importance of interlayer equivalent pores for anion diffusion in clay-rich sedimentary rocks. *Environmental science & technology*, *51*(4), 1998-2006.

Williams, L. B., & Ferrell, R. E. (1991). Ammonium substitution in illite during maturation of organic matter. Clays and Clay Minerals, 39(4), 400-408.

Worden, R. H. (1996). Controls on halogen concentrations in sedimentary formation waters. *Mineralogical Magazine*, *60*(399), 259-274.

Woulé Ebongué, V., Jendrzejewski, N., Walgenwitz, F., Pineau, F., & Javoy, M. (2005). Chlorine isotope residual salt analysis: A new tool to investigate formation waters from core analyses. *AAPG bulletin*, *89*(8), 1005-1018.

Yardley G.S. and Nwozor K.K. (2017) Overpressure Mechanisms and Their Distribution in the Central North Sea. Conference Proceedings, First EAGE Workshop on Pore Pressure Prediction, Mar 2017, cp-506-00009.

Yechieli, Y., Magaritz, M., Levy, Y., Weber, U., Kafri, U., Woelfli, W., & Bonani, G. (1993). Late Quaternary geological history of the Dead Sea area, Israel. Quaternary Research, 39(1), 59-67.

Yu, H., Ma, T., Du, Y., & Chen, L. (2019). Genesis of formation water in the northern sedimentary basin of South China Sea: Clues from hydrochemistry and stable isotopes (D, 18O, 37Cl and 81Br). *Journal of Geochemical Exploration*, *196*, 57-65.

Yu, H., Ma, T., Du, Y., & Chen, L. (2019). Genesis of formation water in the northern sedimentary basin of South China Sea: Clues from hydrochemistry and stable isotopes (D, 18O, 37Cl and 81Br). *Journal of Geochemical Exploration*, *196*, 57-65.

Yuan, G., Cao, Y., Gluyas, J., Li, X., Xi, K., Wang, Y., ... & Oxtoby, N. H. (2015). Feldspar dissolution, authigenic clays, and quartz cements in open and closed sandstone geochemical systems during diagenesis: typical examples from two sags in Bohai Bay Basin, East China. *AAPG Bulletin*, *99*(11), 2121-2154.

Zhao J. and Li J. (2017) Advances in the origin of overpressures in sedimentary basins. Shiyou Xuebao/Acta Petrolei Sinica. DOI: 10.7623/syxb201709001.

Zhao, J., Li, J., Cao, Q., Bai, Y., Wu, W., & Ma, Y. (2019). Quasi-continuous hydrocarbon accumulation: An alternative model for the formation of large tight oil and gas accumulations. Journal of Petroleum Science and Engineering, 174, 25-39.

Ziegler, K., Coleman, M. L., & Howarth, R. J. (2001). Palaeohydrodynamics of fluids in the Brent Group (Oseberg Field, Norwegian North Sea) from chemical and isotopic compositions of formation waters. *Applied Geochemistry*, *16*(6), 609-632.

Zou, Y. R., and Peng, P. A. (2001). Overpressure retardation of organic-matter maturation: a kinetic model and its application. Mar. Petrol. Geol. 18:707–713.